OF APOPTOSOMES AND ONCOGENES:

REPURPOSING A DEATH MACHINE &

DECONSTRUCTING THE ACTION OF P53 MUTATIONS

APPROVED BY SUPERVISORY COMMITTEE

John M. Abrams, Ph.D. (Mentor)

Pier Paolo Scaglioni, M.D., Ph.D. (Chair)

Hongtao Yu, Ph.D.

Jerry Shay, Ph.D.

DEDICATION

Para los Papás y Arturo -

Mis compañeros constantes.

Gracias por apoyar mis sueños.

To Mabe –

The most fascinating person I've ever met.

Without you none of this would be finished.

To the Almighty -

Who gives us all breath and life

whether we recognize it or not.

He. is. good.

ACKNOWLEDGEMENTS

There are way too many people to thank. My wife, Marybeth. She is the best decision I have ever made. Thank you, dear, for believing in me and pushing me to continue in times of weakness and frustration. You truly make this life brighter and more fun. My parents and brother. You three are stable rocks in a sea of shifting sands. Thank you for always having open arms and for teaching me to relax and enjoy life. The Abrams crew. You guys are a fun bunch and challenge me to become a better scientist. Thanks for rejoicing with the successes and being there through the failures. And my mentor, John. You are a legit man. Being under your leadership has made me a better person and scientist. You've not only put up with my inconsistencies and procrastination but helped me overcome them. And thanks for showing us all that science is incredibly fascinating and that life is meant to be enjoyed.

OF APOPTOSOMES AND ONCOGENES:

REPURPOSING A DEATH MACHINE &

DECONSTRUCTING THE ACTION OF P53 MUTATIONS

by

ALEJANDRO D'BROT

DISSERTATION

Presented to the Faculty of the Graduate School of Biomedical Sciences

The University of Texas Southwestern Medical Center at Dallas

In Partial Fulfillment of the Requirements

For the Degree of

DOCTOR OF PHILOSOPHY

The University of Texas Southwestern Medical Center at Dallas

Dallas, Texas

April, 2014

OF APOPTOSOMES AND ONCOGENES:

REPURPOSING A DEATH MACHINE &

DECONSTRUCTING THE ACTION OF P53 MUTATIONS

ALEJANDRO D'BROT, Ph.D.

The University of Texas Southwestern Medical Center at Dallas, 2014

Supervising Professor: John M. Abrams, Ph.D.

It is now well appreciated that the apoptosome, which governs caspase-dependent cell death, also drives nonapoptotic caspase activation to remodel cells. However, determinants that specify whether the apoptosome acts to kill or remodel have yet to be identified. I show here that *Tango7* genetically interacts with the apoptotic machinery but instead of regulating cell death, collaborates with the apoptosome to drive caspase-dependent cellular

remodeling. Specifically, *Tango7* is required for non-apoptotic caspase activity during spermatid remodeling and localizes to the active apoptosome compartment in these cells via its C terminus. Furthermore, Tango7 directly stimulates activity of reconstituted apoptosomes *in vitro*. These and other data presented here suggest that Tango7 physically recruits the apoptosome to specify this complex for nonapoptotic cellular remodeling. *In vivo* genetic model systems are powerful tools to deconstruct activity of genes driving human disease. The tumor suppressor p53 is mutated more than any other gene in human cancer, but unlike other tumor suppressors, it acquires missense mutations which encode oncogenic variants. These gain-of-function mutants promote more aggressive and metastatic cancers *in vivo* but their oncogenic activity is not well understood. To address this problem, I have exploited *Drosophila* as a platform to study and stratify human p53 (hp53) mutants. I replaced fly p53 with either wild-type hp53 or 5 of the most prevalent hp53 mutations in cancer. In this system, hp53 is under control of endogenous *Dp53* regulatory elements and can regulate *in vivo* transcriptional activation and apoptosis like its fly counterpart. Furthermore, wild-type hp53 forms foci in the germline that localize to the same subnuclear compartment as Dp53 foci. This property is compromised in all of the gain-of-function mutants and can thus be used to distinguish oncogenic variants from wild-type hp53. Future studies aim at finding whether this and other properties shared among the 5 mutants can help stratify oncogenic p53 mutations found in human cancer.

TABLE OF CONTENTS

PRIOR PUBLICATIONS

D'Brot A, Chen P, Vaishnav M, Yuan S, Akey CW, Abrams JM. 2013. Tango7 directs cellular remodeling by the *Drosophila* apoptosome. *Genes & development* **27**: 1650-1655.

Wylie A, Lu WJ, **D'Brot A,** Buszczak M, Abrams JM. 2014. p53 activity is selectively licensed in the *Drosophila* stem cell compartment. *eLife* **3**:e01530.

D'Brot A, Abrams J. (in preparation). Making sense out of missense: Gain-of-function mutations in p53. *Oncogene*. *Invited Review*.

LIST OF FIGURES

LIST OF TABLES

LIST OF APPENDICES

LIST OF DEFINITIONS

AO – Acridine Orange

APAF-1 – Apoptotic protease activating factor 1

ATM – Ataxia telangiectasia mutated

BCM – Border cell migration

BH3 – Bcl-2 Homology Domain 3

C4da – class IV dendritic arborization sensory neurons

Caspase – Cysteinyl aspartate-specific protease

Chk2 – Checkpoint kinase 2

Dark – *Drosophila* Apaf-1-related killer

Dcp-1 – Death caspase 1

DHE – Dihydroethidium

Drice – *Drosophila* ICE

Dronc – *Drosophila* Nedd2-like caspase

Ey – Eyeless

GMR – Glass Multiple Reporter

GHP150 – Dp53 cytoplasmic biosensor

hid – Head Involution Defective

Hml – Hemolectin

IAP – Inhibitor of apoptosis proteins

IOCs – interommatidial cells

MOMP – Mitochondrial Outer Membrane Permeabilization

MS1096-Gal4 – a wing specific driver

NS150 – Dp53 cytoplasmic biosensor recombined with $Dp53^{NS}$

OXPHOS – Oxidative phosphorylation

PCI – Proteasome, CSN, Initiation Factor Domain

PCD – Programmed cell death

PML – Promyolocytic leukemia

RFP – Red fluorescent protein

rpr – Reaper

Smac – Second mitochondrial activator of caspases

Tango7 – Transport and Golgi Organization 7

TRiP – Transgenic RNAi Project

UAS – Upstream Activation Sequence

Drosophila gene, protein and mutant nomenclature:

Tango7 – gene, capitalized and italicized

Tango7 – protein, capitalized and non-italicized

$Tango7^{L/+}$ – a genotypically wild-type fly, capitalized and italicized

tango7 – a genotypically mutant fly, lowercase and italicized

$tango7^{L/L}$ – a genotypically mutant fly with specific combination of alleles, lowercase and italicized

DISSERTATION OBJECTIVES

Aim 1: Study the *in vivo* functions of *Tango7* – I mutated the Tango7 gene in the fly and characterized its role in programmed cell death. In the process, I discovered that Tango7 is instead required for cellular remodeling – a caspase-dependent, non-apoptotic cellular program. I went on to study its relationship to the apoptosome using genetic and biochemical assays.

Aim 2: Create an *in vivo* genetic platform to study human p53 mutants– I humanized p53 in *Drosophila* and generated a collection of fly lines that endogenously express either wild-type p53 or 5 of the most common variants found in human cancer. I showed that in this system, humanized p53 can regulate *in vivo* transcriptional activation and apoptosis like its fly counterpart. Using this platform, I have uncovered behaviors and activities that distinguish oncogenic mutants from wild-type p53. Future studies aim at finding whether properties shared among the 5 mutants can help stratify gain-of-function p53 mutations in human cancer.

CHAPTER ONE:

INTRODUCTION

Of Apoptosomes: Cell death and Cellular Remodeling

Apoptosis is the most common form of programmed cell death (PCD) and is intimately involved in development, tissue homeostasis and disease (Thompson 1995). Apoptosis can occur in response to intracellular signals (intrinsic pathway) such as DNA damage, or extracellular signals (extrinsic pathway) such as death ligands from neighboring cells. Both pathways act to tightly regulate activation of a family of proteases called caspases which execute cell death. Deregulation of the apoptotic pathway, and thus inhibition or hyper-activation of caspases, plays a central role in pathologies such as cancer, ischemia, AIDS and neurodegeneration (Fuchs and Steller 2011).

Throughout the animal kingdom, execution of the intrinsic apoptotic pathway relies on the activation of the apoptosome. In mammals, this occurs upon upstream derepression of Bax and Bak which then oligomerize and permeabilize the mitochondrial outer membrane (MOMP) (Kroemer et al. 2007). Upon MOMP, cytochrome c is released, catalyzing apoptosome assembly by promoting oligomerization of Apaf-1 and recruitment of procaspase 9 (Yuan and Akey 2013). Apoptosome assembly then converts the procaspase-9 zymogen into active caspase-9 which subsequently activates executioner caspase-3 and -7. These executioner caspases then cleave a specific set of cellular substrates, including cytoskeletal proteins (Croft et al. 2005), nuclear lamins (Guo et al. 2008) and DNase

inhibitors (Enari et al. 1998) – all which culminate in cell suicide and engulfment by macrophages.

In *Drosophila*, activation of the apoptosome occurs similarly to that of mammals. It involves oligomerization of the adaptor protein Dark (Apaf-1 in mammals) and subsequent recruitment and activation of the initiator caspase Dronc (caspase-9) which in turn activates executioner caspases Drice (caspase-3) and Dcp-1 (caspase-7) (Ryoo and Baehrecke 2010). Unlike its mammalian counterpart, however, the *Drosophila* apoptosome is under constant repression by DIAP1, *Drosophila* Inhibitor of Apoptosis 1, and relies on activation of RHG (Reaper, Hid and Grim) proteins to inhibit this repression of Dronc and Drice (Hay and Guo 2006). Another important difference between the mammalian and the *Drosophila* apoptosome is that the fly counterpart does not require cytochrome c for assembly. Interestingly, a compelling study by Hao et al revealed that Apaf-1 dependent deaths can still occur in mice defective for the apoptotic function of cytochrome c (Hao et al. 2005), suggesting that the mammalian apoptosome (like in *Drosophila*) might have activating factors other than cytochrome c. Thus, the *Drosophila* model system is well suited for the discovery of novel activators of the apoptosome.

Paradoxically, apoptosome activity throughout the animal kingdom has recently been shown to drive diverse cellular processes without promoting cell death (Feinstein-Rotkopf and Arama 2009). Examples of cellular remodeling such as enucleation of erythroblasts (Carlile et al. 2004), keratinocytes (Lippens et al. 2000) and lens fiber cells (Ishizaki et al. 1998), differentiation of macrophages (Sordet et al. 2002), formation of platelet cells from megakaryocytes (De Botton et al. 2002), dendritic pruning (Kuo et al. 2006; Williams et al.

2006), and most recently, synaptic plasticity in the developing brain (Chen et al. 2012) have all been shown to require the apoptosome and/or caspase activity. An early precedent for caspase-dependent cellular remodeling came from studies of spermatid individualization in *Drosophila* (Arama et al. 2003; Huh et al. 2004; Arama et al. 2006). During this process active caspases can be visualized as syncytial spermatids are resolved into mature individual sperm through a specialized cytoskeletal structure known as the individualization complex (IC) which eliminates excess cytoplasmic content and encapsulates each sperm in plasma membrane (Fabrizio et al. 1998). *In vivo*, this process requires the apoptosome and caspase activity, since mutations in *Dark* or *Dronc* prevent normal caspase activation and coordinated IC movement, resulting in spermatogenesis defects and male sterility (Rodriguez et al. 1999; Huh et al. 2004; Arama et al. 2006).

These and other studies establish an essential role for the apoptosome but whether this complex might be converted from a machine that demolishes cells to an engine that remodels them is not known. Furthermore, because the apoptosome is often sufficient for killing, prevailing models do not adequately explain how this complex functions without provoking apoptotic cell death.

Of Oncogenes: p53 Gain-of-Function Mutations in Cancer

Mutations in the TP53 tumor suppressor gene are the most commonly reported genetic alteration in human cancer. The p53 protein functions primarily as a transcriptional hub, converting a diversity of stress-signals into activation or repression of cellular survival and death programs such as cell-cycle arrest, DNA repair, or apoptosis (Vousden and Lane 2007). Unlike other tumor-suppressors which typically acquire frameshift and nonsense mutations that ablate protein function, 75% of mutations acquired by TP53 in the germline and soma are missense mutations which create single-residue substitutions at the protein level, predominantly localized to the DNA binding domain (Soussi 2007). In addition to loss-of-function and dominant negative effects, missense mutations display gain-of-function effects which confer mutants with novel activities unrelated to the wild-type protein. *In vivo* studies in mice strongly suggest that these novel activities give rise to more aggressive and metastatic cancers. Despite considerable ground covered in the last thirty years of mutant p53 research however, a coherent model of how missense mutants exert their oncogenic activity is lacking.

A Brief History: From dominant-negative to gain-of-function effects

From its provocative debut as a viral host protein to its rise as the most highly mutated gene in human cancer, the tumor suppressor p53 has endured a long and complicated history. The odyssey starts in the late 70s in the midst of a hunt for oncogenes co-opted by viruses to transform cells. Multiple groups simultaneously stumbled upon a host protein around 53kD that co-immunoprecipitated with the large T antigen of the simian virus 40 (SV40) from infected mice cells and from human tumors (DeLeo et al. 1979; Kress et al. 1979; Lane and

Crawford 1979; Linzer and Levine 1979). The logical conclusion was made that this protein, named after its product's misleading running molecular size, was an oncoprotein. The TP53 gene was identified and cloned in 1983, followed by overexpression studies with tumor viruses and oncogenes which established that p53 was indeed an oncoprotein (Eliyahu et al. 1984; Jenkins et al. 1984; Parada et al. 1984; Wolf et al. 1984; Eliyahu et al. 1985). Several studies demonstrated the ability of p53 to cooperate with Ha-Ras – at that time a known oncogene - to transform rat embryonic fibroblasts (Eliyahu et al. 1984; Jenkins et al. 1984; Parada et al. 1984). An elegant study by Wolf et al took this observation a step further and showed that reconstitution of transformed p53-null cells with a p53 clone could produce lethal tumors when injected in mice (Wolf et al. 1984).

Shortly thereafter, evidence began to surface which challenged its role as an oncogene: Varda Rotter's group found TP53 to be inactivated by deletions or rearrangements in a human lymphoma cell line (Wolf and Rotter 1984) and Alan Bernstein's group found similar occurrences in erythroleukemic cell lines from mice infected with a leukemia virus (Wolf and Rotter 1984; Mowat et al. 1985; Wolf and Rotter 1985). These data were not enough to slow the field's plowing forward with the oncogene hypothesis, but the mounting suspicions were finally confirmed when Arnold Levine's group began using a TP53 genomic clone derived from embryonic carcinoma cells that failed to co-operate with Ha-Ras to transform cells (Finlay et al. 1988). When this sequence was compared to that of the clones derived from SV40 transformed cell lines and further comparisons done with genomic sequences, it was determined that previous clones which exhibited oncogenic activity actually carried activating mutations (Hinds et al. 1989). It took a few more years of research to rediscover

TP53 as a tumor suppressor, but by 1989 - a decade after its discovery - conclusive evidence put forth by the labs of Bert Vogelstein, Arnold Levine and Moshe Oren settled the matter (Nordling 1953; Baker et al. 1989; Eliyahu et al. 1989). And thus the p53 field blossomed, with study of mutant p53 preceding that of its wild-type counterpart.

p53 mutations in human cancer: what do they tell us?

Foundational work put forth in the 1950s and 60s by Charles Nordling and other groups first advanced the theory that the onset of cancer fits a model in which multiple mutations need be acquired in order for its genesis (Nordling 1953). In 1971, Alfred Knudson convincingly derived the “two-hit” hypothesis to explain the incidence of retinoblastoma in children (Knudson 1971). He correctly hypothesized that a single gene was responsible and that each of its alleles needed to acquire an inactivating mutation in order to give rise to retinoblastoma. This seminal work provided a foundation for the discovery of tumor suppressor genes: genes which acquire nonsense and frameshift mutations that disable one allele and then suffer subsequent loss of their second allele to genetic lesions, typically a chromosomal lesion (Harvey et al. 1993).

As is expected for a tumor suppressor, 60% of tumors harboring p53 missense mutations lose the wild-type allele (Quon and Berns 2001). However, instead of acquiring inactivating mutations like other tumor suppressors, p53 acquires missense mutations. These represent 75% of all p53 mutations (Petitjean et al. 2007) and make up around 40% of all somatic

mutational events that occur in human cancer[1]. Three fourths of these missense mutations occur in the DNA binding domain (DBD)(Figure 1-2), with most of them resulting in loss of consensus sequence binding. If these missense mutations were merely loss-of-function or dominant negative, one would expect an even distribution of mutations across the DBD, since most mutations in this domain have been experimentally shown to impair p53 binding to DNA (Kato et al. 2003). However, their distribution is far from uniform: greater than a third of missense mutations in the DBD occur in six “hot-spot” residues (Figure 1-2). Moreover, four of these hot-spot residues (R175, G245, R249 and R282) are predominantly substituted by a particular amino acid, whereas the other two residues (R248 and R273) are equally substituted by one of two amino acids. It is evident from the non-random distribution of mutations in the DBD that p53 missense mutations have a strong selective advantage that cannot explained by loss-of-function or dominant negative models. Furthermore, the fact that loss of the wild-type allele is required for the full transformation potential of these missense mutations suggests they are not predominantly dominant-negative mutations.

There are eight mutants that are coded for in the six hotspot residues which make up the majority of p53 mutants found in human cancer – R175H, G245S, R248Q, R248W, R249S, R273C, R273H, and R282W (Figure 1-2). Virtually all studies focus on these hot-spot

[1]Thierry Soussi, Christophe Béroud, J.L. Fournier, Dalil Hamroun and Jean Michel Rubio-Nevado. The 2010_R1 release of the UMD_TP53 Mutation database. http://p53/free/fr. July 2010

mutants which are collectively referred to as “mutant p53.” It is clear through crystalography studies, however, that each mutation has a unique impact on protein structure (Joerger and Fersht 2010). These can be broadly divided into two groups: contact site mutants (R248W, R273) and conformational mutants (R175, G245, R248Q R249, R282) (Figure 1-1) (Joerger and Fersht 2007). Contact site mutants specifically ablate residues that directly contact DNA without affecting the overall structure of the protein, whereas conformational mutants shift the conformation of the protein, exposing hydrophobic residues otherwise buried within. These unique structural qualities are reflected in their behavior, with more and more studies reporting unique behaviors both in culture and *in vivo (Lang et al. 2004; Olive et al. 2004; Xu et al. 2011; Hanel et al. 2013)*.

Lessons learned from mouse models

Much of mutant p53 biology has been advanced in cell culture models and although they have provided valuable insight into their oncogenic activity, they are subject to standard caveats associated with cell culture systems. Although animal models have their own disadvantages, they have painted the clearest and most convincing picture of the oncogenic activity of p53 mutants thus far. The earliest studies of mutant p53 *in vivo* were done by the Bernstein lab using transgenic mice shortly after oncogenic p53 was discovered to carry activating mutations (Lavigueur et al. 1989). These mice expressed multiple copies of murine mutant p53 (A135V) under the control of the p53 promoter, rendering them susceptible to tumor formation. These mice presented the first functional *in vivo* evidence that mutant p53 exerts oncogenic function: overexpression of mutant p53 in mice enhanced tumorigenesis. Harvey et al strengthened this observation by examining the effect of the

A135V mutant transgene p53 wild-type, heterozygous and null mice (Harvey et al. 1995). In this study, expression of the mutant transgene in a heterozygous but not a null background resulted in an earlier onset of tumorigenesis. This and similar studies done in cell culture supported a dominant-negative-driven mechanism of action, in which the oncogenicity of mutant p53 is dependent on its ability to oppose its wild-type counterpart's tumor suppressive role. However, these transgenic models were also subject to their own caveats as they relied expression of non-physiological levels of mutant p53. These caveats were circumvented by the labs of Guillermina Lozano and Tyler Jacks in 2004 with the generation of knock-in mutant p53 mouse models (Lang et al. 2004; Olive et al. 2004).

The Lang et al and Olive et al studies presented the most conclusive evidence that p53 mutants have gain-of-function activities: knock-in mice for R172H/- or 270H/- (equivalent to R175H and R273H mutations in human p53) showed an increase in tumor burden, developed novel tumors and exhibited higher incidence of invasive and metastatic tumors compared to $p53^{-/-}$ mice (Lang et al. 2004; Olive et al. 2004). These results argued that mutant p53 can confer oncogenicity *in vivo* independently of its wild-type counterpart, moving the field away from a dominant-negative-driven model to a gain-of-function model. Specifically, R172H/- and R270H/- mice succumbed to tumor burden 25% and 11% higher than that of $p53^{-/-}$ animals. A significant percentage of mutant p53 mice develop a variety of carcinomas which exhibit increased invasiveness, metastasis and other features of advanced human carcinomas that harbor p53 mutations. In contrast, $p53^{-/-}$ mice never develop carcinomas nor do their tumors metastasize, strongly supporting a gain-of-function model for R175H and R273H. Despite these gain-of-function effects, it is interesting to note

that the lifespan of these mutant mice is not affected when compared to $p53^{-/-}$ siblings. However, a recent report by Hanel et al has shown that R248Q mutant mice show shorter survival than p53 null mice (Hanel et al. 2013), demonstrating that not all p53 mutants behave the same and that hot-spot mutants can display greater severity than previously thought.

Taken together, these mouse studies demonstrate the depth of insight that can be obtained *in vivo* and underscore the importance of creating *in vivo* models of human disease. In Chapter 3 of my thesis I present and discuss the creation of a powerful *in vivo* genetic platform with the aim of uncovering and stratifying novel gain-of-function activities of p53 mutants.

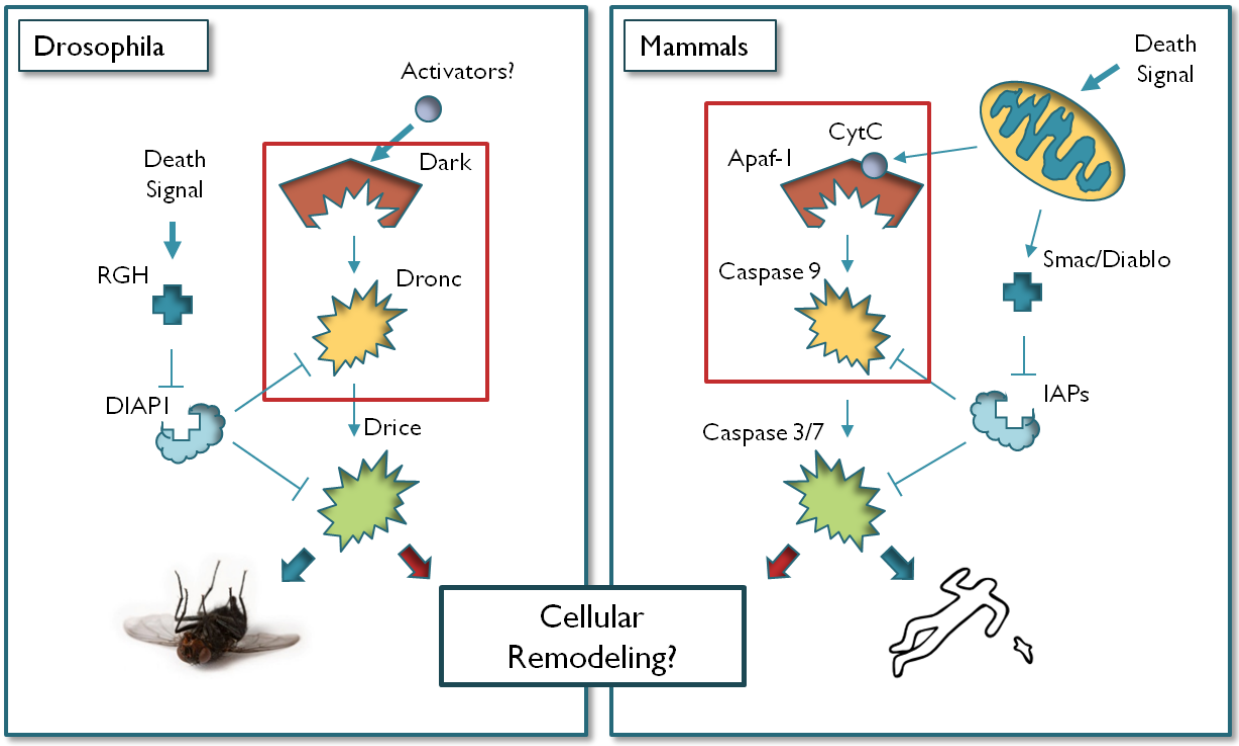

Figure 1-1. The apoptosome in flies and mammals. The apoptosome (in red box) is a well-conserved heptameric complex composed of Apaf-1 and Caspase 9 (Dark and Dronc in flies) that is assembled to launch caspase activation in the cell upon death stimuli. It is now appreciated that caspase activation does not necessarily lead to cell death but can also be used to remodel cells. The apoptosome has several regulatory axes, notably repression by IAPs (DIAP1 in the fly) and activation by cytochrome c. Evidence in mice suggests that other upstream activators exist and in flies, cytochrome c is not required for apoptosome formation. This poises *Drosophila* for discovery novel upstream regulators of the apoptosome.

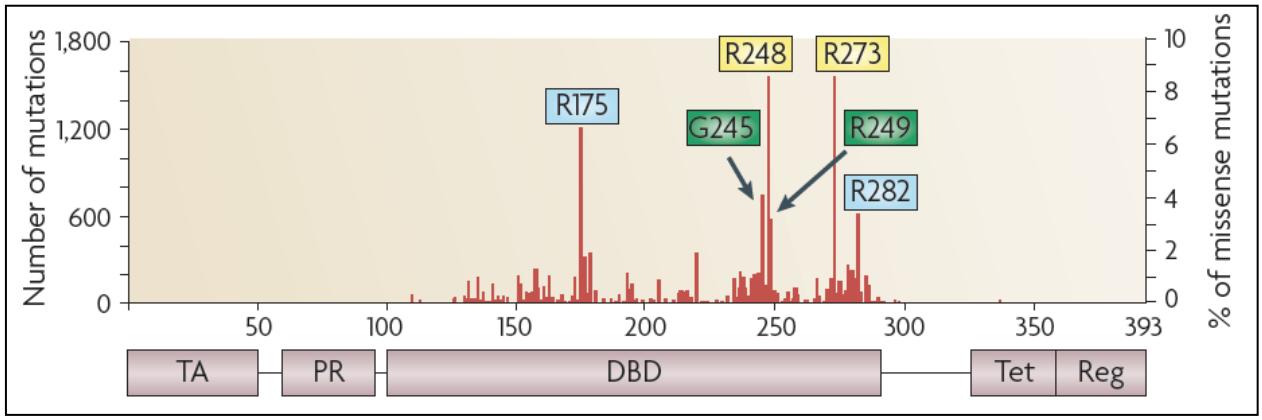

Figure 1-2. Human p53 acquires missense mutations. Missense mutations make up 75% of p53 mutations found in human cancer. Cancers strongly select for mutations in the DNA binding domain (DBD), especially mutations affecting the residues pictured here. One third of all mutations occur in these six residues, encoding oncogenic gain-of-function mutants. Mutations in yellow boxes disrupt residues that contact DNA, those in green and blue boxes disrupt protein conformation either globally (blue) or locally (green). Reproduced with permission from (Brosh and Rotter 2009).

CHAPTER TWO:

IN VIVO FUNCTIONS OF TANGO7 IN DEATH AND REMODELING

Introduction

Tango7 was previously described by our group as an effector of cell death (Chew et al. 2009). Chew et al showed that knocking down *Tango7* in cultured cells protected them from stimulus-dependent apoptosis by various stimuli and that *Tango7* knockdown in the developing eye blocked programmed cell death (PCD) of cells normally fated to die. Mechanistically, knockdown of *Tango7* in cultured cells was shown to prevent caspase activation and lead to a decrease in Dronc protein levels. The dissertation work presented in this chapter follows up on this study and is aimed at disrupting the gene in the fly in order to study how *Tango7* regulates cell death *in vivo*. To our surprise, instead of cell death phenotypes I and others discovered that *Tango7* collaborates with the apoptosome to drive non-apoptotic caspase-activation.

Tango7, Transport and Golgi Organization 7, was initially identified, as the name implies, in a siRNA screen for genes involved in vesicular transport and Golgi organization (Bard et al. 2006). Since then, *Tango7* has appeared in a host of in vitro, cellular and even *in vivo* screens examining neuronal dendrite formation (Sepp et al. 2008), huntingtin aggregation (Doumanis et al. 2009), the mTOR pathway (Lindquist et al. 2011), cell size and cell-cycle progression (Boutros et al. 2004; Bjorklund et al. 2006; Bonke et al. 2013), microtubule interacting proteins (Hughes et al. 2008), the mitotic centrosome (Muller et al. 2010), transcriptional response to hypoxia (Dekanty et al. 2010) and lipid storage (Guo et al. 2008) to name a few.

What *do* we know about *Tango7* function? Functional studies done in yeast, *C.elegans* and more recently, in mice, suggest that *Tango7* is a translation initiation factor subunit. In *S.pombe*, the *Tango7* ortholog, *csn7*, was shown to associate with the eukaryotic initiation factor 3 (eIF3) complex and regulate translation levels (Zhou et al. 2005). Similarly, the *C.elegans* ortholog, *CIF-1*, was described as a shared subunit of the COP9/signalosome (CSN) and the eIF3 complex (Luke-Glaser et al. 2007). *Tango7* is most similar to eIF3 subunit m (eIF3m) in mammals, which has recently been knocked out in mice and shown to affects protein translation in the liver and for stability of the eIF3 complex (Zeng et al. 2013). Sequence identity *Tango7* is an eIF3m ortholog, but this has not been tested in *Drosophila*.

To determine the in vivo functions of Tango7, I disrupted the gene with point mutations in *Drosophila*. I show here that Tango7 is an essential gene required for non-apoptotic caspase activity and collaborates with the apoptosome to drive cellular remodeling processes.

Materials and Methods

Fly strains and husbandry

Canton S flies were used as wild-type controls. All lines were obtained from the Bloomington Stock Center except for Hsp83-Gal4 (gift from Hermann Steller). To obtain *tango7*$^{L/L}$ flies, al^{1}, FRT42D, *Tango7*^{L}, sp^{1} flies were crossed in bottles to flies from the parental *Tango7*^{L} stock and reared at room temperature. *Tango7*^{VK006}; *tango7*$^{L/L}$ and *Tango7*$^{VK006;}$ *tango7*$^{E/E}$ stocks were kept at room temperature.

Ends-out homologous recombination

A donor line was generated by integration of the donor construct (Figure 2-1) into the 3rd chromosome PBac{y+-attP-9A}VK00019 line (Bloomington #9737). Rainbow Transgenic Flies (Camarillo, CA) performed the injection and screening for recombinants. The cross scheme used for targeted recombination is illustrated in Figure 2-1. Over 50,000 F3 progeny were screened and 90 candidate recombinants were recovered over the course of two different knockout attempts.

FLY-TILL point mutant screen

Tango7^{L} and *Tango7*^{E} alleles were recovered by the Seattle *Drosophila* TILLING Project (Till et al. 2003; Cooper et al. 2008a; Cooper et al. 2008b), which screened for point mutations in the 2nd chromosome *Canton S*-derived Hawley lines. Screening consists of amplifying small fragments of your gene of interest from the mutagenized lines and incubating them with corresponding amplified fragments from the parental non-mutagenized lines and allowing the two to form heteroduplexes. By using a single-strand specific endonuclease, amplicons

containing single nucleotide mismatches are identified and traced back to the original mutagenized stocks from which they were derived.

Recombination-mediated chromosome cleanup of Tango7^{L} and Tango7^{E} chromosomes

Mutagenized lines were crossed to multiply marked 2nd chromosomes carrying either al^{1}, dp^{1}, bl^{1}, pr^{1}, c^{1}, px^{1}, sp^{1} markers (Bloomington #156) or al^{1}, dp^{1}, bl^{1}, pr^{1}, c^{1}, cn^{1}, px^{1}, sp^{1} (Bloomington #4187). F1 females trans-heterozygous for the mutagenized chromosome and the multiply marked chromosome were crossed to CyO/Sp males and F2 balanced males were crossed back to the multiply marked chromosome line. Males that produced F3 progeny with markers for either al^{1}, dp^{1}, bl^{1}, pr^{1} (2L) or px^{1}, sp^{1} (2R) but not c^{1} (7cM from *Tango7*) were used to make stocks. These were then crossed to FRT42D, cn^{1}, px^{1}, sp^{1} chromosomes (Bloomington #8210) to generate al^{1}, FRT42D, *Tango7^{L}*, sp^{1} (Tango7^{L} in the text) and FRT42D, *Tango7^{E}* (*Tango7^{E}* in the text). These alleles were used for most of the studies presented in this dissertation.

Tango7^{VK006} rescue

The *Tango7^{VK006}* line was generated by inserting the rescue construct described below onto an attP site on the X chromosome of the PBac{y+-attP-9A}VK00006 line (Bloomington #9726). Rainbow Transgenic Flies (Camarillo, CA) performed the injection and screening for recombinants. *Tango7^{VK006}*; *tango7$^{L/L}$* and *Tango7$^{VK006;}$ tango7$^{E/E}$* stocks are kept at room temperature as they become progressively infertile at 18^{o}C.

Immunofluorescence

Whole testes were dissected in PBS, fixed in PT (1X PBS, 0.1%Triton) with 4% Formaldehyde and heptane at a 1:3 volume/volume ratio for 20 minutes. Fixed samples were then washed with PT 4x7 minutes, blocked with PTA (1X PBS, 0.1% Triton, 1.5%BSA) for 1 hr, and incubated overnight at 4ºC with primary antibody diluted in PTA. On the second day, the samples were rinsed 3 times with PT, washed with PTA 4x7 minutes, incubated with appropriate secondary antibody for 2 hrs at room temperature, rinsed again with PT 3 times and washed with PT overnight at 4ºC. On the third day, the samples were rinsed with PBS once and mounted with VECTASHIELD + DAPI (Vector Labs).

The following antibodies and dilutions were used: rabbit anti-Cleaved-Caspase-3 (Cell Signaling) at 1:500; mouse anti-AXO49 (Bressac et al. 1995) at 1:20; Rhodamine-phalloidin (Invitrogen Molecular Probes) at 1:40; mouse anti-Tango7 (1N13) at 1:1000; rabbit anti-GM130 at 1:500 (Abcam); rat anti-slbo (Jekely et al. 2005) at 1:100. Alexa-488 and Alexa-568 secondary antibodies (Invitrogen Molecular Probes) were used at 1:250. A custom monoclonal antibody (1N13) against Tango7 was raised at Abmart Antibody Company (Shanghai, China) against epitope ELLGTYTADN.

Immunofluorescence on S2R+ cells

2mm circular coverslips were coated with 1mg/ml concanavalin A (Sigma-Aldrich, St. Louis, Missuori), allowed to dry at room temperature and then placed in a 6-well dish (5 coverslips/well) right before plating cells. S2R+ cells were split and plated (according to Cell Culture methods below) and after two days, media was aspirated, wells rinsed twice with PBS then incubated in 200ul of 1XPBS with 4% Formaldehyde for 20 minutes. Coverslips were then rinsed once with PBS, incubated in 200ul of 1XPBS with 0.5% Triton X-100 for 10

minutes and washed with PBS 3x5 minutes. 20ul drops of antibody diluted in PTA (1XPBS, 0.1% Triton, 1.5% BSA) were pipetted onto Parafilm and coverslips were incubated for one hour at room temperature cell-face down on each drop. Coverslips were then placed cell-side up into a 24-well plate, washed with PBS 3x5 minutes and then incubated in 100ul of appropriate secondary antibody diluted in PTA for 30 minutes. Coverslips were then rinsed with PBS 3x5 minutes and mounted onto slides with 20ul of VECTASHIELD + DAPI (Vector Labs).

The following antibodies and dilutions were used: rabbit anti-Dark (from Lai) at 1:100; rabbit anti-GM130 (Abcam) at 1:100; rabbit anti-Syntaxin 16 (Abcam) at 1:100; mouse anti-Tango7 (1N13) at 1:1000.

Acridine Orange staining in embryos and wing discs

Embryos were collected for 2.5 hrs, aged for 2.5 hrs, exposed to 40 gray of ionizing radiation in a Cs-137 Mark 1-68A irradiator (J.L. Shepherd & Associates) and then allowed to recover for 1.5 hrs. Embryos were then dechorionated with 50% bleach for 2-3 minutes, rinsed with water and placed into a 5ml glass vial with 2ml of Heptane and 2ml of 5ug/ml Acridine Orange in 1M Phosphate Buffer. Samples were shaken by vortex for 5 minutes and then the embryos were isolated and mounted onto glass slides with halocarbon oil 700 (Sigma). Wing discs were dissected from wandering 3rd instar larvae in PBS on a watchglass, incubated for 5 minutes in 5ug/ml Acridine Orange in 1M Phosphate Buffer, rinsed in PBS and mounted in PBS using two coverslips as “stands” so as to not squash the wing disc with the mounting coverslip.

Clonal analysis

All clones used FRT42D, *Tango7*^{L} or *Tango7*^{E} chromosomes in trans to FRT42D, GFP or FRT42D, RFP chromosomes except for eye clones in Figure 2-22 which used a FRT42D chromosome carrying a recessive lethal cl mutation (Newsome et al. 2000) (See appendix A for stocks). Eye disc clones were induced with ey-FLP and wing disc clones with MS1096-Gal4, UAS-FLP. hs-FLP clones were induced by heatshocking bottles at 37^{o}C for 2 hrs on days 3 and 4 after egg laying.

Dominant Female Sterile clones

Maternal and zygotic mutant embryos were generated using the ovoD system. For this, FRT42D, Tango7^{L}/CyO or FRT42D, Tango7^{E}/CyO females were crossed to hs-FLP;FRT42D, ovoD/CyO males in bottles. These bottles were heatshocked at 37^{o}C for 2 hrs on days 2, 3 and 4 after egg laying. Female progeny transheterozygous for both FRT42D chromosomes were crossed to Tango7E/CyO, twist-GFP males and their embryos examined for PCD phenotypes.

dHb9^{+} *and Kr*$^{+}$ *cell counts*

Staged 13-16hr embryos were collected, dechorionated in 50% bleach and fixed in a 1:1 volume ratio of heptanes and PBS with 4% formaldehyde. Embryos were rehydrated with increasing volume:volume ratios of PT (1XPBS, 0.1% Triton X-100):Methanol, blocked for one hour in PTAN (1XPBS with 0.1% Triton X-100, 0.1% BSA, 5% normal goat serum) and stained overnight at 4^{o}C with primary antibody diluted in PTAN. The next day, embryos washed with PTA and stained for 2 hrs with corresponding secondary antibodies diluted in

PTAN, then washed again. Stained embryos were mounted using 30μl of VECTASHIELD + DAPI (Vector Labs). Confocal micrographs of the ventral side (for dHb9) or lateral side (for Kr) were taken using 1μm Z-sections. $dHb9^{+}$ cells were found and selected in Volocity software (Perkin Elmer) and counted by eye. For dHb9 embryos, two hemisegments from T2-A9 were counted, totaling 22 hemisegments per embryo. Guinea pig anti-Kruppel (Kosman et al. 1998) was used at 1:600 and rabbit anti-dHb9 was used (Broihier and Skeath 2002) at 1:500.

Interommatidial cell counts

Pupal retinas from 46-48 hr old pupae were dissected, fixed and stained with anti-discs large (Developmental Studies Hybridoma Bank) at 1:500 using the immunofluorescence protocol detailed above. IOCs were counted as described in (Chew et al. 2009). Hexagonal units connecting six 'ommatidia centers' that completely surround one ommatidium were counted. Secondary or tertiary pigment cells inside or partly inside hexagonal assemblies were counted as one cell.

Microscopes and image processing

Confocal micrographs were taken with Leica TCS SP5 and Carl Zeiss LSM780 laser confocal microscopes and either Leica software or Zeiss Zen software. Fluorescent light micrographs were taken with a Zeis Axioplan 2E microscope using Openlab software. Microcraphs of adult eyes and wings were taken with a Zeiss SteREO Discovery V.12 stereomicroscope using 0.63X or 1.5X PlanApoS lenses with an MRc5 digital camera (Axiocam) and Axiovision Release 4.6 software. All images were processed with Volocity

Demo Version 6.1.1 (Perkin Elmer) unless noted otherwise. Figures were prepared with Microsoft PowerPoint.

Caspase activity assay

Activity assays were performed as in (Yuan et al. 2011). Recombinant 6His-Dark-6His, Dronc-6His and Tango7-V5-6His were mixed on ice, incubated at 37°C for 30 min, and then incubated at 25°C overnight to form the apoptosome complex. The next day, recombinant pro-Drice$^{C/A}$-6His was added and incubated at 25°C for 6 hrs. Subsequently, the proteins were resolved by SDS-PAGE, and blotted with anti-His-HRP antibody (Invitrogen).

Immunoprecipitation

For *in vitro* IPs, recombinant 6His-Dark-6His, Dronc-6His and Tango7-V5-6His were mixed on ice, incubated at 37°C for 30 min, and then incubated at 25°C overnight to form the apoptosome complex. The proteins were diluted in buffer A (20 mM HEPES-KOH, pH7.5, 10 mM KCl, 1.5 mM MgCl2, 1 mM sodium EDTA, 1 mM sodium EGTA, 1 mM DTT), and immunoprecipitated using anti-V5 antibody (Bethyl Laboratories) and protein G Dynabeads. For IPs from cells, equal amounts of cell lysates were pre-cleared with 40 ul of protein A/G Sepharose (Santa Cruz Biotechnology Inc) for 1 h at 4°C. Lysates were then incubated overnight at 4°C with 2 ug of mouse anti-V5 (Bethyl labs), rabbit anti-Myc (Invitrogen), or rabbit anti-Flag (Sigma). The following day 40μl of protein A/G Sepharose was added to the lysates and the complexes were allowed to bind to the beads for 2 h at 4°C. Immunoprecipitates were then washed three times with 1 ml of ice-cold Triton Lysis Buffer and the bound complexes were eluted with SDS sample buffer.

Immunoblotting and antibodies

Recombinant proteins, lysates and immunoprecipitated proteins were separated by SDS-PAGE, transferred to Immobilon-P membranes (Millipore) using a semi-dry transfer apparatus (Biorad), and immunodetected with respective antibodies. Blots were further developed by incubation with corresponding secondary antibody and visualized using enhanced chemiluminescence (GE Healthcare). Mouse anti-V5-HRP (Invitrogen) was used at 1:5000, mouse anti-Myc (Invitrogen) at 1:5000, mouse anti-Flag-HRP (Sigma) at 1:5000, and mouse anti-His-HRP (Invitrogen) at 1:5000.

Cell culture and transfections

S2R+ cells were maintained in Schneider's medium (Gibco) supplemented with 10% (v/v) fetal bovine serum (Atlas Biologicals) and 100 units/ml each of penicillin and streptomycin (Gibco) and grown at 25°C. Cells were plated onto 100 mm dishes, grown to 75% confluence and *Tango7*-V5 was co-transfected with either Flag-Dronc or Dark-Myc with Effectene (Qiagen). Tango7 and Dark expression was induced by adding 250 uM CuSO4 into the Schneider's growth medium. After 48 hrs, cells were washed twice with ice-cold PBS and lysed with Triton Lysis Buffer (50 mM Tris pH 8, 150 mM NaCl, 1 mM EDTA, 10% glycerol, 1mM DTT, 1% Triton X-100, and protease inhibitor cocktail (Roche)). The lysate was clarified by centrifugation at 13000 rpm at 4°C for 15 min, and the protein concentration determined by Bradford assay.

RT-PCR

Total RNA from embryos or ovaries was isolated using TRIzol reagent (Life Technologies). 1ug of total RNA was used to make cDNA using iScript cDNA synthesis kit (BioRad). 1ul of cDNA was used for PCR with GoTaq DNA polymerase (Promega). Rp49 was used for normalization.

Tango7 rescue construct

The *Tango7*^{VK006} rescue construct was engineered by recombineering a 22,609bp fragment containing the *Tango7* locus from BAC clone CH321-18D10 into a modified Pacman construct with Gateway sites (kind gift from Michael Buszczak). The parent BAC was obtained from the P[acman] Resource (Venken et al. 2009).

Cell culture constructs

The Tango7-V5 construct was a kind gift from Vivek Maholtra. The Dark-Myc construct was a kind gift from Xiaodong Wang. The Tango7-V5-6xHis construct was made by ligating a PCR amplified Tango7-V5 fragment from the Tango7-V5 construct using primers 1 and 2 into a SacI/ pnI digested pFB vector. The Flag-Dronc construct was made by ligating a PCR amplified Dronc fragment using primers 3 and 4 into a BamHI/EcoRI digested pAFW vector (*Drosophila* Gateway Vector Collection, Carnegie Institute of Washington). For primer sequences see Appendix C.

UASp-Tango7 constructs

To make UASp-FLAG-HA-Tango7^{FL}, UASp-FLAG-HA-Tango7^{L}, UASp-FLAG-HA-Tango7$^{PCI+30aa}$, and UASp-FLAG-HA-Tango7$^{\Delta PCI}$, Tango7 cDNA was amplified using primers

with SalI and NotI restriction sites and cloned into the pPFHW vector (*Drosophila* Gateway Vector Collection, Carnegie Institute of Washington). UASp-FLAG-HA-Tango7^{FL} used primers 5 and 6; UASp-FLAG-HA-Tango7^{L} used primers 7 and 8 ; UASp-FLAG-HA-Tango7$^{PCI+30aa}$ used primers 9 and 10; UASp-FLAG-HA-Tango7$^{\Delta PCI}$ was made by first amplifying the regions 5' and 3' of the PCI domain using primers 5 and 12 for the 5' end and primers 11 and 2 for the 3' end and then splicing these two fragments together using the overlap between both fragments to perform PCR SOEing[2].

[2]http://openwetware.org/wiki/PCR_Overlap_Extension

Results

Generating Tango7 mutants: Ends-out homologous recombination

In order to characterize *Tango7* function *in vivo*, I targeted the gene for knockout using ends out homologous recombination (Gong and Golic 2003). For this, I first created a "donor" line that carries the donor DNA that will be used to target and replace the native Tango7 ORF with a selectable marker (Figure 2-1B and see Materials and Methods). The donor DNA was mobilized and linearized using a heatschock inducible FLPase and ISce-I endonuclease. This linearized fragment targets the native ORF for replacement via homologous recombination (Figure 2-1B). I performed the targeting experiment twice and isolated a total of 90 candidates, most of which targeted the correct chromosome. None of the homozygous viable candidates showed loss of the native ORF by PCR. Three candidates were homozygous lethal and of these, only one, KK, failed to complement a deficiency that deletes the *Tango7* locus. Unfortunately, this line showed a duplication event of the locus by Southern blot analysis (Figure 2-2A) and none of the three lethal lines showed loss of the native ORF by PCR (Figure 2-2B). Stocks for these three lines are available and could be revisited for complementation analysis with known alleles (See Appendix 1). Although this was very disappointing, it was extremely fortuitous in that it forced me to look for other alternatives to generate *Tango7* alleles.

Generating Tango7 mutants: Isolating point mutations

To isolate the two point mutants used in this study, I accessed FLY-TIL^{L} (Till et al. 2003; Cooper et al. 2008a; Cooper et al. 2008b) and screened for deleterious point mutations in the *Tango7* locus (See Materials and Methods). Ten variants were recovered (Figure 2-3A)

and placed in *trans* to Df(2R)Exel7130, a deficiency that deletes the *Tango7* locus. One variant was lethal, another was viable but male-sterile, and the remaining variants had no obvious phenotypes. I confirmed the lethal variant to be nonsense mutation Q135* and the male-sterile variant to be nonsense mutation W358* (Figure 2-3B), which I designated *Tango7*^{E} and *Tango7*^{L}, respectively. The probability of uncovering nonsense mutations using FLY-TIL^{L} is a little over 3%[3], so the fact that I recovered two nonsense mutations was pleasantly unexpected.

Of the remaining 8 alleles, 7 were missense mutations and one (V230H, ΔFLEG232-235, I244H) was a compound mutation consisting of an in frame 4 amino acid deletion flanked by 2 missense mutations. Five of the mutations (E33K, C53S, G268S, E292K and V230H, ΔFLEG232-235, I244H) affect highly conserved residues, and of these, three (G268S, E292K and V230H, ΔFLEG232-235, I244H) reside in the PCI domain (Figure 2-4). None of the alleles were lethal or male sterile *in trans* to *Tango7*^{E} or *Tango7*^{L}. All but one of the alleles (E292K) were homozygous lethal yet all were viable over Df(2R)Exel7130, indicating that the majority of these chromosomes contain lethal background mutations.

To remove background mutations from *Tango7*^{E} and *Tango7*^{L} chromosomes, I selectively replaced most of the mutagenized chromosome with a non-mutagenized chromosome (Figure 2-3C and see Materials and Methods). After two rounds of recombination with two

[3] http://tilling.fhcrc.org/fly/FAQ_Fly-TILL.html

different chromosomes, the cleaned up alleles were sequence verified and used for characterization.

Tango7 is an essential gene and its C-terminus is required for male fertility

In order to characterize the *Tango7*^{E} and *Tango7*^{L} alleles, I conducted complementation analysis, which consists of placing mutations in *trans* to one another and to genomic deletions. *Tango7*^{E} is lethal at the first instar larval stage when tested in *trans* to itself and deficiencies *Df(2R)Exel7130* and *Df(2R)50C-38*, which delete the *Tango7* locus (Table 2-1, for deficiencies, see Figure 5A). *Tango7*^{L}, however, was viable in *trans* to both deficiencies as well as *Tango7*^{E}, but these flies are male sterile and most die during eclosion or soon after (Table 2-1). Furthermore, when the cleaned up *Tango7*^{L} strain was crossed back to the parental strain, I obtained healthy but male sterile *tango7*$^{L/L}$ flies. Although not quantified, these flies consistently show a delay in eclosion and come out at a slight lower than expected Mendelian ratio. Lethality and male sterility of the alleles did not map to any genes uncovered by Df(2R)BSC401, a deficiency that overlaps with the 3' end of Df(2R)Exel7130 but does not delete the *Tango7* locus (Table 2-1 and Figure 2-5A). Because *Tango7*^{E} is lethal in combination with deficiencies but *Tango7*^{L} is viable, I concluded that *Tango7*^{E} is a null allele and that *Tango7*^{L} is a hypomorphic allele.

To confirm that *Tango7*^{L} produces a truncated protein, Po Chen blotted lysates from wild-type, heterozygous mutant or homozygous mutant tissue with a monoclonal Tango7 antibody that was raised (Figure 2-5C; for antibody, see *Material and Methods*). Samples from cultured Kc167 cells, wild-type embryos and wild-type testes all showed a prominent band at the expected ~44kD size (Figure 2-5C). The premature stop in the *Tango7*^{E} allele

eliminates the epitope recognized by anti-Tango7 but heterozygous *Tango7*$^{L/+}$ testes produced both the full length protein and the predicted shorter variant at ~40kD. Furthermore, the homozygous *tango7*$^{L/L}$ testes produced only the shorter variant as expected (Figure 2-5C). Taken together with the complementation studies, these data establish that *Tango7*^{E} is a null allele and *Tango7*^{L} is a truncated variant that lacks the C terminal 30 amino acids, which are required for male fertility.

Tango7L phenocopies apoptosome mutants

Like mutants for the apoptosome components *Dark* and *Dronc* (Rodriguez et al. 1999; Chew et al. 2004; Huh et al. 2004; Xu et al. 2005; Arama et al. 2006), all viable *Tango7* mutants were male sterile and exhibited several wing phenotypes. A wrinkled wing phenotype characteristic of cell death mutants (Abbott and Lengyel 1991; Grether et al. 1995) appears at a modest frequency in *tango7*$^{L/L}$ adults and at higher frequencies in *tango7*$^{L/E}$ and *tango7*^{L}/*Df(2R)Exel7130* flies (Figure 2-6 and Table 2-1). We also noted a low penetrance of mild blemishing and upward curved wings similar to mutants for *Dark* and *Dronc* (Chew et al. 2004; Xu et al. 2005) (Figure 2-6). These phenotypes are temperature dependent, with higher penetrance at higher temperatures. Additionally, *tango7*$^{L/L}$ and *tango7*$^{L/E}$ mutants exhibited extra scutellar bristles that have also been reported for *Dark* and *Dronc* mutants (Chew et al. 2004; Mendes et al. 2006). Strikingly, *Tango7* mutants are 100% penetrant for male sterility. Interestingly, male infertility was one of the earliest reported phenotypes of Apaf-1-/-mice (Honarpour et al. 2000), and is also characteristic of strong mutations for Dark and Dronc (Arama et al. 2006).

Zygotic Tango7 mutants do not exhibit gross cell death defects

Although viable *tango7* mutants exhibit wing and bristle phenotypes characteristic of apoptotic mutants (Abbott and Lengyel 1991; Chew et al. 2004; Xu et al. 2005), I did not observe global cell death defects in zygotic null embryos as examined by acridine orange staining (Abrams et al. 1993) (Figure 2-7B). It is possible that, like *dark* and *dronc* embryos, zygotic expression of *Tango7* might be dispensable for embryonic PCD because of maternally loaded transcript (Chew et al. 2004; Akdemir et al. 2006). In support of this, I detected abundant *Tango7* transcript in *Df(2R)Exel7130* homozygous embryos which genetically lack the *Tango7* locus (Fig. 2-8A and B). Additionally, both wild-type and mutant transcripts were detected in *tango7*$^{L/L}$ embryos by sequencing (Figure 2-8C) but only wild-type transcript was detected in *tango7*$^{E/E}$ embryos, suggesting that *Tango7*^{E} mutant transcript is degraded by nonsense mediated decay (Figure 2-8D). In conclusion, zygotic sources of *Tango7*, like other apoptosome mutants (Chew et al. 2004; Akdemir et al. 2006), are not rate limiting for most cell deaths in the embryo. More detailed examination of cell death phenotypes are described later in this chapter.

Tango7 mutants are defective for caspase activity and apoptosome-dependent cellular remodeling

To determine whether the sterility of *tango7* males, like apoptosome mutants (Rodriguez et al. 1999; Huh et al. 2004; Arama et al. 2006), might be caused by defective caspase activation prior to spermatid individualization, I stained wild-type, *tango7*$^{L/L}$ and *tango7*$^{L/E}$ testes with cleaved-Caspase-3 antibody (anti-CC3), a marker of Dronc substrate cleavage (Fan and Bergmann 2010). Strikingly, *tango7* mutant testes completely failed to stain for

anti-CC3, indicating that Dronc fails to cleave its substrates in *tango7* mutant cysts (Figure 2-9A). Furthermore, wild-type and *tango7* mutant spermatids were similarly positive for AXO49 (Figure 2-9B), a marker for advanced spermatogenesis (Bressac et al. 1995). Therefore, the absence of anti-CC3 staining in *tango7* mutants reflects an authentic and specific failure in caspase activation rather than developmental arrest. Hence, *Tango7* is required for Dronc activity in this remodeling context.

To examine whether failure in caspase activation was coupled to spermatid individualization defects, I stained wild-type and *Tango7* mutant testes with phalloidin, which binds to the actin of the investment cones that make up the individualization complex (IC). In wild-type testes, ICs form at the nuclei of spermatids and then migrate synchronously through the syncytia toward the opposite end of the cyst, expelling cytoplasmic content and wrapping each sperm in plasma membrane (Fig. 2-10C). However, like animals compromised for *Dronc* and *Dark* (Huh et al. 2004), *Tango7* mutant ICs do form properly but either stall at the nuclei or move asynchronously through the syncytia (Figure 2-9C and see also Figure 2-13C).

Since *Tango7* was originally described in a siRNA screen for genes involved in Golgi organization (Bard et al. 2006), it is possible that defects in the Golgi could account for the caspase activation and individualization phenotypes. To examine this possibility, I stained *tango7*$^{L/L}$ testes with anti-GM130, a marker for the cis-Golgi, but found no difference in cis-Golgi structure or organization in these mutants when compared to *Tango7*$^{L/+}$ heterozygotes (Figure 2-11).

To definitively assign these phenotypes to *Tango7*, we generated a rescue strain by site-specific integration of a 20kb BAC spanning the *Tango7* locus into the fly genome, which we named *Tango7*^{VK006}. One copy of this genomic fragment expresses full length Tango7 in the testes at levels comparable to wild-type (Fig. 2-5C) and can effectively rescue sterility (Table 2-1) as well as caspase activation and individualization defects in *tango7*$^{L/L}$ and *tango7*$^{E/E}$ males (Fig. 2-10B and C). Additionally, *Tango7*^{VK006} reversed the lethality of the *Tango7*^{E} allele, the semi-viability of *tango7*$^{L/E}$ adults and all of the observed wing phenotypes (Table 2-1).

Taken together, these genetic data demonstrate that, like the apoptosome components *Dronc* and *Dark*, *Tango7* is similarly required for nonapoptotic caspase activation and individualization in the *Drosophila* testes.

Tango7 localizes to the active apoptosome compartment via its C-terminus in individualizing spermatids

In spermatids that are being remodeled, the active apoptosome localizes to the individualization complex (IC) at the nuclei and at the cystic bulge, as indicated by active Dronc staining (Huh et al. 2004). To determine whether Tango7 also localizes to this structure, I stained wild-type testes with anti-Tango7. Indeed, Tango7 conspicuously localized to the cystic bulge and the waste bag (Figure 2-12A-C" and Figure 2-13B, white and yellow boxes). Furthermore, this protein notably colocalized with anti-CC3 at these structures but not at other regions (Fig. 2-12A-C"), suggesting that Tango7 plays a role in caspase activation specifically at the IC. We further observed that Tango7 discretely localized to the leading edge of wild-type investment cones in the cystic bulge (Figure 2-

13B, yellow arrow). In contrast, the truncated Tango7^{L} protein (which lacks C-terminal 30aa) was notably absent from the leading edge of asynchronously moving investment cones in *tango7*$^{L/L}$ spermatids (Figure 2-13C, yellow arrow). These findings suggest that the extreme C-terminus of Tango7 is required for its localization to the IC, and thus, its function in cellular remodeling.

Tango7 interacts with components of the apoptosome and stimulates apoptosome activity

Our *in vivo* observations suggest that Tango7 interacts with the apoptosome to regulate nonapoptotic caspase function. To test whether Tango7 might directly affect apoptosome activity, Po Chen reconstituted the apoptosome *in vitro* using recombinant Dronc and Dark in the presence or absence of recombinant Tango7 and assayed for caspase activity using catalytically dead pro-Drice$^{C/A}$ as a substrate. As seen in Figure 2-14A, the presence of Tango7 stimulated cleavage of pro-Drice$^{C/A}$ by the apoptosome in a dose dependent manner. This enhancing effect was heat sensitive (Figure 2-14B, lane 3) and was not seen when a catalytically dead active site Dronc mutant (Meier et al. 2000) was used (Figure 2-14B, lane 4). Furthermore, consistent with previous studies on the fly apoptosome (Yuan et al. 2011), cytochrome c was not similarly active in these assays (data not shown). To probe whether Tango7 interacts with the apoptosome directly, we tested for interactions between recombinant proteins *in vitro*. Tango7 did not interact with an irrelevant His-tagged protein (data not shown) but did bind to Dronc or Dark individually or together (Fig. 2-14C). Combined, these results show that Tango7 can directly stimulate apoptosome activity *in vitro*.

To test whether similar physical interactions occurred *in vivo*, Mahesh Vaishnav performed co-immunoprecipitation experiments in cultured $S2R^{+}$ cells co-transfected with Tango7-V5 and either Flag-Dronc or Dark-Myc constructs. In these experiments, Tango7 interacted with Dronc (Fig. 2-14D) and with Dark (Fig. 2-14E). Likewise, in reciprocal immunoprecipitation experiments, these same interactions were detected (data not shown). In these assays, we also observed that Dronc and Dark interacted with a modified form of Tango7 (Fig. 2-14D and data not shown). Additionally, I tested for colocalization of Tango7 and Dark in S2R+ cells by immunofluorescence (IF). For the most part, these cells had diffuse and rather low levels of anti-Tango7 and anti-Dark staining. However, Tango7 and Dark colocalized at discrete foci in cells that exhibited Dark punctae and higher levels of Tango7 (Figure 2-15A-C). Furthermore, I looked for localization of Tango7 to the Golgi in these cells but found no colocalization to cis- or trans-Golgi markers, GM130 or Syntaxin 16, respectively (Figure 2-16A and B).

Taken together, these results demonstrate that Tango7 interacts with the apoptosome components Dark and Dronc *in vitro* and *in vivo*.

Caspase activity in spermatid remodeling is not required for SREBP activity

Spermatids are unique in that they exhibit high amounts of caspase activation during remodeling but do not undergo apoptosis. Why caspases are activated during cellular remodeling and what substrates they are cleaving are important questions that arise from this dissertation work. One hypothesis is that the apoptosome is cleaving a different set of substrates that are uniquely required for cellular remodeling.

SREBP has long been known as a caspase substrate (Wang et al. 1996). Besides the S1P and S2P cleavage sites that are normally used to process SREBP, it has a highly conserved caspase cleavage site that is cleaved by Drice during larval development. However, the role of SREBP cleavage during apoptosis remains a mystery (Amarneh et al. 2009). In spermatid individualization, 64 syncytial spermatids are separated and wrapped in their own plasma membrane. Since SREBP is a potent lipid synthesis regulator, we hypothesized that it might be cleaved during individualization to coordinate massive *de novo* lipid synthesis in order to generate enough plasma membrane for individualization.

To determine whether SREBP is cleaved in spermatid remodeling, I used an *in vivo* transgenic SREBP reporter (Kunte et al. 2006) as a read out for SREBP cleavage. This reporter consists of a Gal4 domain which replaces the original helix-loop-helix transactivation domain. Upon cleavage, the Gal4 domain is released and imported into the nucleus where it binds and activates a UAS-GFP transgene (Figure 2-17E). Indeed, the SREBP reporter was active in remodeling spermatids (Figure 2-17A). The reporter was mostly expressed at the base of the testes (Figure 2-17C) but was also seen along elongated spermatids (Figure 2-17D). To test whether SREBP cleavage in spermatids required caspase activity, I examined SREBP reporter activation in *tango7*$^{L/L}$ testes. No significant difference was observed in *tango7*$^{L/L}$ testes compared to *Tango7*$^{L/+}$ heterozygotes (Figure 2-17B, C' and D'). In addition, *tango7*$^{L/L}$ testes were stained with anti-SREBP, an antibody that recognizes the transcriptional activation domain of SREBP (Seegmiller et al. 2002) to test whether this SREBP domain was being translocated into the nuclei of individualizing spermatids. Although no difference was seen in elongated, individualizing

spermatids (data not shown), *tango7*$^{L/L}$ testes exhibited accumulation of anti-SREBP staining in the primary spermatocyte region (compare Figure 2-17H' to 2-17G'). Primary spermatocytes do not normally activate caspases (data not shown), so this accumulation of SREBP cannot be due to caspase activation defects in *Tango7* mutants. Taken together, these results suggest that although SREBP is cleaved in the testes, this cleavage does not require caspase activation.

Tango7 mutants have phenotypes in other remodeling contexts

To determine whether *Tango7* is required for non-apoptotic caspase activity in other cellular remodeling contexts, I examined border cell migration (BCM). BCM is a migratory event during oogenesis in which stationary epithelial cells in the developing egg detach from the epithelium and migrate to the opposite end. This process has become a productive model for understanding the cellular and molecular mechanisms that govern invasive and migratory behavior of tumor cells (Montell 2003). Regulation of caspase activation levels is important for proper BCM since deregulation of the apical caspase Dronc either by loss of DIAP1 (increased caspase levels) or Dark (decreased caspase levels) lead to defects in BCM (Geisbrecht and Montell 2004). To determine whether *Tango7* mutants exhibit defects in caspase-dependent BCM, I stained mutant ovaries with anti-slbo to label migrating border cells. BCM was impaired in roughly 45% of *tango7*$^{L/L}$ stage 9.5 and 10 egg chambers (Figure 2-18B-B") compared to less than 5% defects in *Tango7*$^{L/+}$ heterozygotes (Figure 2-18A-A"). Additionally, an "accelerated" BCM phenotype was observed in *tango7*$^{L/L}$ stage 10 egg chambers (Figure 2-18C) which was never observed in heterozygote controls. These BCM phenotypes are consistent with the hypothesis that *Tango7* collaborates with the

apoptosome to drive cellular remodeling. However, further analysis is required to determine whether the defects seen here are in fact due to defects non-apoptotic caspase activation.

Is Tango7 involved in programmed cell death?

The previous data collectively establish *Tango7* as an effector of non-apoptotic caspase activation required for different cellular remodeling contexts. However, it was still not clear whether *Tango7* was required for programmed cell death (PCD). Although I did not observe global cell death phenotypes in the *tango7*$^{E/E}$ embryos (Figure 2-7B), this was likely masked, as is the case in apoptosome mutants, by maternal loading of wild-type transcript (Figure 2-8). To determine whether *Tango7* is involved in PCD, I conducted classic PCD and clonal analysis assays.

Mutations in Tango7 can suppress forced cell death in the developing eye

Early on in the field, it was discovered that forcing expression of IAP antagonists, known as RHG proteins (rpr, hid and grim), in the developing retina ablates the adult eye, which provided a powerful tool to look for enhancers and suppressors of apoptosis. Apoptosome mutants can fully suppress these eye-killing phenotypes, which demonstrate that RGH killing occurs via the apoptosome (Kondo et al. 2006). To determine whether *Tango7* is required in this context, I tested whether losing one copy of *Tango7* can suppress RHG-killing in the developing eye. Unlike Dark or Dronc, *Tango7*$^{L/+}$, *Tango7*$^{E/+}$, Df(2R)Exel7130/+ flies did not suppress eye killing phenotypes (Figure 2-19D). However, *tango7*$^{L/L}$ mutants suppressed the roughness and small size of GMR-grim and GMR-hid (Figure 2-25A and B), but not GMR-rpr (Figure 2-25C), showing that *Tango7* genetically interacts with apoptotic genes.

These results suggest that *Tango7* is not rate limiting for RHG-induced cell death but that it does interact with cell death machinery in sensitized contexts. This supports our finding that Tango7 physically interacts with the apoptosome and can enhance its activity. However, because these experiments rely on forced expression of apoptotic proteins, one cannot conclude that *Tango7* normally participates in cell death. As an example of this, the caspase Dredd (Caspase 8) can suppress eye-killing phenotypes (Chen et al. 1998) but is not required for developmental or stress-induced cell death (Kondo et al. 2006).

Is Tango7 required for programmed cell death in the embryo?

As mentioned before, *tango7*$^{E/E}$ embryos did not exhibit reduced levels of PCD by AO staining (Figure 2-7B). There are two possible explanations for this: 1) *Tango7* is not required for PCD or 2) *Tango7* is required for PCD but maternally provided sources of wild-type *Tango7* are sufficient to carry out PCD in mutant embryos. Since *Tango7* is a maternally loaded gene (Figure 2-6) the second hypothesis is certainly plausible. I took three approaches to circumvent the complications afforded by maternal loading of *Tango7*.

First, to determine whether *tango7*^{L} embryos had global cell death defects in the absence of maternal wild-type transcript, I crossed *tango7*^{L}/Df(2R)Exel7130 mothers to *Tango7*^{E}/CyO fathers (Figure 2-20A). The resulting embryos only had *Tango7*^{L} as a maternal source and have only one zygotic copy *Tango7*^{L} (with the other being either *Tango7*^{E} or a deletion). These embryos presented a low penetrance of developmentally aborted embryos but did not show reduced levels or altered patterns of PCD by AO staining (Figure 2-20B). Interestingly, a low penetrance of embryos exhibited a head involution defect – a phenotype characteristic of mutants for Hid (Grether et al. 1995), a pro-apoptotic gene upstream of DIAP1 (Figure 2-

20C). However, these results demonstrate that *Tango7*^{L} does not have gross PCD phenotypes in the embryo.

Second, to examine more subtle programmed cell death phenotypes in the embryo, I stained for dHb9 and Kr, which mark for specific neurons in the embryo that undergo programmed cell death (Rogulja-Ortmann et al. 2007). In *tango7*$^{L/E}$ embryos produced by *tango7*$^{L/L}$ mothers, some extra dHb9^{+} neurons were detected (Figure 2-21A,B) but I did not see persisting Kr^{+} cells (Figure 2-21C,D). Therefore, *Tango7*^{L} exhibits maternal effect PCD-associated phenotypes in some but not all contexts of the developing embryo.

Third, to determine whether *tango7*$^{E/E}$ embryos had global cell death defects, I used the ovoD dominant female sterile technique to create embryos that were both zygotically and maternally null (see methods). Surprisingly, *tango7*$^{E/E}$ germline clones never developed into embryos (data not shown), suggesting that *Tango7* is an essential gene required for cell viability. In support of this, *tango7*$^{E/E}$ clones in the developing wing fail to undergo more than 2-3 cell divisions (Figure 2-22D-D'). Thus, the null state is inaccessible in the embryo and is currently limited to clonal analysis in larval tissues.

Taken together, these data demonstrate that in the developing embryo, *Tango7*^{L} does not exhibit gross cell death phenotypes but does lead to extra cells in a subset of ventral nerve chord neurons.

Is Tango7 required for cell death in the other contexts?

To determine whether *Tango7*^{L} has PCD defects in other developmental contexts, I examined interommatidial cell (IOC) death in pupal retinas. PCD of these cells is necessary

for the proper patterning of the adult compound eye and has been shown to require Dark and Dronc (Mendes et al. 2006). Additionally, Chew et al (Chew et al. 2009) demonstrated that knockdown of *Tango7* in the retina resulted in extra IOCs (Figure 2-23B). *Tango7* mutant retinas, however, did not display extra IOCs, suggesting that *Tango7*^{L} does not cause PCD defects in this context (Figure 2-23C-E). Nevertheless, *tango7*$^{L/L}$ retinas exhibited low penetrance defects in cell specification (Figure 2-23C) and both *tango7*$^{L/E}$ and *tango7*^{L}/Df(2R)Exel7130 retinas had missing IOCs and extra ommatidia also at low penetrance (Figure 2-23D and E). Because these defects are not characteristic of cell death mutants, I conclude that other signaling pathways must be affected.

The apoptosome is also essential to launch stress-induced apoptosis (Chew et al. 2004; Daish et al. 2004; Mills et al. 2006). To determine whether *Tango7*^{L} is defective for stress-induced apoptosis, I examined radiation-induced cell death in the developing wing of *Tango7* mutants. Irradiated wing discs from *tango7*^{L}/Df(2R)Exel7130 (Figure 2-24B) larvae showed similar AO staining as *Tango7*$^{L/+}$ wing discs (Figure 2-24A), demonstrating that *Tango7*^{L} does not prevent stress-induced cell death in the wing disc.

Next, I asked whether cells in *tango7*$^{E/E}$ clones can undergo stress-induced cell death. To answer this, I stained irradiated *tango7*$^{E/E}$ mosaic wing discs with anti-CC3, a marker for executioner caspase cleavage. Although the null clones are small in size, there were multiple instances of clones that contained a CC3 positive cell (white arrows, Figure 2-23B-C'), demonstrating that *tango7* null cells can indeed undergo PCD. The possibility exists, however, that residual Tango7 from the heterozygote parent cell from which the clone arose

still lingers in *tango7*$^{E/E}$ clones. Staining for Tango7 in this mosaic tissue revealed that this might be the case (data not shown), but this needs to be definitively addressed.

Taken together, these results show that *Tango7* mutants are not defective for typical developmental or stress-induced cell death, suggesting that this gene is not required for PCD in the animal. However, the essential cellular functions of *Tango7* make it difficult to study the null state and address whether death can occur without *Tango7*. Looking for other tissues that do not show sensitivity to *Tango7* levels might provide a more definitive answer to this question. To this end, I tried using different FLP expressing lines to create *tango7*$^{E/E}$ clones in different tissues (Figure 2-26). Clones in the eye disc or wing disc were small irrespective the driver used (MS1096-FLP, Ey-FLP or hs-FLP), but clones in the ovary using hs-FLP seemed larger in size and in cell number, particularly in the follicle cells. Thus, follicle cell clones in the ovary might be a good system to test for null phenotypes.

Characterization of a Tango7 transgenic shRNA line

Recently, a collection of transgenic UAS-shRNA lines were made available by Harvard Medical School's Transgenic RNAi Project (TRiP) (Ni et al. 2008). These TRiP lines have been shown to provide more efficient knockdown both in somatic and germline tissue than its UAS-dsRNA predecessors. I acquired a TRiP line targeting *Tango7* (*Tango7*^{HMS00667}) but I decided not to pursue this reagent as it is difficult to rule out off-target effects and thus map phenotypes to the targeted gene. Nevertheless, I did examine this line for phenotypes in different developmental stages and tissues. The results are summarized in Table 2-2. Below I comment on a few interesting observations.

In embryos, *Tango7* knockdown using ubiquitous drivers resulted in lethality at the L1 larval stage, whereas knockdown with a tissue-specific driver in the embryo did not (Table 2-2). These results are consistent with the finding that *Tango7* is an essential gene, but in addition suggest that *Tango7* is not required in all tissues for proper development. Furthermore, *Tango7* knockdown with Daughterless-Gal4 did not result in reduced AO levels, suggesting that lethality of *Tango7* knockdown with this driver is not due to PCD defects (data not shown).

In larvae, *Tango7* shRNA was driven in the CNS and the developing eye and wing (Table 2-2). Surprisingly, knockdown with Eyeless- and MS1096-Gal4, which express very early in the developing eye and wing, respectively, was pupal lethal. In contrast, knockdown with GMR- and Vestigial-Gal4, which express late in the developing eye and wing, respectively, was not. Knockdown with Eyeless-Ga4 results in headless flies, which is consistent with a phenomenon called “developmental pathway interference,” in which developing tissues compromised for essential signaling pathways are aborted (Jiao et al. 2001). This phenomenon could also explain the lethality seen with MS1096-Gal4 and supports the hypothesis that *Tango7* has essential functions in the cell.

In adults, *Tango7* shRNA was driven in the the germline, the testes and the central nervous system (CNS) (Table 2-2). Knockdown in these tissues produced viable, fertile flies with the exception of germline knockdown using Nanos-Gal4 which resulted in male and female sterility. Examination of these flies revealed atrophied ovaries and testes, suggesting that *Tango7* is required for viability of germline cells. Although *Tango7* knockdown in the testes using Hsp83-Gal4 did not result in male sterility, these testes exhibited caspase activation

defects, albeit in a different manner than *Tango7* mutants (data not shown). Surprisingly, flies expressing *Tango7* shRNA in the CNS are viable, suggesting that *Tango7* is not required for the viability of neurons or that the Elav driver does not efficiently express the *Tango7* shRNA in the CNS.

In conclusion, the *Tango7* TRiP line produces phenotypes consistent with what we know from *Tango7* mutants, suggesting the *Tango7* TRiP line indeed targets *Tango7*. Additionally, the lethality seen in embryos and pupae suggest efficient and potent knockdown. However, I did not directly test for knockdown efficiency of the TRiP line, so if one wishes to pursue a specific phenotype listed in Table 2-2 it is recommended to validate that *Tango7* levels are in fact reduced in the tissue of interest.

Targeting eIF3, CSN or proteasome components in spermatids

Studies of *Tango7* orthologs in *C. elegans* (Luke-Glaser et al. 2007) and in yeast (Zhou et al. 2005) suggest the protein could also act as a non-core factor associated with the COP9 signalosome (CSN) complex and/or the eIF3 translation complex. To test whether *Tango7* functions through these complexes to promote spermatid remodeling, I used Nanos-Gal4 to drive expression of shRNA targeting eIF3 or CSN components in the male germline and looked for phenocopy of *Tango7* individualization defects. The results are summarized in Table 2-3.

As proof of principle, I targeted different genes involved in apoptosis to test whether this resulted in defective caspase activation in spermatids. Knockdown of Dronc, Dark and Drice resulted in decreased caspase activation, whereas knockdown of DIAP1 resulted in

atrophied testes (Table 2-3). Knockdown of these genes with Hsp83-Gal4, which expresses in remodeling spermatids, yielded similar results (Table 2-3). Unfortunately, knockdown of eIF3 and CSN subunits resulted in atrophied testes, suggesting these complexes are essential for proper germline development (Table 2-3).

Unfortunately, these results were inconclusive and do not help determine whether *Tango7* functions through the eIF3 or CSN complexes. Evidence arguing against this possibility is considered in the discussion.

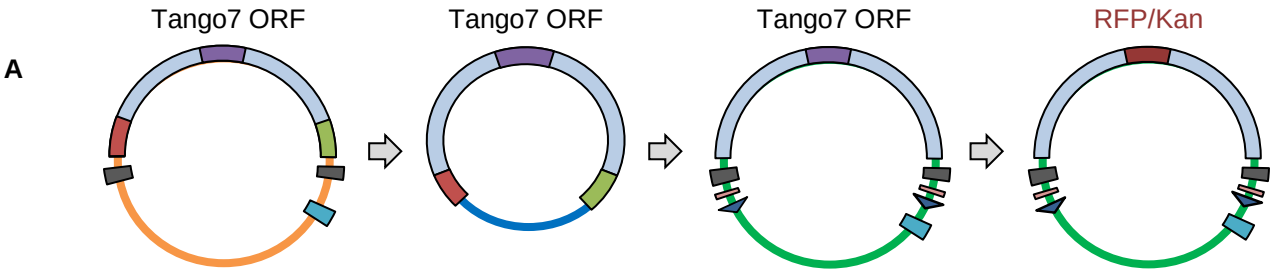

Construct	Parent	Shuttle	Wildtype Donor	Knockout Donor
Vector	P[acman]	pENTR	P[acman] GW	P[acman] GW
Method	-	*Recombineering*	*Gateway Rxn.*	*Recombineering*

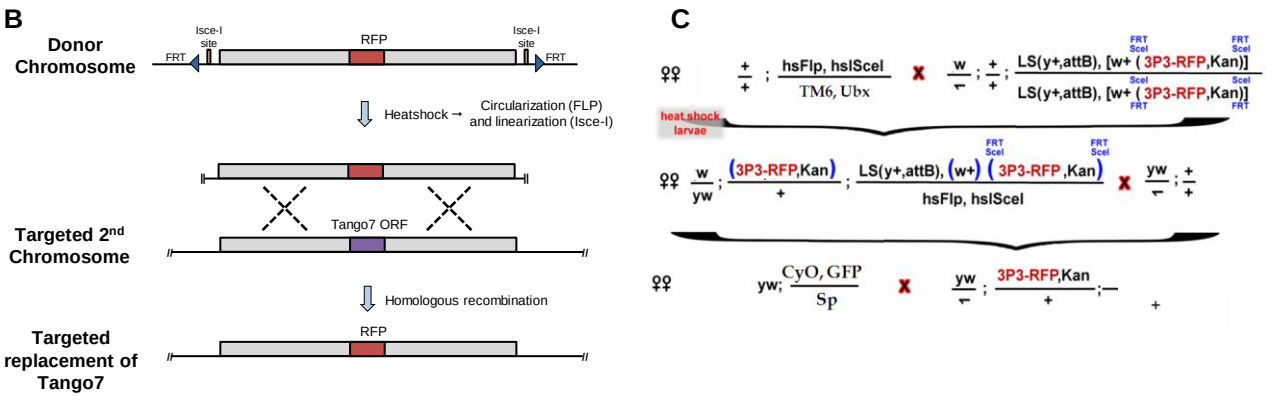

Figure 2-1. Generating *Tango7* mutants via ends-out homologous recombination. (A) Vector sequence used to clone the donor construct. (B) Targeting scheme for replacement of *Tango7* ORF with an RFP marker. (C) Crossing scheme for screening targeted recombinants. The donor construct has a y+ marker from the attP site and a w+ marker from the P[acman] chromosome. Upon hs-FLP and hs-Isce-I induction, the 3P3-RFP,Kan cassette is mobilized and unlinked from y+ and w+. Progeny that are y-,w- and RFP+ are potential targeted recombinants. (C) is adapted with permission from Dr. Robin Hiesinger.

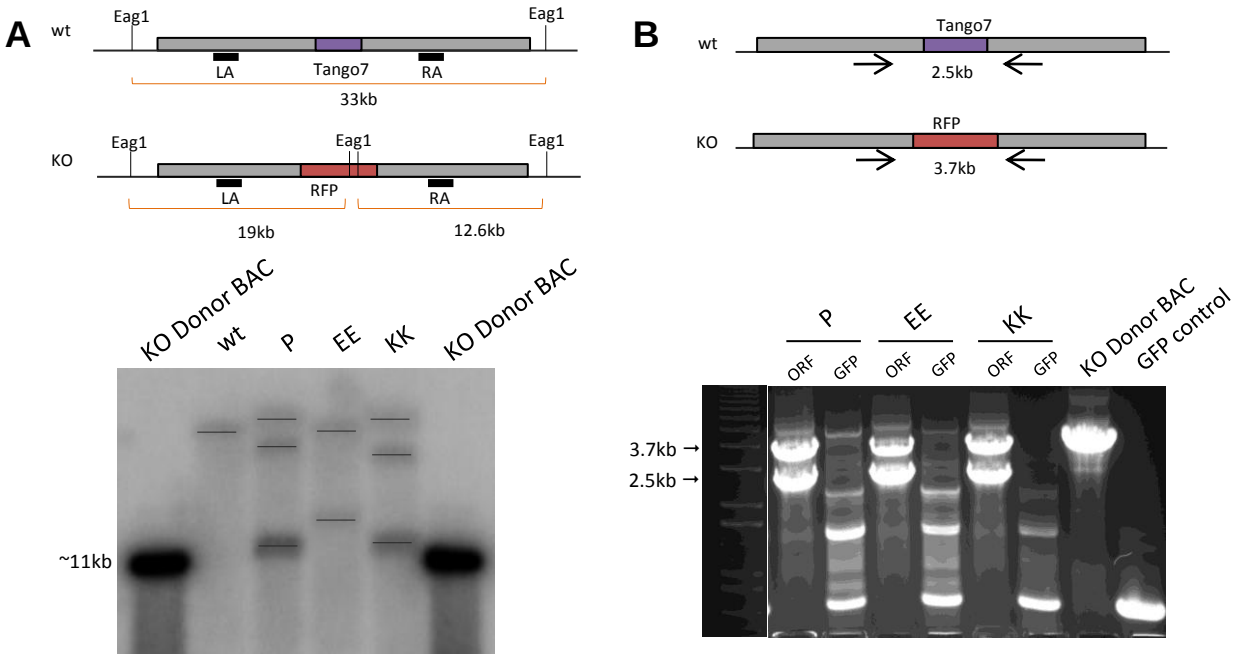

Figure 2-2. Validating candidate *Tango7* knockouts. We screened candidate targeted recombinants for homozygous lethality, which we expected. 3 of the candidates were homozygous lethal (P,EE and KK). These were validated by Southern blot (A) and PCR for the ORF in homozygote embryos (B). (A) A probe for the right arm of homology of the targeting construct (RA) was used to blot Eag1 digested genomic DNA from wild-type flies and heterozygote knock-out candidates. The knock-out donor BAC was used as a positive control. The RA probe should recognize a 33kb Eag1 fragment from the wild-type and a 12.6kb fragment from the knock-out. All three candidates had a band above 11kb but two of them (P and KK) presented two bands around the 33kb wild-type band, suggesting a duplication event. The EE candidate had bands of the correct size (~12kb and ~33kb) but still had the native ORF as determined by PCR from homozygote embryo genomic DNA (B). (B) PCR for the ORF was performed on genomic DNA from homozygote embryos sorted against a GFP marker on the 2nd chromosome balancer. The gel shows two lanes per genotype: one for the ORF and one for GFP to detect contamination of heterozygote embryos. Although this gel shows GFP contamination, clean preps still retained the native ORF (not shown). Additionally, although the EE candidate was homozygous lethal, it was viable over the deficiency, suggesting that mapped to a background lethal.

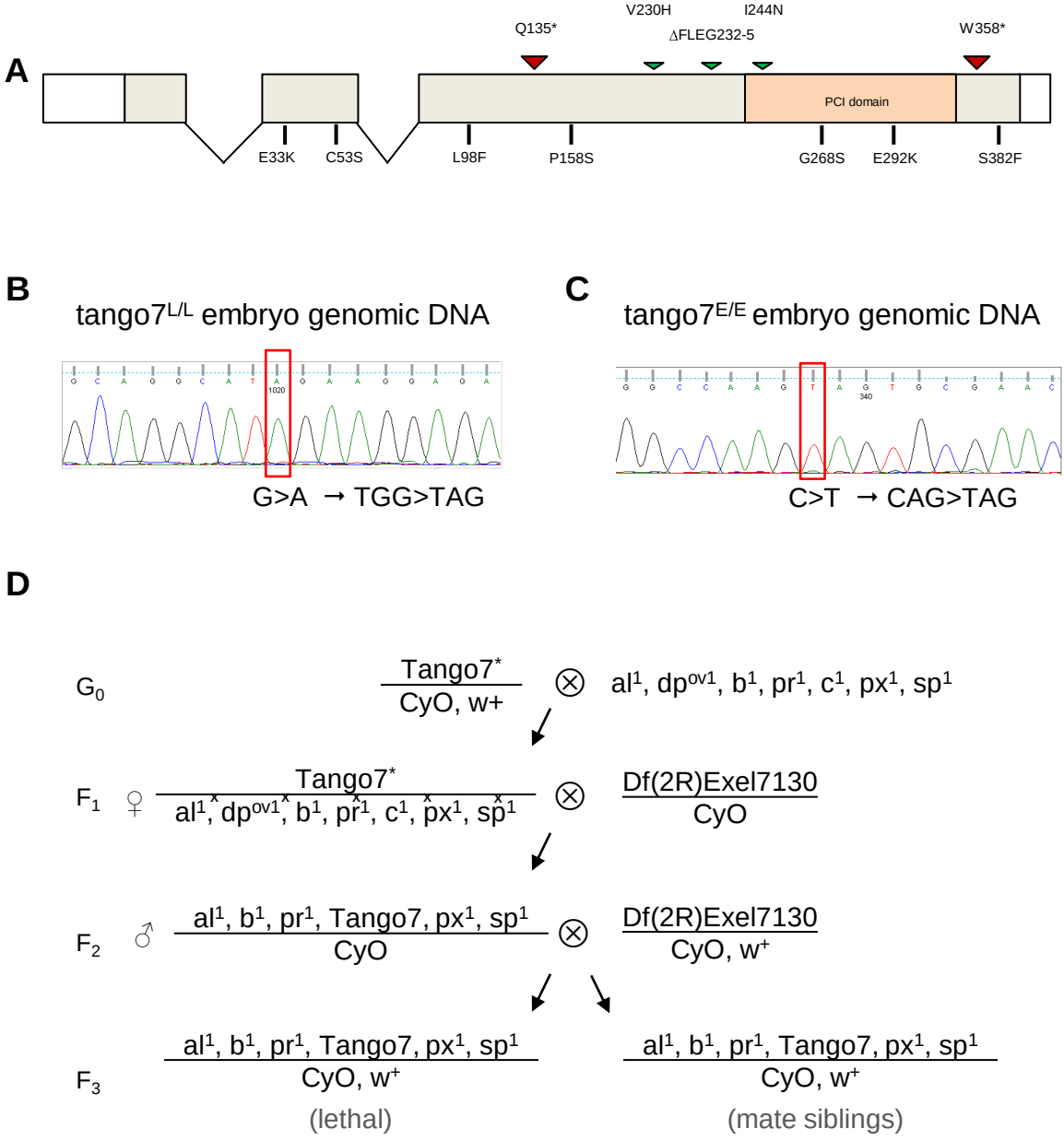

Figure 2-3. *Tango7* point mutations, validation and clean up. (A) 10 point mutations were were recovered by FLY-TILL. Two of these were nonsense mutations (red arrowheads), 7 were missense mutations and one (V230H, DFLEG232-235, I244H) was a compound mutation consisting of an in frame 4amino acid deletion flanked by 2 missense mutations. Five of the mutations (E33K, C53S, G268S, E292K and V230H, DFLEG232-235, I244H) affect highly conserved residues (see Figure 2-4), and of these, three (G268S, E292K and V230H, DFLEG232-235, I244H) reside in the PCI domain. (B) The *Tango7*^{L} and Tango7^{E} chromosomes were confirmed by Sanger sequencing to carry the predicted nonsense mutations. (D) Crossing scheme used to clean up the *Tango7*^{L} and *Tango7*^{E} mutagenized chromosomes. Both went through this crossing scheme three times (once to clean up the right arm, another to clean up the left arm and the last time to recombine onto FRT42D chromosome). FRT42D,*Tango7*^{L} and FRT42D,*Tango7*^{E} were used for most of the experiments in this thesis work.

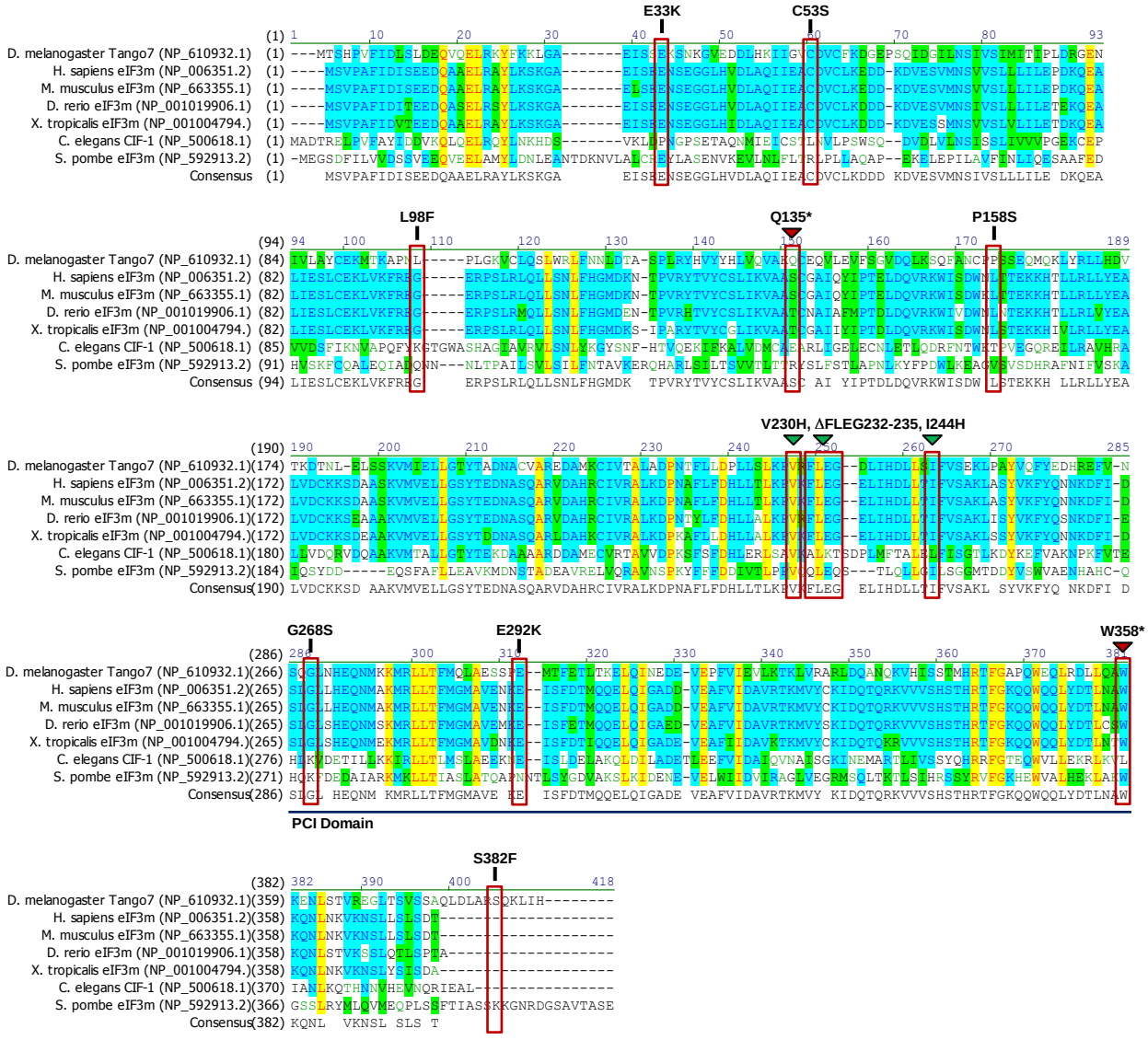

Figure 2-4. Tango7 protein sequence alignment. Tango7 protein was aligned with eIF3m orthologs in the indicated organisms, including *Homo sapiens*. The amino acid alterations of the point mutations recovered by FLY-TILL are boxed in red. Red arrowheads indicate nonsense mutants. Green arrowheads indicate one compound mutant. Vector NTI was used to make the alignment.

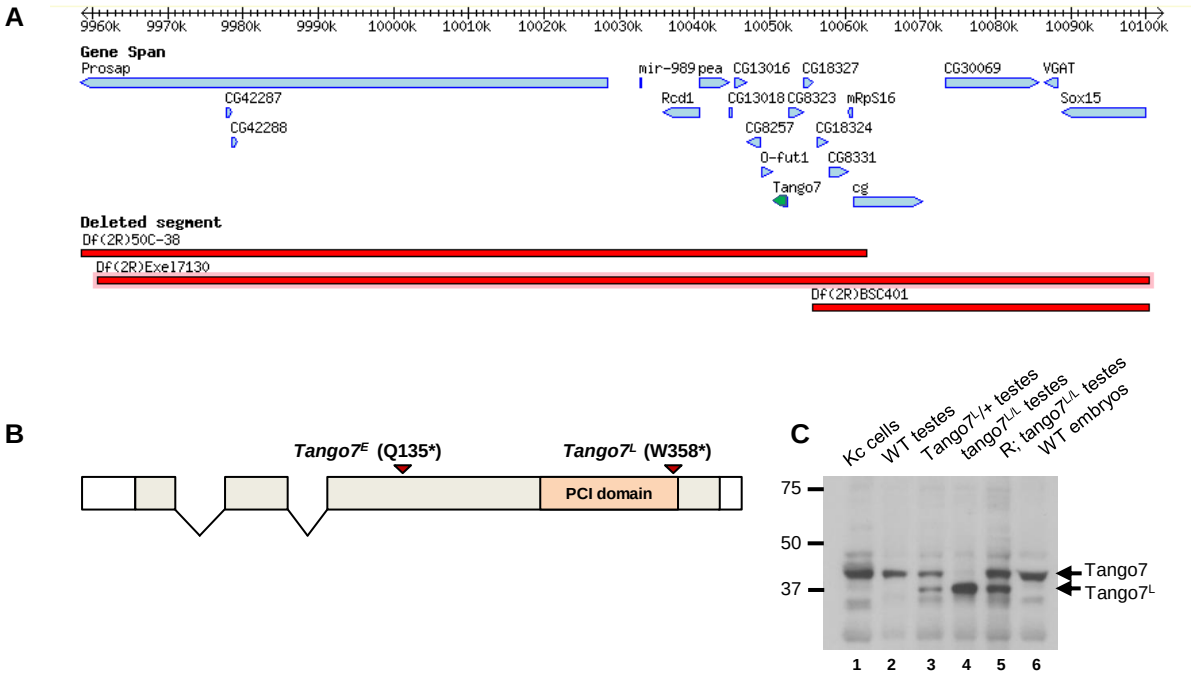

Figure 2-5. *Tango7* is an essential gene and its C-terminus is required for male fertility. (A) The *Tango7* locus region on chromosome 2. *Tango7* is highlighted in green. The three deficiencies used in this study are shown in red below the genes. (B) *Tango7* encodes a 387aa protein with a conserved PCI domain. 10 variants were recovered by FLY-TILL. Two of these carried nonsense mutations (red arrowheads above gene structure). Gray boxes are exons, white boxes are untranslated regions. *(C)* Lysates from Kc167 cultured cells, wild-type embryos and testes of various genotypes were blotted with anti-Tango7 (see Methods). Note that the mutant Tango7^{L} protein was stably expressed in both heterozygote and mutant testes in lanes 3 and 4, respectively. One copy of the *Tango7^{VK006}* rescue (R) in the mutant background effectively expresses the full length protein in the testes (lane 5).

Genotype	Viability	Male Fertility	Wrinkled wings
tango7$^{L/L}$	Viable	Sterile	15%, n= 255
tango7$^{L/E}$	Semi-viable	Sterile	33%, n=157
tango7^{L}/Df(2R)Exel7130	Semi-viable	Sterile	31%, n=232
tango7^{L}/Df(2R)Exel7130	Semi-viable	Sterile	NA
tango7^{L}/Df(2R)Exel7130	Viable	Fertile	NA
tango7$^{E/E}$	Lethal	-	-
tango7^{E}/Df(2R)Exel7130	Lethal	-	-
tango7^{E}/Df(2R)50C-38	Lethal	-	-
tango7^{E}/Df(2R)BSC401	Viable	Fertile	N A
Tango7^{VK006}; tango7$^{L/L}$	Viable	Fertile	1%, n=166
Tango7^{VK006}; tango7$^{L/E}$	Viable	Fertile	5%, n=121
Tango7^{VK006}; tango7$^{E/E}$	Viable	Fertile	3%, n=323

Table 2-1. Lethality, sterility and wing phenotypes observed in *Tango7* mutants. (*B***) *Tango7^{L}* is viable but male sterile in all allelic combinations. *Tango7^{E}* is lethal in *trans* to itself, *Df(2R)Exel7130* and semi-viable in trans to *Tango7^{L}*. Viable *Tango7* mutants also exhibited a "wrinkled" wing phenotype characteristic of *W^{1}* mutants, a dominant negative Hid allele (Abbott and Lengyel 1991). A genomic fragment rescue, *Tango7^{VK006}*, rescued viability, male sterility and the wrinkled wing phenotype of *Tango7* mutants. *Df(2R)BSC401* – a deficiency that overlaps with the 3' end of *Df(2R)Exel7130* but does not delete the *Tango7* locus (see Figure 2-5A) – did not exhibit any phenotypes over *Tango7^{L}*, *Tango7^{E}* or *Df(2R)Exel7130*.

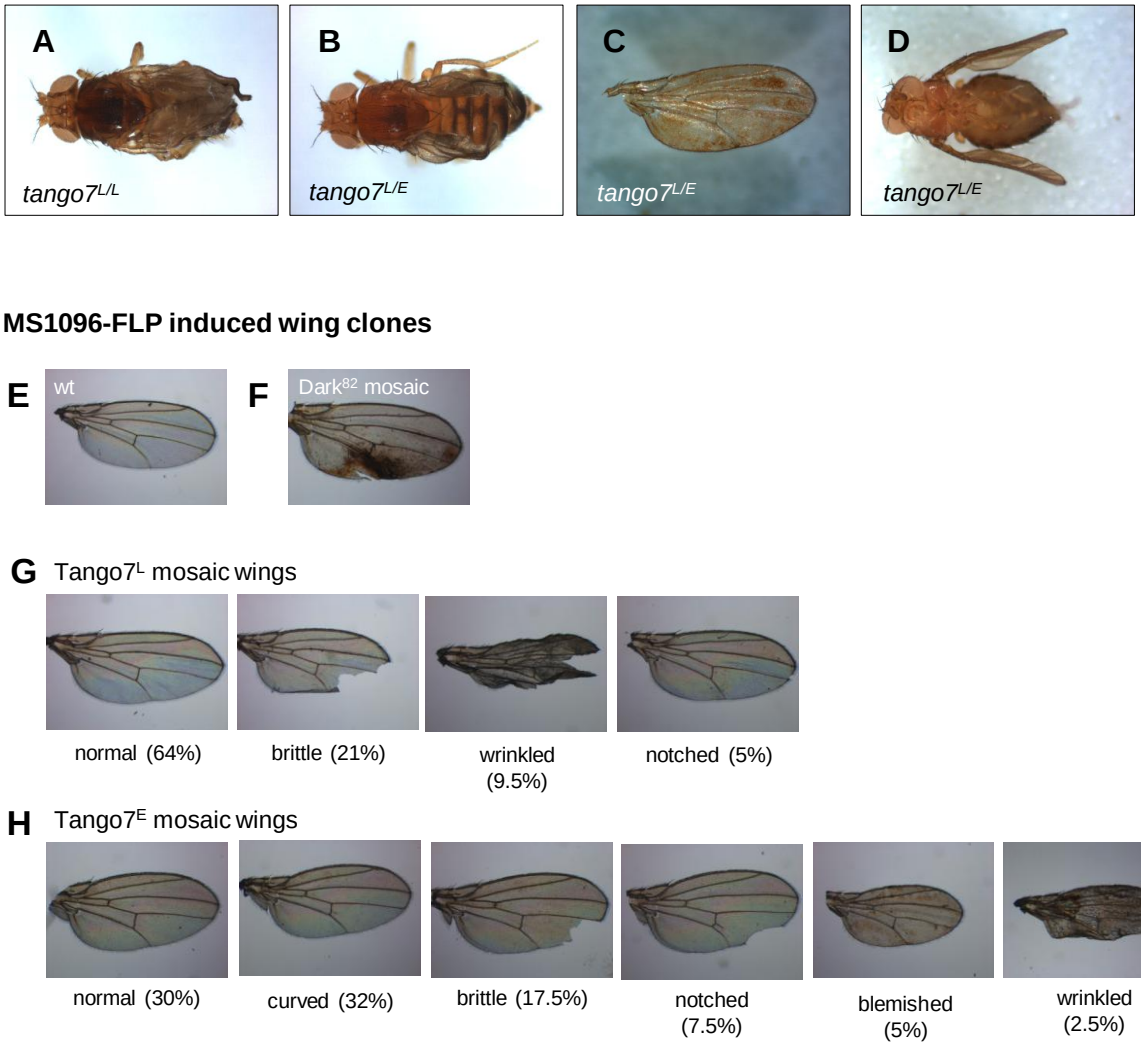

Figure 2-6. Wing phenotypes in *Tango7* mutants. Stereoscope micrographs of adult flies and wings. The wrinkled wing phenotype in *tango7*$^{L/L}$ (*A*) and *tango7*$^{L/E}$ (*B*) flies (see Table 2-1) for quantification. Tango7 mutants also presented mild blemishing (*C*) and curved wings (*D*), characteristic of apoptotic mutants. (E-H) Mosaic wings for *Dark*^{82} (F). *Tango7*^{L} (G) or *Tango7*^{E} (H). Note that *Tango7*^{E} mosaics wings (H) have a greater percentage of defects and exhibit curved wings (30%) and moderate blemishing (5%). For *Tango7*^{L} mosaics, n=73 and for *Tango7*^{E} mosaics, n=40. For mosaics, FRT42B *Dark*^{82}, FRT42D *Tango7*^{L} or FRT42D *Tango7*^{E} were placed *in trans* to a FRT42D GFP chromosome and mitotic recombination was induced using MS1096-FLP.

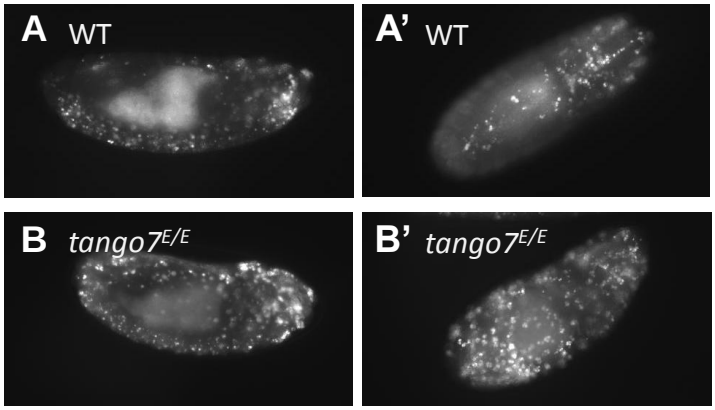

Figure 2-7. Zygotic *Tango7* mutants do not exhibit gross cell death defects. Acridine Orange (AO) staining of 13-16hr old embryos. (B) Homozygous mutant embryos from heterozygous parents (Tango7^{E}/CyO,twist-GFP) did not display cell death defects by AO staining. Compare staining to that of WT embryos (A). (A) and (B) are lateral views. (A') and (B') are ventral views. tango7$^{E/E}$ embryos were phenotyped using the twist-GFP marker in the balancer. In (A), WT background is *yw*.

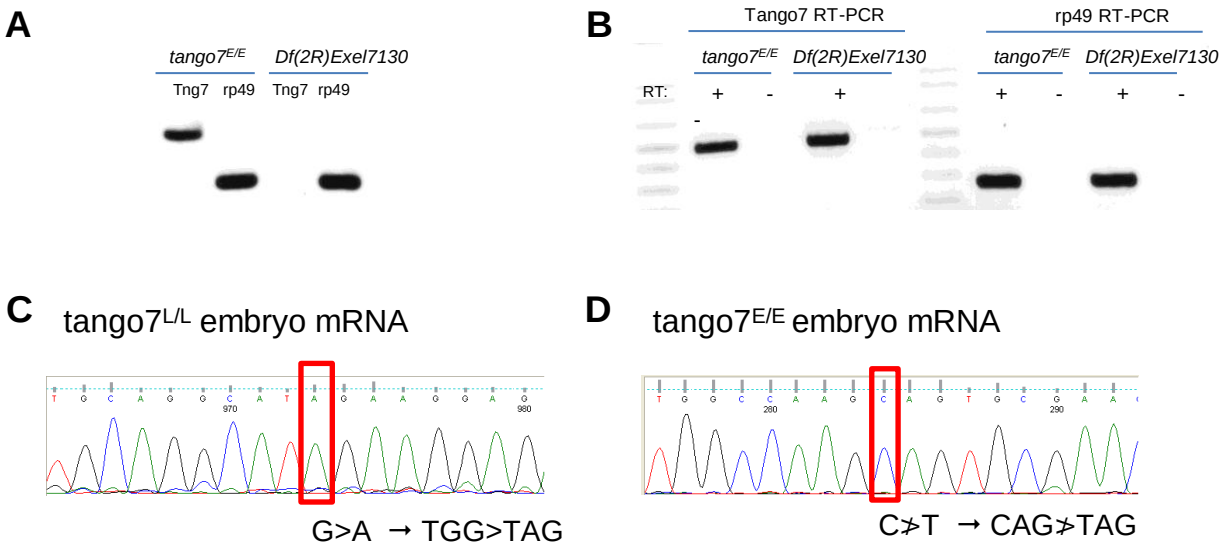

Figure 2-8. *Tango7* is a maternally loaded gene. *(A)* PCR for genomic DNA from *tango7*$^{E/E}$ and *Df(2R)Exel7130* zygotic null embryos from heterozygous mothers. Homozygous embryos were sorted against a GFP marked balancer. Notice that *Df(2R)Exel7130* deletes the *Tango7* locus, but *tango7*^{E}, a point mutant, has an intact locus. *Rp49* was used as an gDNA input control. (B) RT-PCR with (+) or without (-) reverse transcriptase (RT) of RNA from *tango7*$^{E/E}$ and *Df(2R)Exel7130* zygotic null embryos from heterozygous mothers. Homozygous embryos were sorted against a GFP balancer. Although *Df(2R)Exel7130* embryos completely lack the *Tango7* locus, *Tango7* transcript levels were comparable to that of *tango7*^{E} embryos, indicating this is a maternally loaded transcript. *Rp49* was used as an input control. (C-D) Sanger sequencing results off excised RT-PCR products from tango7$^{L/L}$ (C) and tango7$^{E/E}$ (D) embryos.

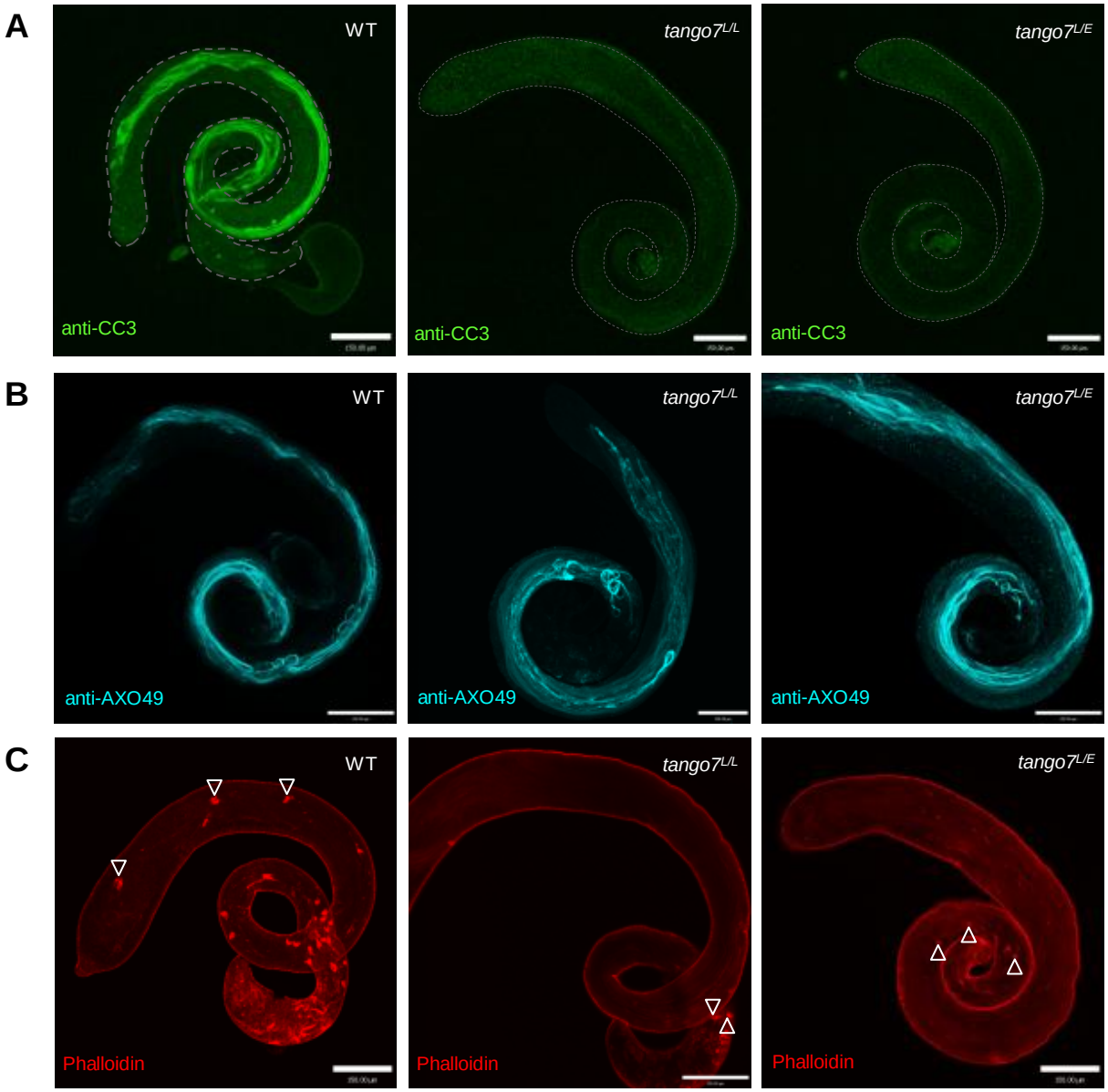

Figure 2-9. *Tango7* mutants are defective for caspase activity and apoptosome-dependent cellular remodeling. (A-E) Confocal micrographs of immunofluorescence on whole-mount testes. (A) Testes stained with anti-CC3, a surrogate for Dronc substrate cleavage (Fan and Bergmann 2010). Spermatid cysts in wild-type testes are positive for anti-CC3, but over 90% tango7 mutant cysts failed to stain, reflecting a defect in Dronc activity (~10% stained weakly for anti-CC3). (B) Testes stained with anti-AXO49, which binds polyglycated b2 tubulin at the onset of individualization (Bressac et al. 1995). tango7 mutant cysts are positive for anti-AXO49, indicating spermatogenesis proceeds normally in these mutants. Signal here was pseudocolored cyan. (C) Testes stained with phalloidin which binds to the actin in individualization complexes (ICs, open arrowheads). Wild-type ICs form at the basal end of cysts and then migrate towards the distal end, whereas tango7 mutant ICs form at the basal end but then either stall or move in an asynchronous fashion (see also Fig 3F). Scale bars are 150um.

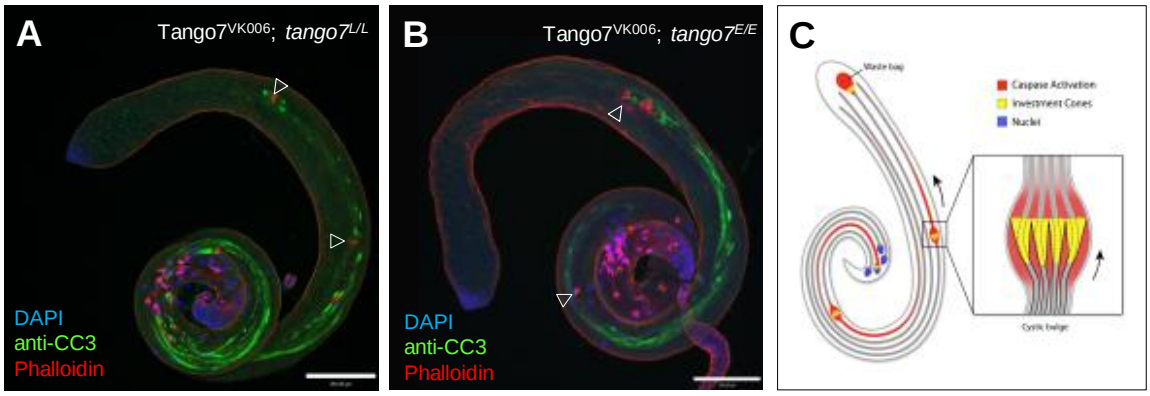

Figure 2-10. Caspase activity and individualization phenotypes are rescued by a *Tango7* genomic fragment. (A-B) One copy of the Tango7^{VK006} rescue fragment restored fertility, caspase activation (anti-CC3) and individualization (Phalloidin) in spermatid cysts of tango7$^{L/L}$ (C) and tango7$^{E/E}$ (B) testes. **.** (A) Schematic of spermatid individualization in the testes. Each spermatid cyst (gray lines) contains 64 syncytial spermatids. Caspase activation occurs upon formation of the individualization complex (IC) at spermatid nuclei and is most prominent at the cystic bulge, which forms as the IC translocates through the syncytia. Inset shows a more detailed view of the cystic bulge, where 64 syncytial spermatids (only four are shown for simplicity) are resolved into individual sperm by the IC and wrapped in their own plasma membrane (black lines). Arrows represent direction of individualization. Red: caspase activation; blue: nuclei; yellow: IC. Scale bars are 150um.

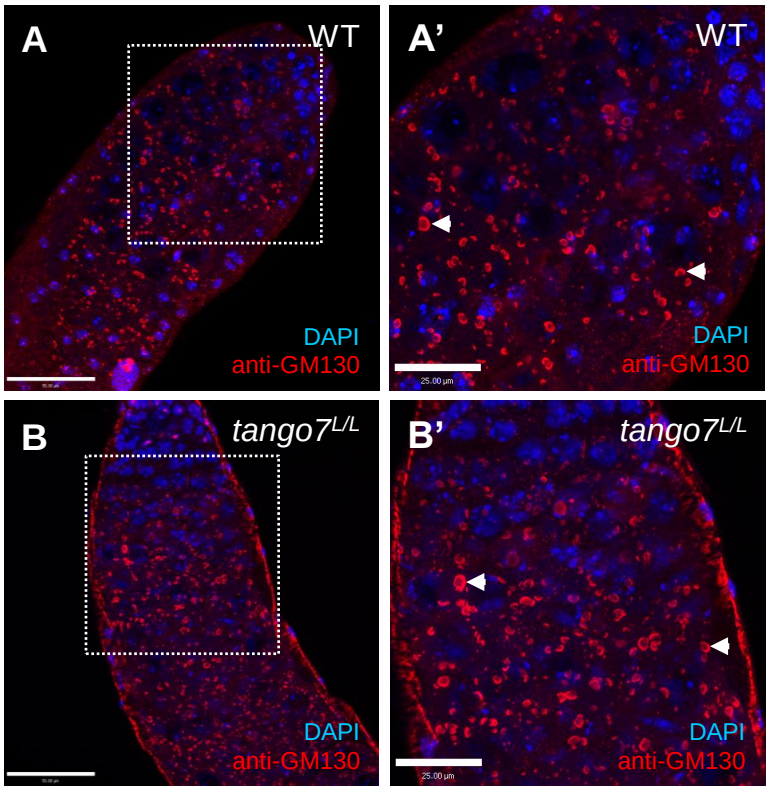

Figure 2-11. *tango7*$^{L/L}$ flies are not disrupted for the Golgi apparatus. Confocal micrographs of immunofluorescence on whole-mount testes. Both wild-type testes (*A-A'*) and *tango7*$^{L/L}$ testes (*B-B'*) have similar patterns of anti-GM130 staining, a *cis*-Golgi marker. (*A'*) and (*B'*) are higher magnification images of boxed areas in (*A*) and (*B*), respectively. Notice that Golgi organization is similar in both genotypes. White arrows indicate representative *cis*-Golgi. Scale bars are 50um in *(A)* and *(B)*, and 25um in *(A')* and *(B')*.

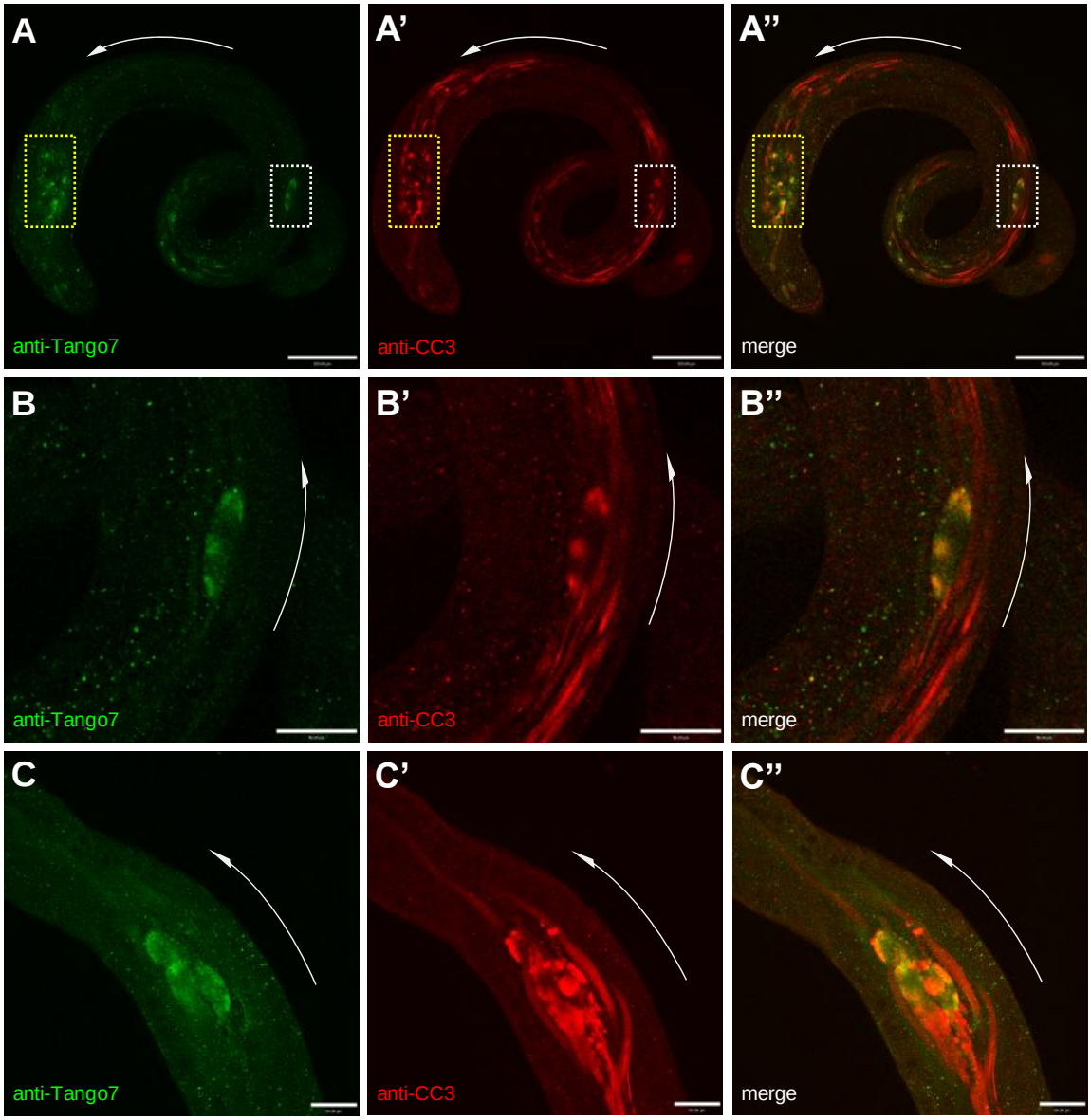

Figure 2-12. Tango7 localizes to the active apoptosome compartment via its C-terminus in individualizing spermatids. Confocal micrographs of immunofluorescence on whole-mount testes. (*A-C″*) Wild-type testes stained with anti-Tango7 and anti-CC3, a marker of Dronc substrate cleavage (Fan and Bergmann 2010). (*A-A″*) Tango7 colocalizes with anti-CC3 in the cystic bulge (white box) and in waste bags (yellow box), which harbor active Dronc caspase (Huh et al. 2004). (*B-B″*) Higher magnification of the cystic bulge in (*A*). (*C-C″*) Higher magnification of a waste bag from a different wild-type testis. Scale bars are 150um for (A-A'') and 50um for (B-C''). Curved arrows represent direction of individualization.

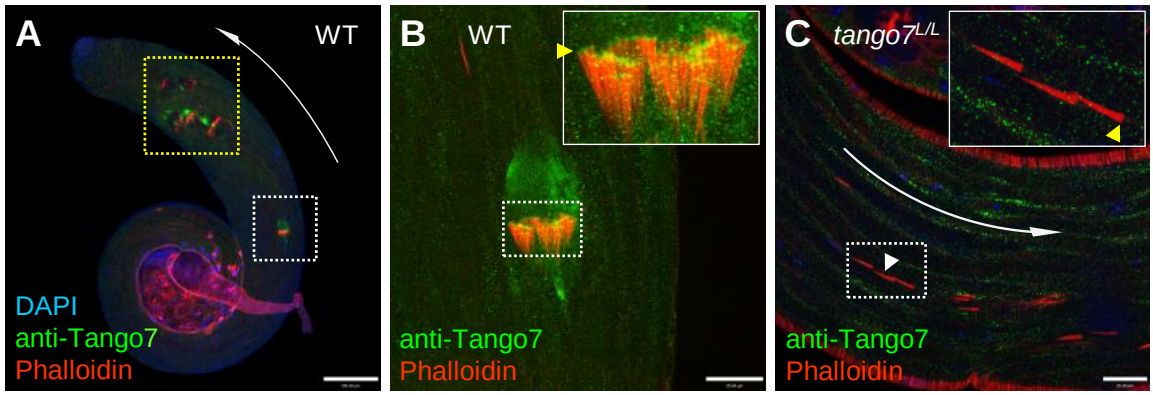

Figure 2-13. Tango7 localizes to the active apoptosome compartment via its C-terminus in individualizing spermatids. (A-C) Testes stained with DAPI (blue), anti-Tango7 (green), and phalloidin (red). (A) In wild-type testes, Tango7 is associated with the IC in the cystic bulge (white box) and in the waste bag (yellow box). (B) Higher magnification of the cystic bulge in (D). Within the cystic bulge, Tango7 is discretely localized to the upper edge of investment cones (inset, yellow arrow). (F) In tango7$^{L/L}$ testes, the C-terminal truncated Tango7^{L} protein failed to localize to the upper edge of investment cones (inset, yellow arrow) and ICs move asynchronously (white arrows). Scale bars are 150um for (A) and 25um for (B-C). Curved arrows represent direction of individualization.

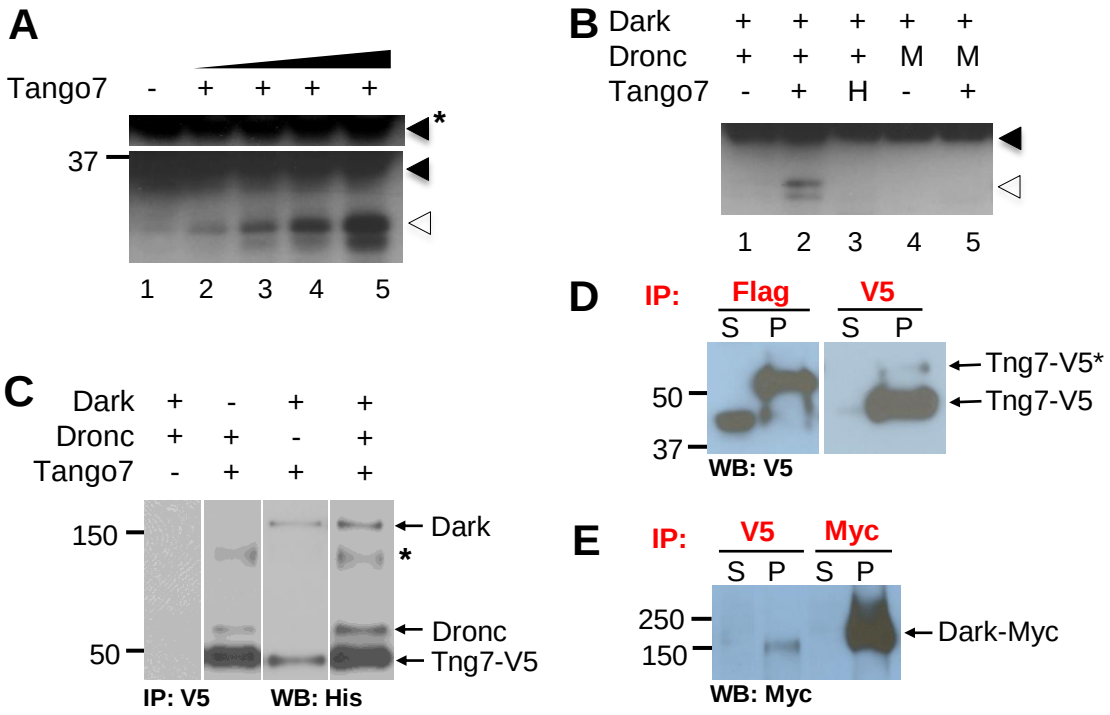

Figure 2-14. Tango7 interacts with components of the apoptosome and stimulates apoptosome activity. (A-B) Apoptosome activity assays detecting cleavage of pro-Drice substrate by the apoptosome. In (A) and (B), filled arrowheads denote substrate (pro-Drice$^{C/A}$-6xHis and open arrowheads indicate product (cleaved Drice$^{C/A}$-6xHis). (A) Tango7 stimulates cleavage of Drice by the apoptosome in a dose-dependent manner. The upper blot in (A) is a lighter exposure of the pro-Drice$^{C/A}$ band, indicated by *. (B) This stimulation effect by Tango7 was heat sensitive (Lane 3) and the appearance of product required wild-type Dronc (Lanes 4 and 5). "H" in lane 3 indicates that Tango7 was heat inactivated before it was added to the reaction. "M" in lanes 4 and 5 indicates that recombinant active site mutant Dronc, Dronc$^{C/A}$, was used. (C) Tango7 directly interacts with Dark and Dronc in vitro. Recombinant 6xHis-Dark-6xHis, Dronc-6xHis and Tango7-V5-6xHis were incubated together in the combinations indicated. Complexes were immunoprecipitated using anti-V5 and detected using anti-His. This interaction is specific as Tango7 does not pulldown an irrelevant protein control (not shown). * indicates a cross reacting background band. (D-E) Tango7 physically interacts with Dark and Dronc in cultured cells. (D) Flag-Dronc interacted with Tango7-V5 in cultured cells. Notice that Flag-Dronc also bound a post-translationally modified form of Tango7, Tango7-V5*. This modified form of Tango7 was not affected by phosphatase treatment (data not shown). (E) Tango7-V5 interacted with Dark-Myc in cultured cells.

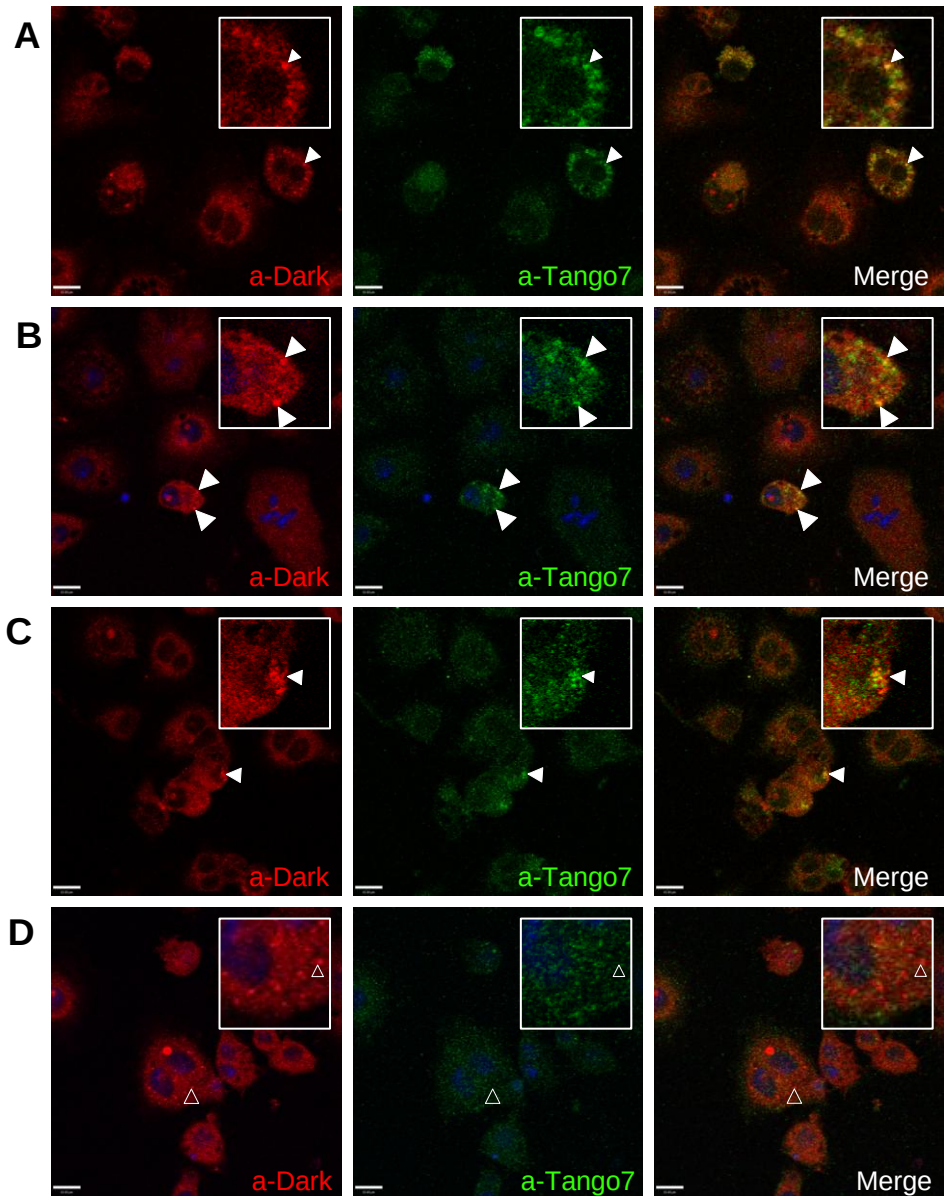

Figure 2-15. Tango7 interacts with components of the apoptosome in cultured cells. Confocal micrographs of S2R+ cells plated on Concanavalin A coated coverslips. (A-D) Images of cells stained for Dark and Tango7 that exhibited Dark punctae in the cytoplasm. In these cells, there was often colocalization of Tango7 and Dark signal (white arrowheads). Notice that cells that exhibit colocalization of both signals in (A-C) often present increased Tango7 staining. (D) A cell exhibiting Dark punctae (open arrowheads) that do not colocalize with Tango7. Notice in the inset that Tango7 staining is diffuse in this cell.

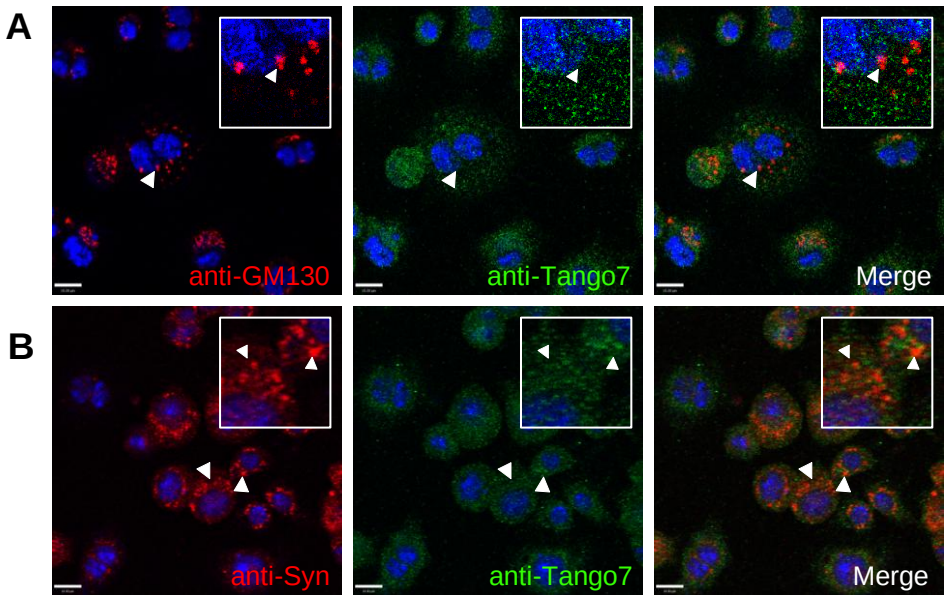

Figure 2-16. Tango7 does not localize to the Golgi in S2R+ cells. Confocal micrographs of S2R+ cells plated on Concanavalin A coated coverslips. (A) Cells stained for anti-GM130, a cis-Golgi marker ,and Tango7 showing that Tango7 does not localize to the cis-Golgi in cultured cells. (B) Cells stained for anti-Syntaxin 16, a trans-Golgi marker, and Tango7 showing that Tango7 does not localize to the trans-Golgi in cultured cells. Notice that anti-Tango7 stains diffusely throughout the cell and seems to localize preferentially in the cytoplasm. Arrowheads indicate representative cis- or trans-Golgi structures.

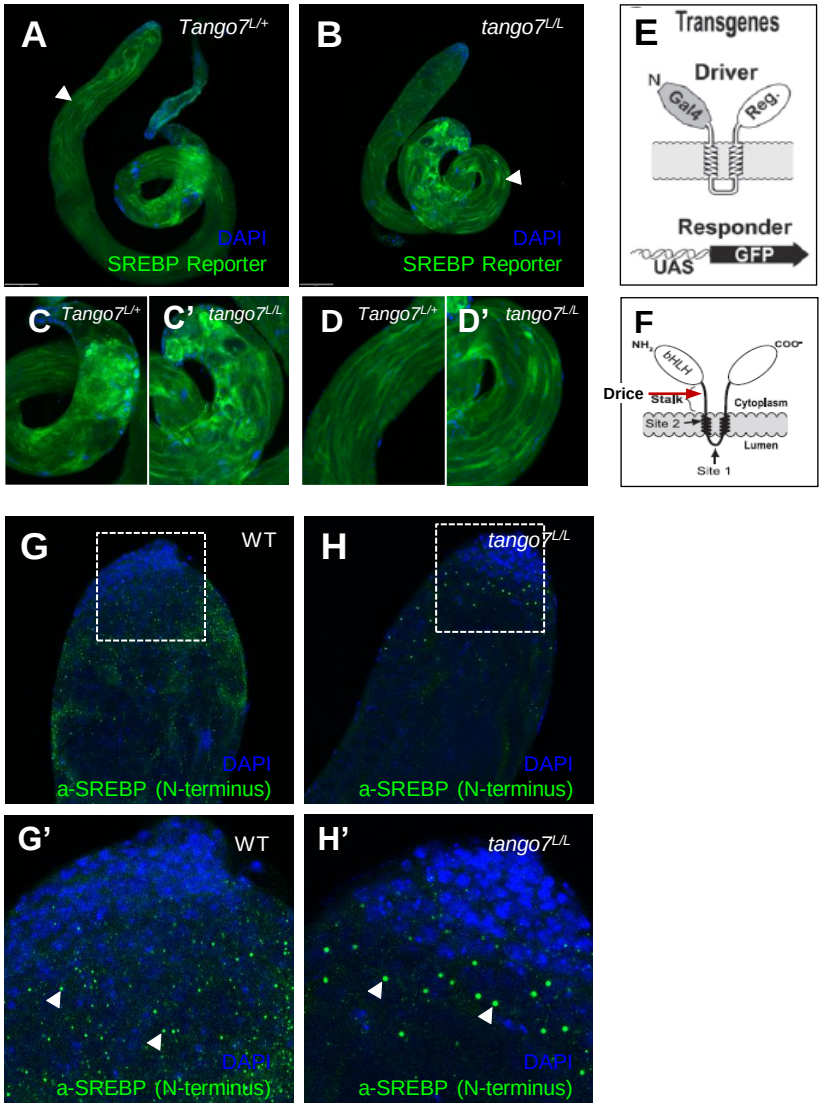

Figure 2-17. Caspase activity in spermatid remodeling is not required for SREBP activity. Confocal micrographs of immunofluorescence on whole-mount testes. (*A-D'*) GFP-staining of testes from *Tango7*$^{L/+}$ (A) or *tango7*$^{L/L}$ (B) flies carrying a SREBP reporter. These flies express a *SREBP* transgene that has replaced the bHLH transactivation domain for a Gal4 transactivation domain (I). Upon cleavage, either by SP1, SP2 or Drice (J), the Gal4 domain is released and translocated into the nucleus where it can bind and activate a UAS-GFP transgene (I). Note that there is not an obvious difference in GFP intensity in spermatids of *Tango7L/+* or (A) *tango7L/L* (B) testes (white arrows). (C-C') The basal end of the testes pictured in (A-B). (D-D') Spermatids from testes pictured in (A-B). (G-H') Staining with an N-terminal specific SREBP antibody in *WT* (G,G') or *tango7*$^{L/L}$ (H,H') testes. (G') and (H') are higher magnification images of boxed regions in (G) and (H). Notice that SREBP seems to accumulate in dividing spermatocytes of *tango7*$^{L/L}$ testes (H', white arrows). WT background is *CantonS*. (E) and (F) adapted with permission from Matthews et al 2010 and Amarneh et al 2009, respectively.

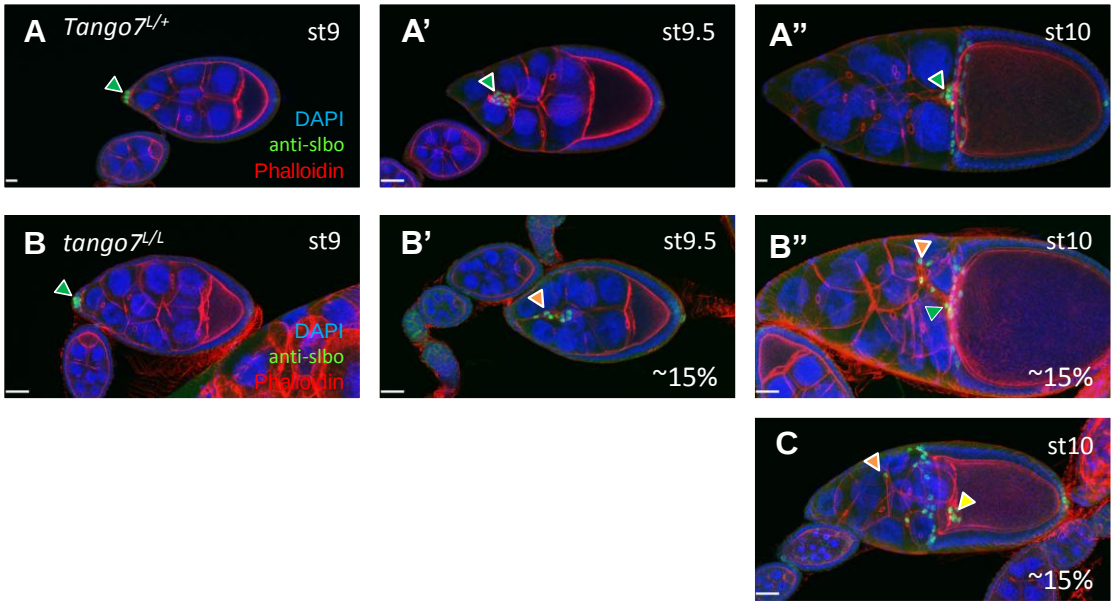

Figure 2-18. *Tango7* mutants have phenotypes in other caspase dependent remodeling contexts. Confocal micrographs of ovaries stained with anti-slbo, a marker for migrating border cells, and rhodamine-phalloidin, which binds the actin cytoskeleton. (A-A") *Tango7*$^{L/+}$ ovaries display normal border cell migration (BCM). Border cells appear at the apical end of the egg chamber in stage 9 (A), migrate through the nurse cells in stage 9.5 (A') and reach the oocyte in stage 10 (A"). Green arrowheads indicate normal border cell clusters. (B-C) *tango7*$^{L/L}$ ovaries display a range of border cell migration phenotypes such as loss of clustering (B, orange arrowhead), failure of cells to reach the oocyte (B' and C, orange arrowheads), and an "accelerated BCM" phenotype (C, yellow arrowhead). These defects totaled to around 45%,whereas only 5% of heterozygotes exhibited defects in BCM..

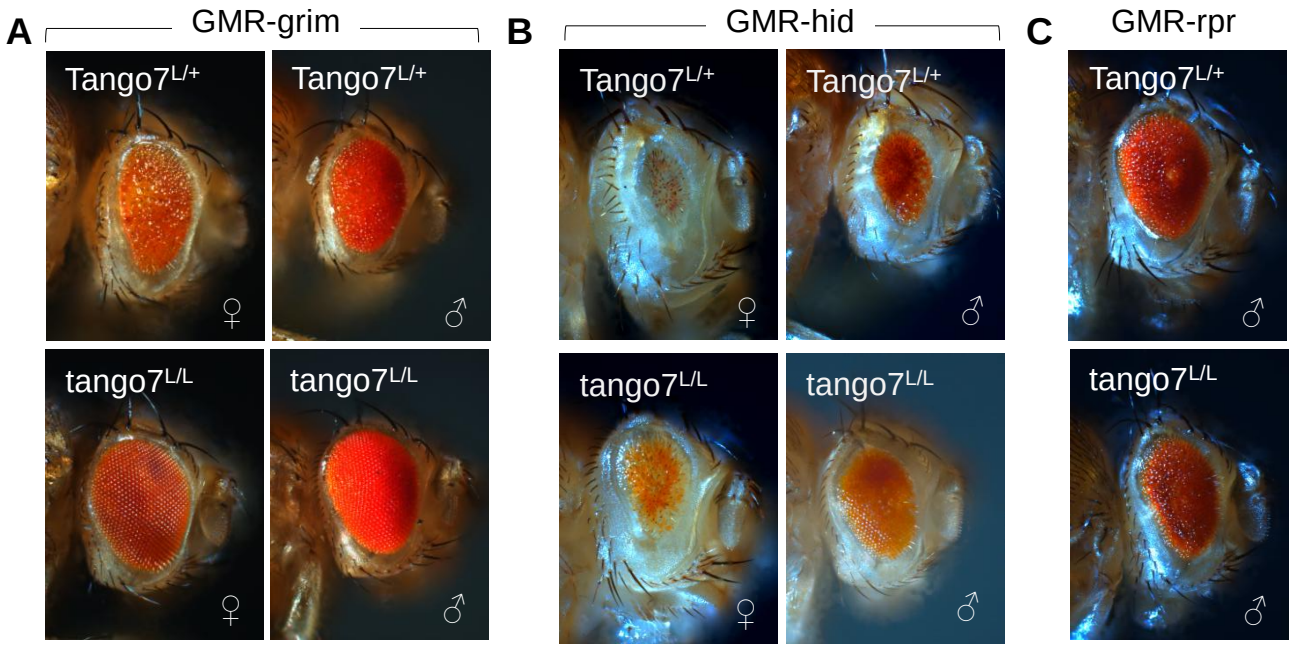

D

	GMR-rpr	GMR-grim	GMR-hid
+/+	Rough (+)	Rough (+ to ++)	Rough (+++)
***Tango7^{L}*/+**	Rough (+)	Rough (+ to ++)	Rough (+++)
***Tango7^{E}*/+**	Rough (+)	Rough (+ to ++)	Rough (+++)
***Df(2R)Exel7130*/+**	Rough (+)	Rough (+ to ++)	Rough (+++)
GMR-DIAP1/+	Normal	=	=

Figure 2-19. *Tango7^{L}* suppresses of forced cell death phenotypes in the eye. Ectopic eye killing by GMR-rpr, GMR-grim or GMR-hid in different mutant backgrounds. (A-C) Roughness and small size of GMR-grim (A) and GMR-hid (B) but not GMR-rpr (C) compound eyes were suppressed in *tango7$^{L/L}$* mutants. GMR-grim eye killing was variable but consistently suppressed in tango7$^{L/L}$ homozygotes. (D) *Tango7^{L}*, *Tango7^{E}* and *Df(2R)Exel7130* were tested for hemizygous suppression of eye killing phenotypes but no difference was seen in eye roughness or size when compared to a wild-type (+/+) background.

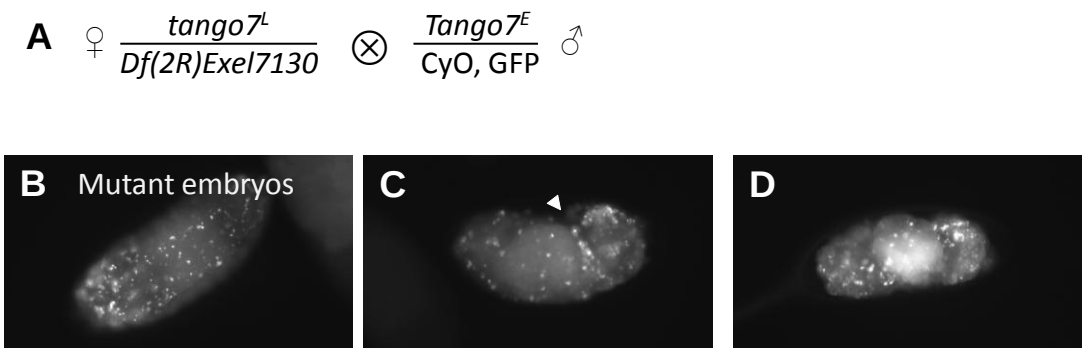

Figure 2-20. Zygotic and maternal *Tango7*^{L} embryos do not exhibit gross cell death defects. Acridine Orange (AO) staining of 13-16hr old embryos. (A) To eliminate maternal loading of wild-type transcript, tango7L/Df(2R)Exilexis7130 mothers were crossed to heterozygote *Tango7*^{E} males. (B) Mutant embryos that have only *Tango7*^{L} maternal transcript do not have decreased PCD levels but do show low penetrance defects such as hid-like phenotypes (C, white arrow) and irregular morphology (D). Mutant embryos were phenotyped by lack of GFP from the 2nd chromosome balancer.

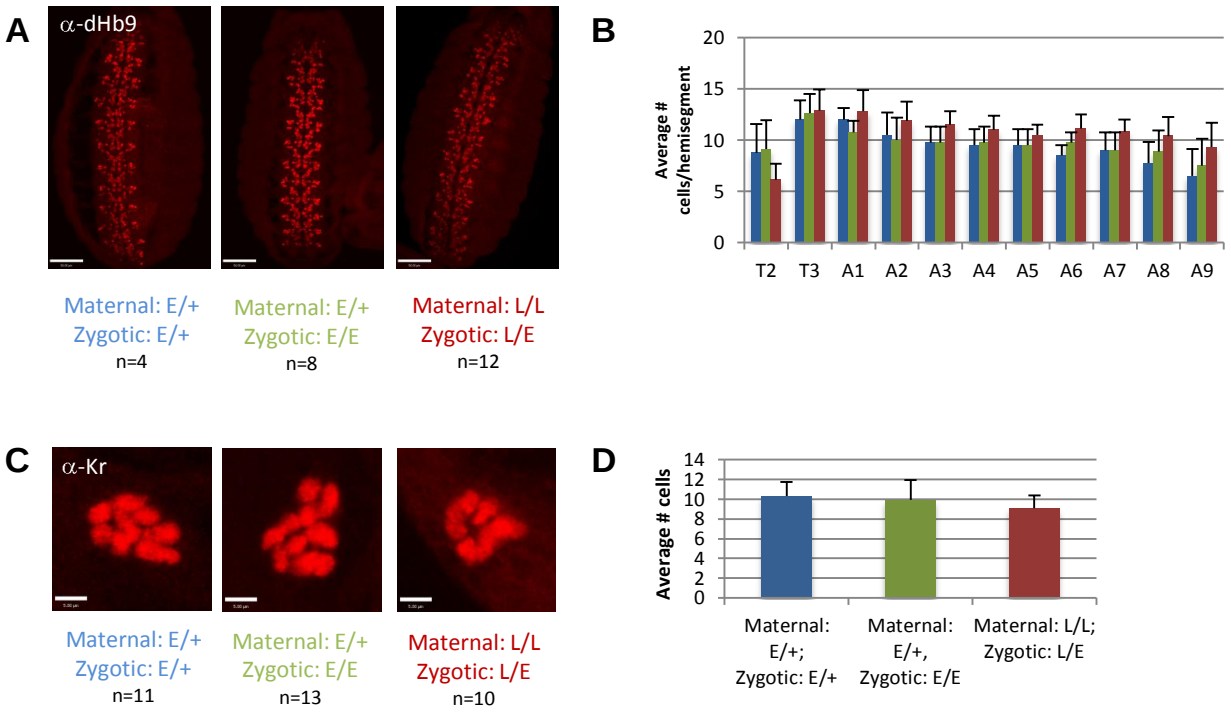

Figure 2-21. *Tango7*^{L} exhibits maternal effect PCD-associated phenotypes in some but not all contexts of the developing embryo. Stage 16 embryos were stained with either anti-dHb9 (C-D) or anti-Kruppel (E-F) to test for persisting neuronal cells (Rogulja-Ortmann et al. 2007). In *tango7*$^{L/E}$ embryos produced from *tango7*$^{L/L}$ mothers extra dHb9^{+} cells occurred in the abdominal hemisegments (A1-A9) of the ventral nerve cord (D) but persisting Kr^{+} cells were not seen in the Bolwig Organ (F). *Tango7*$^{E/+}$ embryos and *tango7*$^{E/E}$ embryos from *Tango7*$^{E/+}$ heterozygous mothers were also examined. These showed similar numbers of dHb9^{+} and Kr^{+} cells when compared to zygotic heterozygous controls (D,F), suggesting that one copy of maternal contribution is sufficient to carry out *Tango7* function in null embryos. Mutant embryos were sorted against a GFP marked balancer. Scale bars are 50um for (C) and 5um for (E).

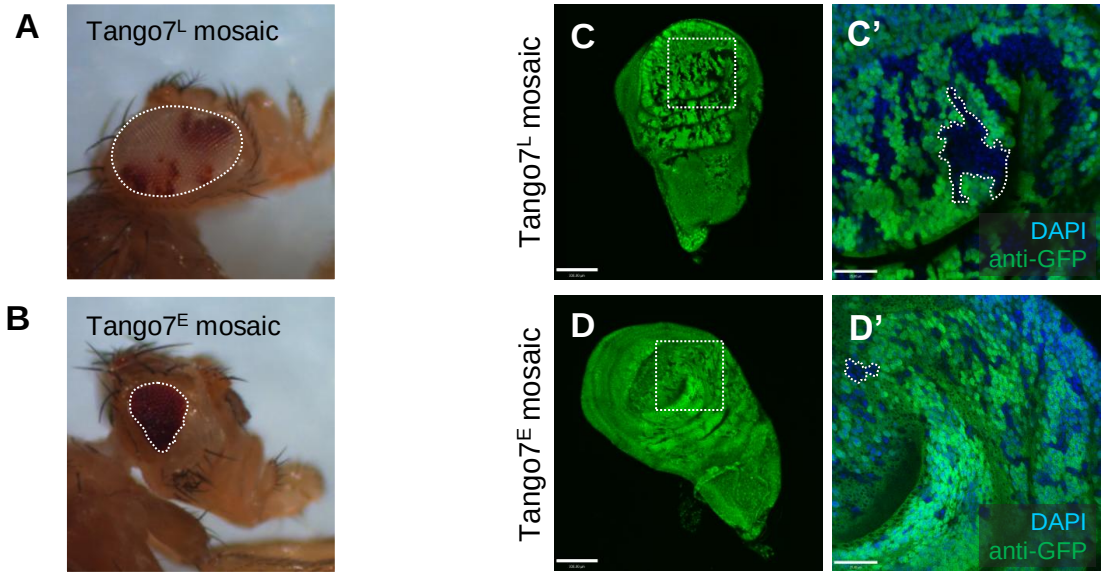

Figure 2-22. *Tango7*^{L} uncouples essential functions of *Tango7* from remodeling functions. Clonal analysis of *Tango7*^{L} and *Tango7*^{E} was performed in the adult eye (A-B) and in the developing wing (C-D'). Eye clones were made using Ey-FLP in flies with an FRT chromosome carrying a recessive lethal *cl* mutation (Newsome et al. 2000) in *trans* to an FRT chromosome carrying either *Tango7*^{L} or *Tango7*^{E}. In these mosaics, most of the adult eye will be composed of *white*$^{-}$ mutant tissue while the remainder will be *white*$^{+}$ heterozygous mutant tissue compromised for growth because it is also heterozygous for a deleterious *cl* mutation. *tango7*$^{L/L}$ tissue is able to form a complete adult eye (dotted outline) in *Tango7*^{L} mosaics (A), whereas *tango7*$^{E/E}$ tissue fails to do so (dotted outline) and is not seen in *Tango7*^{E} mosaics (B). (C-D') Confocal micrographs of immunofluorescence on wing discs. Clones in the developing wing were made using MS1096-Gal4,UAS-FLP in flies with a GFP marked FRT42D chromosome in trans to an FRT chromosome carrying either *Tango7*^{L} (C-C') or *Tango7*^{E} (D-D'). *tango7*$^{L/L}$ clones (GFP^{-} tissue) grow normally (C-C'), whereas *tango7*$^{E/E}$ clones (GFP^{-} tissue) remain small (D-D'). Dotted outlines in (C') and (D') are representative clones to highlight size difference. Scale bars are 100um in (C) and (D) and 25um in (C') and (D').

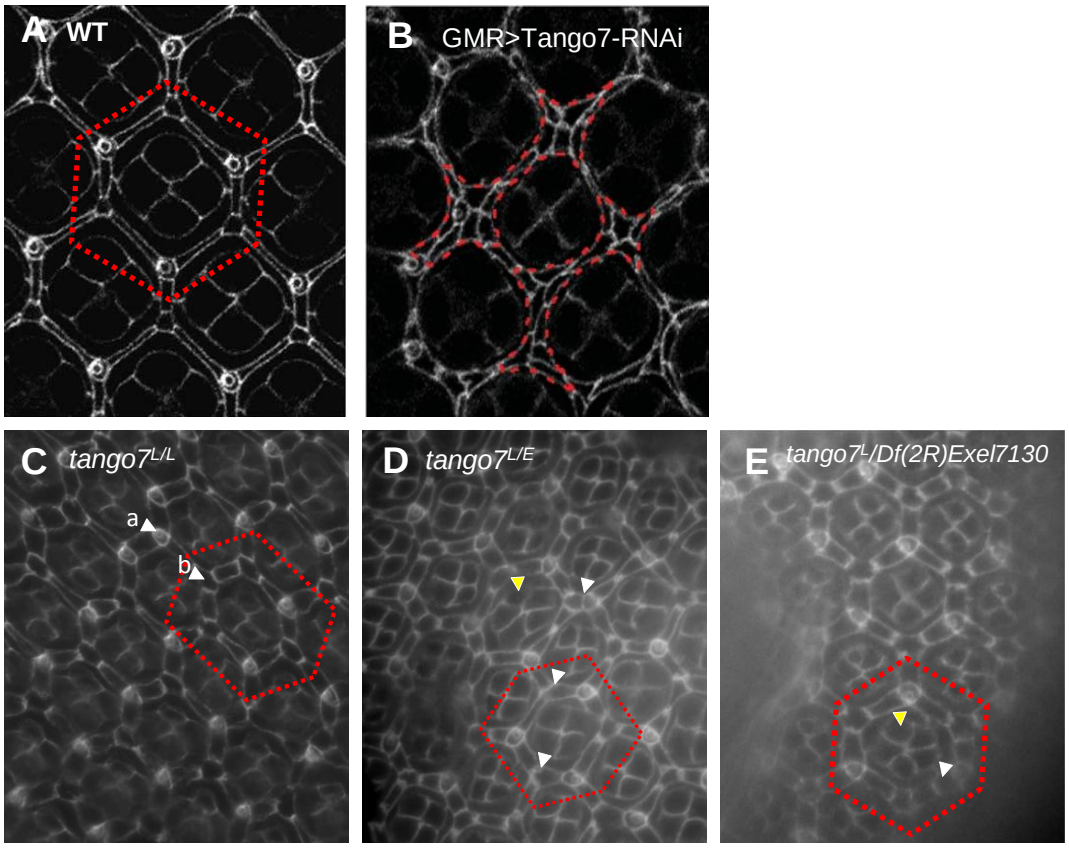

Figure 2-23. *Tango7* mutants do not have extra interommatidial cells. Light micrographs of immunofluorescence on pupal retinas. Retinas from 42 hour old pupae were dissected, fixed and stained with anti-dlg, which stains cell membranes of retinal cells. At the center of each hexagon are "rossettes" which eventually become the ommatidia of the adult compound eye. The cells between each of these "rossettes" are interommatidial cells. (A) Retinas from wild-type pupae form a finely patterned lattice with only one interommatidial cell between each edge of the rosette. (B) Retinas expressing *Tango7* dsRNA show extra interommatidial cells outlined in red. Retinas from *tango7*$^{L/L}$ (C), *tango7*$^{L/E}$ (D) and *tango7*^{L}*/Df(2R)Exel7130* do not have extra interommatidial cells like in (B). (C) *tango7*$^{L/L}$ retinas show low penetrance bristle specification defects (cell marked by 'a' should be in place of the cell marked by 'b'). (D) *tango7*$^{L/E}$ retinas are missing interommatidial cells (white arrows), and occasionally show an extra ommatidial cell (yellow arrow). (E) *tango7*^{L}*/Df(2R)Exel7130* have occasional ommatidial cells (yellow arrow). In this filed of view, there is one extra interommatidial cell (white arrow). (A) and (B) were adapted from Chew et al 2009 with permission.

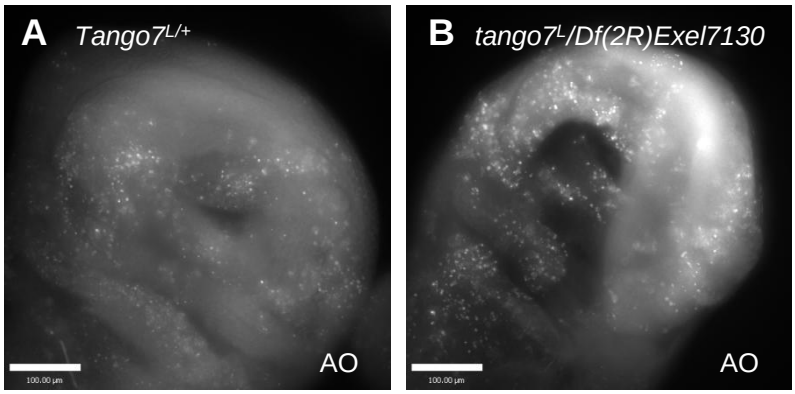

Figure 2-24. *Tango7* mutants are not compromised for radiation-induced apoptosis. Acridine Orange (AO) staining of live wing discs.4 hours after irradiation at 40 Gray. Both heterozygotes (A) and mutant (B) wingdiscs show a ubiquitous AO staining in the wing disc in response to irradiation.

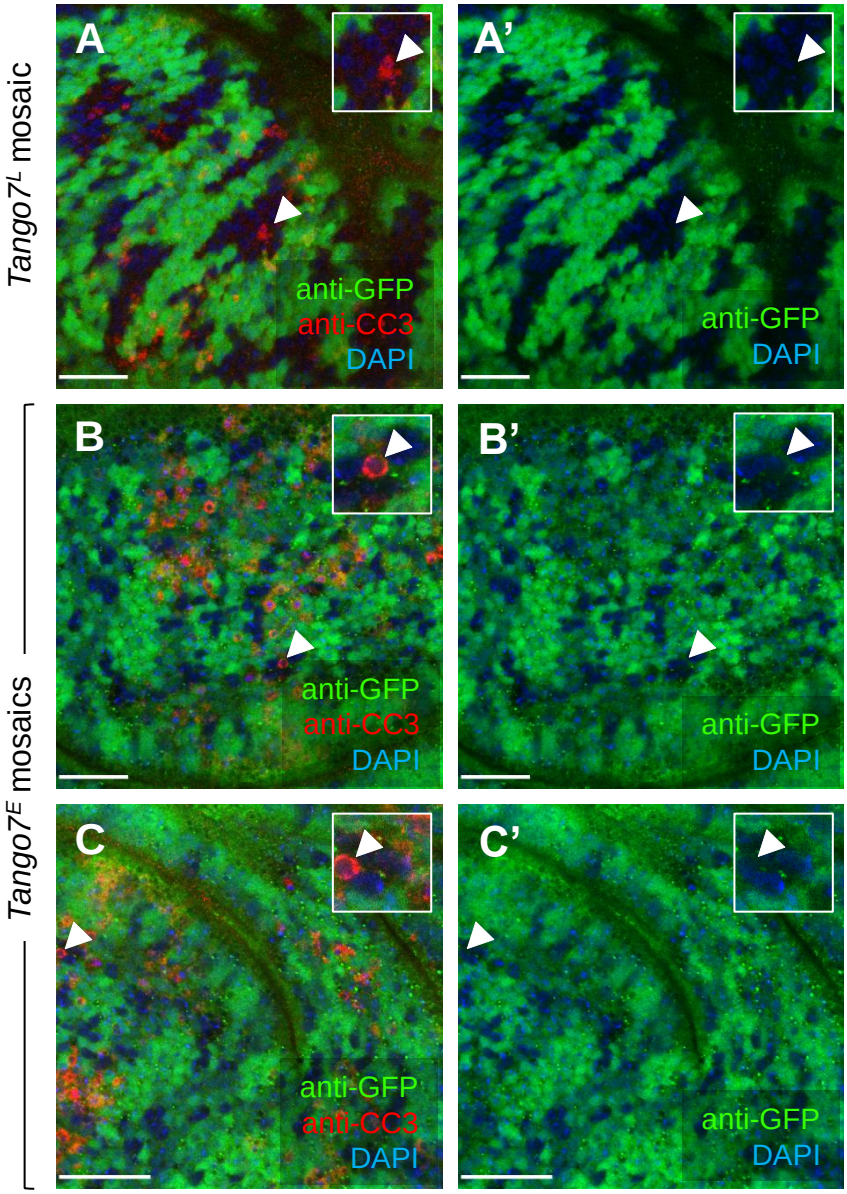

Figure 2-25. *tango7$^{E/E}$* cells can undergo programmed cell death. Confocal micrographs of immunofluorescence on mosaic wing discs 4 hours after irradiation at 40 Gray. Both *tango7$^{L/L}$* clones (A-A', GFP^{-} tissue) and *tango7$^{E/E}$* clones (B-C', GFP^{-} tissue) have dying cells as marked by anti-CC3 (white arrows). *Tango7^{L}* (A-A') or *Tango7^{E}* mosaics were generated using MS1096-Gal4,UAS-FLP in flies with a GFP marked FRT42D chromosome in trans to an FRT chromosome carrying the respective *Tango7* allele.

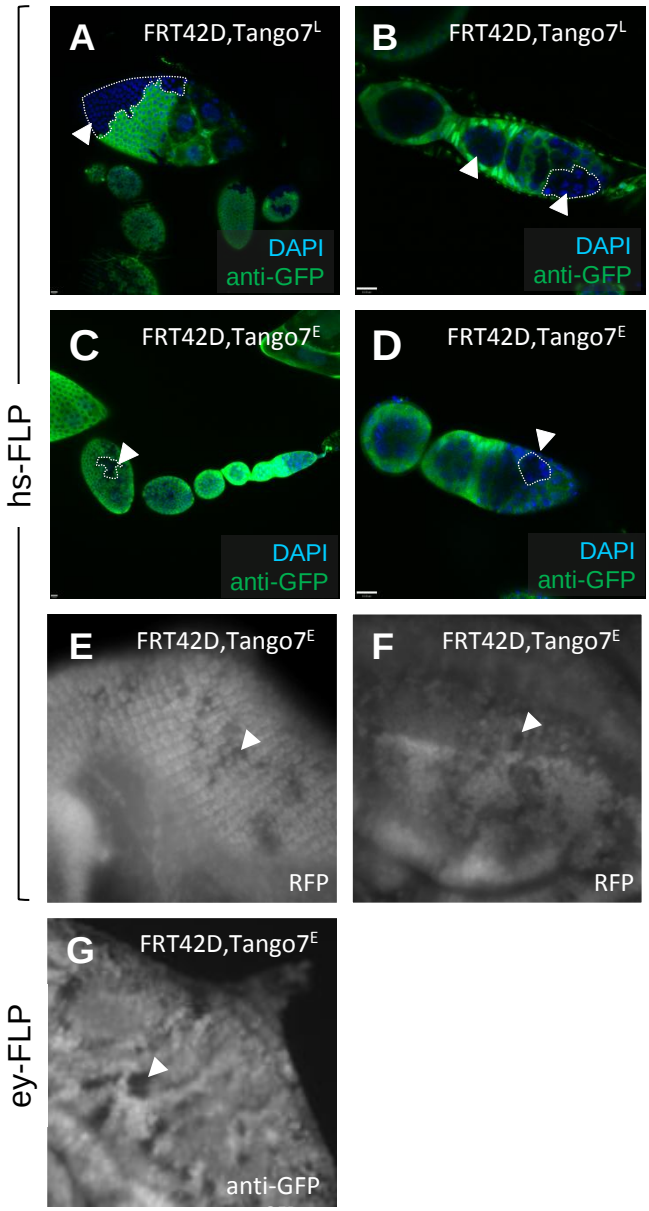

Figure 2-26. Generating *tango7*$^{E/E}$ clones in different tissues, using different FLP drivers and different marked chromosomes. Confocal and light micrographs of immunofluorescence on mosaic ovaries (A-D), eye discs (E and G) and wing disc (F) generated by hs-FLP (A-F) or ey-FLP (G). Mosaics were generated using either hs-FLP (A-F) or Ey-FLP to induce mitotic recombination in flies with a GFP-marked (A-D,G) or RFP-marked (E-F) FRT42D chromosome in trans to a FRT42D, *Tango7*^{E} chromosome. RFP marked tissue was fixed and imaged, without antibody staining.

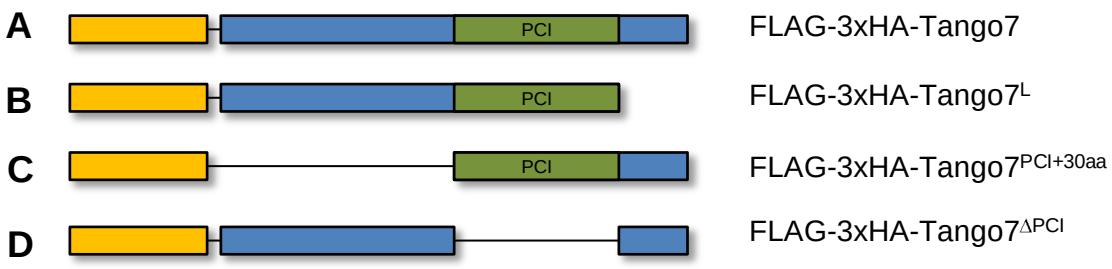

Figure 2-27. UASp-FLAG-3xHA constructs and flies. Four UASp-FALG-3xHA-*Tango7* constructs were made and three of them (A,B and C) were transformed into flies and exist as stocks (see Appendix A). All four constructs can be used for transient expression in cell culture when transformed in conjunction with armadillo-Gal4.

		Phenotypes			
Tissue	**Driver**	**Viability**	**Fertility**	**Wings**	**Eyes**
Embryo	**Engrailed-Gal4**	Lethal - L1	-	-	-
	Armadillo-Gal4	Lethal - L1	-	-	-
	Daughterless-Gal4	Lethal - L1	-	-	-
	Mesoderm-Gal4	Viable	Fertile	Normal	Normal
Eye	**Eyeless-Gal4**	Lethal – Headless pupae	-	-	-
	GMR-Gal4	Viable	-	-	Melanotic eyes
Wing	**MS1096-Gal4**	Lethal – Liquefied pupae	-	-	-
	Vestigial-Gal4	Viable	-	Normal	-
CNS	**Elav-Gal4**	Viable	Fertile	-	-
Germline	**Nanos-Gal4**	Viable	Sterile	-	-
Testes	**Hsp83-Gal4**	Viable	Fertile	-	-

Table 2-2. Knockdown of *Tango7* with a UAS-shRNA line. *Tango7*^{HMS00667} was used to knockdown Tango7 in different tissues. The tissues in which the shRNA was expressed, the Gal4 drivers used and the phenotypes observed are listed.

		Nos-Gal4:VP16			Hsp83-Gal4			Da-Gal4
Process/ Complex	**UAS-shRNA**	**Fertility**	**Testes**	**Caspase Activity**	**Fertility**	**Testes**	**Caspase Activity**	**Viability**
	Tango7	Fertile	Atrophied	-	Fertile	Normal	Altered	Lethal
Apoptosis	**Dark**	Fertile	Normal	Normal	Fertile	Normal	Normal	Viable
	Dronc	Fertile	Normal	Normal	Fertile	Normal	Normal	Viable
	Drice	Fertile	Normal	Normal	Fertile	Normal	Altered	Lethal
	DIAP1	Sterile	Atrophied	-	Fertile	Normal	Normal	Lethal
eIF3	**S9**	Sterile	Atrophied	-	-	-	-	Lethal
	S10	Sterile	Atrophied	-	-	-	-	Lethal
	Trip1	Sterile	Atrophied	-	-	-	-	Lethal
	S69b	-	-		-	-	-	Viable
CSN	**Csn7**	Sterile	Atrophied		-	-	-	-

Table 2-3. Targeting eIF3 and CSN components in testes and embryos. Phenotypes observed using UAS-shRNAs with nos-Gal4:VP16, hsp83-Gal4 and da-Gal4. Nos-Gal4:VP16 expresses in the germline. Hsp83-Gal4 expresses in testes in early spermatocytes and late spermatids. Da-Gal4 expresses strongly in the embryo.

Discussion

Like animals mutated for apoptosome genes, I show here that viable *Tango7* males are sterile because they fail to initiate a caspase-dependent process that remodels syncytial cysts to produce individualized sperm. These characteristic defects established a classic precedent for how apoptosome activation does not inevitably drive cell killing but can, instead, be repurposed for non-apoptotic processes during spermatogenesis (Arama et al. 2003; Huh et al. 2004; Feinstein-Rotkopf and Arama 2009).

How might *Tango7* collaborate with the apoptosome as spermatids are remodeled? Since *Tango7* was originally described in a collection of targets linked to Golgi organization (Bard et al. 2006), we examined a Golgi marker in *tango7*$^{L/L}$ tissue but found no indication that this organelle was affected (Figure 2-11). Studies of *Tango7* orthologs in *C. elegans* (Luke-Glaser et al. 2007) and in yeast (Zhou et al. 2005) suggest the protein could also act as a non-core factor associated with the COP9 signalosome complex and/or the eIF3 translation complex. These modalities could certainly be relevant *in vivo*, but the *in vitro* activities seen here with recombinant Tango7 (Figure 2-14) suggest functions independent from these multiprotein complexes. Furthermore, since *tango7*$^{L/L}$ mutants are fully viable it seems doubtful that systemic defects in either of these complexes could account for caspase-dependent spermatogenesis defects seen in these animals. Instead, I propose that *Tango7* directly engages the apoptosome to specify this holoenzyme for cellular remodeling. Several pivotal observations support this. First, the action of *Tango7* is clearly required for apoptosome-dependent caspase activity and remodeling of spermatids. Second, Tango7 localizes to the active holoenzyme compartment *in vivo* and physically binds apoptosome

proteins *in vitro* and in cultured cells. Third, Tango7 is one of few proteins (and the first of its kind in *Drosophila*) able to stimulate apoptosome activity *in vitro*. Together these observations suggest that *Tango7* functions as a direct regulatory component of this complex, acting also perhaps as a scaffold or chaperone that could promote remodeling by recruiting the active apoptosome to the IC. Consistent with this, Tango7^{L} (which truncates 30 amino acids from the C terminus) fails to localize to the IC in caspase defective *tango7*$^{L/L}$ testes. Furthermore, like active Dronc, Tango7 localized to the investment cones of migrating ICs and correlated with active caspases at this structure but not with anti-CC3 staining elsewhere in the testes. To further explore this scenario, I sought to localize active Dronc in *tango7* spermatids but, unfortunately, this particular antisera is no longer available.

The above data combined with my genetic observations establishes that the C terminus of Tango7 is dispensable for viability but required for apoptosome-dependent remodeling. Hence, *Tango7*^{L} is an allele specific variant that uncouples essential functions from non-essential functions. Consistent with this, *Tango7*^{L} clones in the eye, wing and germline grew normally but *Tango7*^{E} clones arrested after several cell divisions and failed to give rise to embryos (Figures 2-, 2- and data not shown).

What essential functions might *Tango7* have? It is clear from protein sequence data that the mammalian ortholog of *Tango7* is eukaryotic initiation factor 3 subunit m (eIF3m). eIF3m is the best hit when *Tango7* is BLASTed against the human proteome. It has 95% query coverage and is 47% identical and 68% similar to *Tango7* (see also Figure 2-). Functionally, the eIF3m orthologs in yeast (Zhou et al. 2005) and C.elegans (Luke-Glaser et al. 2007) have been implicated in global protein translation and more recently, knocking out eIF3m in

mice has been shown to reduce stability of the eIF3 complex as well as reducing protein translation levels in the liver (Zeng et al. 2013). The latter study revealed that eIF3m is an essential gene required for early embryonic development and tissue homeostasis, which is consistent with data for the *Tango7*^{E} allele thus far. If *Tango7* is in fact the *Drosophila* ortholog of eIF3m, it is likely involved in protein translation. If this is the case, then *Tango7*^{L} uncouples *Tango7*'s role in translation initiation from its role in remodeling, underscoring the fortuitous nature of this allele.

Does *Tango7* function in PCD? The strongest precedent for this are *ex vivo* studies done by Chew et al showing that *Tango7* depletion in cultured cells protects them from Smac-mimetic killing (Chew et al. 2009). In this dissertation work, I show that *tango7*$^{L/L}$ mutants suppress Hid-killing in the eye (Figure 2-19B), exhibit extra dHb9^{+} neurons in the embryo (Figure 2-21A and B) and show PCD phenotypes in the wing (Figure 2-6A-D). These argue in favor of a role for *Tango7* in PCD. However, it is clear that *Tango7*^{L} does not behave like a global PCD mutant. Specifically, *tango7*$^{L/L}$ mutants do not show defective global PCD in embryos with maternal *Tango7*^{L} (Figure 2-20), interommatidial cell death (Figure 2-23) or radiation induced apoptosis (Figure 2-24). The most parsimonious explanation of these data is that *Tango7* can participate in PCD but that the C-terminus is dispensable for this role in most, but not all contexts.

How is the apoptosome functioning to remodel cells without provoking cell death? Mechanisms that recruit the apoptosome to subcellular structures, together with restraints imposed by the ubiquitin-proteasome system (Kuo et al. 2006; Arama et al. 2007; Kaplan et al. 2010) could restrict caspase activity to discrete subcellular compartments. This scenario

explains how partial demolition of subcellular structures might occur but, conceivably, the apoptosome could also exert constructive roles during remodeling. There are two interesting scenarios for how this could happen: the remodeling apoptosome might target a specific subset of substrates or it might cleave different substrates altogether. Experiments to address these hypotheses are currently underway by other members of the lab.

Finally, there are a couple of lessons learned from this dissertation work. The first is that you get what you screen for. Even though *Tango7* came out of a siRNA screen for apoptotic effectors, it turns out what was really being screened for was caspase activation. *Tango7* is required for caspase activation, but non-apoptotic caspase activation. The second lesson is that all biology discovered in cell culture and in vitro should also be studied in model systems. We would have never discovered the role of Tango7 in caspase-dependent cellular remodeling had we not translated our cell culture work into the living animal. Finally, hypomorphic alleles are incredibly valuable. *Tango7* is an essential cellular gene and if we hadn't fortuitously recovered the *Tango7*^{L} hypomorph the extent of our observations would have been just that. *Tango7*^{L} allowed us to uncouple its essential cellular functions from its remodeling functions and has become an exciting entry point to understanding how the apoptosome might be diverted from death programs to cellular remodeling.

Future Directions

The findings from this dissertation work have spawned many questions and directions for future research. Of highest priority are questions aimed at understanding how the apoptosome can launch caspase activation without killing the cell. It will be interesting to test whether the remodeling apoptosome has different substrate specificity or different substrates altogether and whether these properties are affected by *Tango7*. Indeed, proof-of-principle experiments for a non-biased proteomic screen aimed at uncovering remodeling-specific substrates are currently underway. Actin and myosin share roles in cellular remodeling (Noguchi and Miller 2003; Noguchi et al. 2006; Isaji et al. 2011; Lucas et al. 2013) and in apoptosis (Mashima et al. 1999; Croft et al. 2005), and are thus good candidates to examine for different cleavage in remodeling vs. dying cells. Functionally, non-apoptotic caspase activity has been shown to promote learning and memory in the zebra finch and, more recently, in *Xenopus laevis* (Huesmann and Clayton 2006; Chen et al. 2012). Similarly, *Dronc* has also been shown to be required for dendrite pruning in a subset of neurons during metamorphosis (Kuo et al. 2006). It would be fascinating if *Tango7* were required for apoptosome dependent neuron remodeling and consequently, learning and memory. To examine this possibility, existing transgenic lines that label certain neurons can be tested in *Tango7* mutants for presence of dendrite pruning defects.

Does*Tango7* function in PCD? To definitively answer this, *Tango7* null tissue has to be tested. A group of cells that have been used to study PCD in our lab (Chew et al. 2004) but that has not been tested in *Tango7* mutants are hemocytes - the *Drosophila* equivalent of blood cells. A Gal4 strain that drives GFP and FLP expression in hemocytes is available

(see Appendix A) and can be used in conjunction with *Tango7*^{E} and RFP-labeled FRT chromosomes to test for PCD in *Tango7* null hemocytes.

Although not directly related to our lab's focus, it will be important to determine what the essential function of *Tango7* is. Like cytochrome c, it could be that *Tango7* is a dual function protein that links apoptosome activation to a vital cellular process as a way to protect it from acquiring deleterious mutations and thus maintain the cell's ability to activate the remodeling apoptosome when it is needed.

One of the most powerful tools for gene discovery are genetic screens. Because reversion of sterility is relatively simple to phenotype, the *Tango7*^{L} allele presents a unique opportunity to screen for genes that are involved in apoptosome-dependent, non-apoptotic caspase activation. Specifically, one could conduct a F3 mutagenesis screen for dominant mutations that revert the male sterile phenotype. In a screen like this, one could screen massive numbers of males by crossing them *en masse*. If a particular cross produces progeny, then the fertile male(s) can be isolated and the causal mutation mapped by whole genome sequencing.

Lastly, what are the molecular functions of the C-terminal 30 amino acids? How do these function to promote non-apoptotic caspase activation? One can speculate that the 30 amino acids specify the apoptosome for remodeling by modulating its substrate specificity by either affecting the conformation of the apoptosome or by binding and presenting remodeling substrates to the apoptosome. Discovering the mechanism by which the apoptosome is redirected from death to remodeling and vice versa will undoubtedly cause us to reevaluate

how cells execute life or death decisions and reexamine the role of the apoptosome in cancer and other pathologies.

Chapter 2 Acknowledgements

I would like to thank Xiaoquin Tu, Nichole Link, and Leslie Durham for help with experiments and reagents. Thanks to Marie-Hélène Bré for the AXO49 antibody, Joachim Seemann for the GM130 antibody and Peter Michaely for the NV18-6His recombinant protein. Special props to Angela Diehl for the individualization schematic. And lastly, many thanks to Dr. Michael Buszczak, Dr. Helmut Kramer and Dr. Robin Hiesinger for their advice and comments.

CHAPTER THREE:

DECONSTRUCTING ONCOGENIC ACTIVITY

ENCODED BY P53 MUTATIONS IN HUMAN CANCER

Introduction

Though mutant p53 was first discovered over thirty years ago, much remains to be discovered about how p53 mutants exert their oncogenic activities. Although cell-based studies are valuable and offer cellular insight, *in vivo* studies using knock-in mice have yielded unprecedented cellular, developmental and pathological insight into p53 mutant activity, underscoring the power of *in vivo* models. In this chapter of my thesis, I discuss the creation of an *in vivo* platform aimed at uncovering gain-of-function activities of p53 mutants using the *Drosophila* model system.

Studying human p53 mutants in the fly has several advantages. First of all, *Drosophila* is a powerful *in vivo* model system with unparalleled genetic tools and community resources. Second, the majority of genes, pathways and cellular programs that govern human biology are conserved in the fruit fly. Third, it benefits from a simpler genome with lower complexity and redundancy; thus, one can ask directed questions about mutant p53 gain-of-function activities without having to parse out dominant negative activity against p53 family members. Finally, creation of transgenics and their genetic manipulation are relatively simple and benefit from short generation cycles and low maintenance costs. In contrast, laborious genetic manipulation, longer generation times and high maintenance costs of mice

are most likely the reason that there have only been seven mutant p53 mouse models generated since 2004.

I rationalized that if human p53 could complement fly p53 in *Drosophila*, I could exploit the power of the *Drosophila* genetic model system to uncover mutant p53 gain-of-function activities (Figure 3-1). At the outset of this project, several observations suggested hp53 could complement *Dp53*. First of all, the core of the p53 regulatory network is well conserved in *Drosophila*. Upstream ATM and Chk2 kinases control *Dp53* activity in flies like in humans (Brodsky et al. 2004) and, like human p53, fly p53 targets genes involved in apoptosis and DNA repair in order to preserve genomic stability in response to cellular stress (Brodsky et al. 2004). Furthermore, the p53 binding site is highly conserved, reflected by the fact that Dp53 can bind the hp53 consensus binding site (Brodsky et al. 2000) and that hp53 can engage the *Dp53* genetic circuitry (Yamaguchi et al. 1999).

Human p53 studies in the fly thus far have been limited to ectopic expression systems which are hampered because overexpression of hp53, like *Dp53*, potently induces cell death (Yamaguchi et al. 1999). I bypassed this limitation by humanizing *Drosophila* p53 such that hp53 is under control of the native regulatory elements that control *Dp53* expression. These humanized p53 flies express hp53 in the same tissues as *Dp53* with the same dynamics, thus allowing the study of hp53 in biologically and developmentally relevant contexts in *Drosophila*.

There are two overarching goals of this platform. First is to uncover novel gain-of-function activities of p53 mutants. As discussed in Chapter 1, studies in mice and in cultured cells have shown that p53 mutants can exert gain-of-function activity via dominant negative

effects on other proteins such as p63 and p73 (Lang et al. 2004; Olive et al. 2004; Adorno et al. 2009; Muller et al. 2009; Xu et al. 2011). However, p63 and p73 null mice display severe developmental defects that are not seen in p53 mutant mice (Mills et al. 1999; Yang et al. 1999; Pozniak et al. 2000; Yang et al. 2000), suggesting that dominant negative activity toward p63 and p73 cannot be a principal mechanistic role of mutant p53. Because *Drosophila* does not have orthologs for p63 or p73, this poises our platform for discovery of novel gain-of-function activities independent of p63 and p73 inhibition.

The second goal is to uncover phenotypic differences that can be used to stratify p53 mutations for prognostic use. One third of all tumors acquire missense mutations that target six residues in the p53 protein (Soussi 2007). *In vivo* studies have shown that some hot-spot mutants give rise to more aggressive cancers than others and have shorter survival. This emphasizes the need to distinguish between the severity of gain-of-function mutations in order to offer accurate prognoses. However, two-thirds of human p53 missense mutations remain largely understudied. Thanks to the ease of genetic manipulations in *Drosophila*, humanized flies can be generated for novel or understudied p53 mutations and then stratified according to how they behave in comparison to humanized hot-spot p53 mutants.

Materials and Methods

Fly strains and husbandry

yw flies were used as wild-type controls unless noted otherwise. *Dp53*^{NS}, *Dp53*$^{5A-1-4}$ and GHP150 were inherited lab stocks. w;UAS-eGFP/TM3,Sb (Bloomington #5430) and w;TM3,Sb,Tb-RFP (Bloomington #36338) stocks were obtained through Bloomington. CyO, Ubi-Cre was a kind gift of M. Buszczak. All flies were reared at 25^{o}C or room temperature. hp53^{1} ;NS/TM3,Sb,Tb-RFP and hp53^{2};NS/TM3,Sb,Tb-RFP flies are noticeably healthier at room temperature.

Generation of Dp53 rescue line

The *Dp53* rescue strain was engineered by phiC31 integration of a 20kb genomic fragment BAC containing the *Dp53* locus into an attP site on the X chromosome of the PBac{y+-attP-9A}VK00006 line (Bloomington #9726). The parent BAC CH322-115D03 was obtained from the P[acman] resource library [38] and Rainbow Transgenic Flies performed the injection and screening for recombinants.

Generation of humanized p53 lines

Similarly, the humanized p53 lines were generated by replacing the *Dp53* ORF of BAC CH322-15D03 with either wild-type or mutant human p53 cDNA via recombineering and then integrating into the attP site on the X chromosome of the PBac{y+-attP-9A}VK00006 line (Bloomington #9726). Primers 13-26 were used for recombineering (See Appendix C). The five p53 hot-spot mutants, which represent the five most mutated hot-spot codons, were

generated by site-directed mutagenesis of the p53 cDNA before recombineering onto the BAC (see Appendix C for primer sequences).

Generation of NS150 chromosome

The NS150 chromosome was created by conventional chromosome recombination. F1 females trans-heterozygous for the *Dp53*^{NS} allele and GHP150 ctyoplasmic reporter were crossed to w; TM3,Sb/TM6,Tb,Hu double balancer males in vials. Single F2 male progeny with dark red eyes (indicating presence of *Dp53*^{NS}) were crossed to 3-5 w; TM3,Sb/TM6,Tb,Hu double balancer females and their progeny examined for presence of GFP (from the GHP150 transgene) by PCR (see Appendix C for primer sequences).

Acridine Orange staining in embryos and wing discs

Embryos were collected for 2.5 hrs, aged for 2.5 hrs, exposed to 40 gray of ionizing radiation in a Cs-137 Mark 1-68A irradiator (J.L. Shepherd & Associates) and then allowed to recover for 1.5 hours. Embryos were dechorionated with 50% bleach for 2-3 minutes, rinsed with water and placed into a 5ml glass vial with 2ml of Heptane and 2ml of 5ug/ml Acridine Orange in 1M Phosphate Buffer. Samples were shaken by vortex for 5 minutes and then the embryos were isolated and mounted onto glass slides with halocarbon oil 700 (Sigma). Wing discs were dissected from wandering 3rd instar larvae in PBS on a watchglass, incubated for 5 minutes in 5ug/ml Acridine Orange in 1M Phosphate Buffer, rinsed in PBS and mounted in PBS using two coverslips as “stands” so as to not squash the wing disc with the mounting coverslip.

Immunofluorescence

Whole ovaries were dissected in PBS, tips teased apart, fixed in PT (1X PBS, 0.1%Triton) with 4% Formaldehyde and heptane at a 1:3 volume/volume ratio for 15 minutes. Fixed samples were then washed with PT 4x7 minutes, blocked with PTA (1X PBS, 0.1% Triton, 1.5%BSA) for 1 hr, and incubated overnight at 4°C with primary antibody diluted in PTA. On the second day, the samples were rinsed 3 times with PT, washed with PTA 4x7 minutes, incubated with appropriate secondary antibody for 2 hrs at room temperature, rinsed again with PT 3 times and washed with PT overnight at 4°C. On the third day, the samples were rinsed with PBS once and mounted with VECTASHIELD + DAPI (Vector Labs).

The following antibodies and dilutions were used: mouse anti-hp53 DO-1 (Santa Cruz Biotechnology) was used at 1:1000, rabbit anti-hp53 7F5 (Cell Signaling) at 1:1000, rabbit anti-hp53 FL-393 (Santa Cruz Biotechnology) at 1:1000, rabbit anti-GFP (Invitrogen Molecular Probes) at 1:500, mouse anti-lamin Dm0 ADL894.12 (Developmental Studies Hybridoma Bank) at 1:100, mouse anti-Dp53 25F4 concentrated (Developmental Studies Hybridoma Bank) at 1:1000, rat anti-HTS/spectrin alpha (Developmental Studies Hybridoma Bank) at 1:500, mouse anti-γ-tubulin (Sigma) at 1:100, mouse anti-BEAF32 (Developmental Studies Hybridoma Bank) at 1:100, rabbit anti-lsm11 (kind gift from Mike Buszczak) at 1:1000, rabbit anti-Coilin (kind gift from Mike Buszczak) at 1:1000, and rabbit anti-dSUMO2/dSmt3 (Lehembre et al. 2000) at 1:500. Alexa-488 and Alexa-568 secondary antibodies (Invitrogen Molecular Probes) were used at 1:250. Custom Dp53 monoclonal antibodies (ID3 and IF6) were raised at Abmart Antibody Company (Shanghai, China) against epitope QDERQLNSKK.

Microscopes and image processing

Confocal micrographs were taken with Leica TCS SP5 and Carl Zeiss LSM780 laser confocal microscopes and either Leica software or Zeiss Zen software. Fluorescent light micrographs were taken with a Zeis Axioplan 2E microscope using Openlab software. All images were processed with Volocity Demo Version 6.1.1 (Perkin Elmer) unless noted otherwise. Figures were prepared with Microsoft PowerPoint.

Figure 3-15 image processing

All samples were dissected, fixed and stained in parallel. Confocal micrographs were taken with a Zeiss LSM780 (Carl Zeiss) laser confocal microscope using a 40X objective lens with 4X digital zoom. All imaging was done with the same laser intensities and master gain settings. Z-stacks were taken at 0.5um sections. Images were deconvolved in AutoQuant (AutoQuant, Albany, NY) software using 10 iterations of 3D blind deconvolution. Images were then processed using Imaris 7.6.5 software (Bitplane, Zurich, Switzerland). All channels were background substracted at 8.39 and then the red channel was baseline substracted at 37895.9. Nuclear foci were isolated by masking all hp53 signal that was outside of the DAPI surface. Nuclear foci contacting lamin were isolated by masking all nuclear foci that was outside of lamin surface.

Immunoblotting and antibodies

Protein lysates were separated by SDS-PAGE, transferred to Immobilon-P membranes (Millipore) using a wet transfer apparatus (Biorad) and immunoblotted with respective antibodies. Blots were visualized using enhanced chemiluminescence (GE Healthcare). Mouse DO-1 anti-hp53 (Invitrogen Molecular Probes) was used at 1:1000, rabbit anti-GFP

(Invitrogen Molecular Probes) at 1:500 , mouse E7 anti-tubulin (Developmental Studies Hybridoma Bank, University of Iowa) at 1:5000 and anti-mouse-HRP/anti-rabbit-HRP (Jackson Immuno Research Laboratories, Inc) at 1:5000.

RT-PCR and quantitative RT-PCR

Total RNA from embryos or ovaries was isolated using TRIzol reagent (Life Technologies). 1ug of total RNA was used to make cDNA using iScript cDNA synthesis kit (BioRad) and this was used for either RT-PCR or quantitative RT-PCR. RT-PCR was performed using GoTaq DNA polymerase (Promega). Quantitative PCR was performed using iQ SYBR Green Supermix (BioRad) on the BioRad CFX96 real time PCR machine. Primer efficiency was taken into account for all reactions. Rp49 was used for normalization.

Results

Overexpression of hp53 in the germline can complement Drosophila p53

It is known that *Drosophila* p53 (*Dp53*) can bind the human p53 (hp53) response element *in vitro* (Brodsky et al. 2000). To determine whether hp53 could functionally replace *Dp53*, I tested whether hp53 can activate a biosensor for *Dp53* transcriptional activity. This *Drosophila* p53 biosensor (p53R-GFPcyt/GHP150) is endogenously activated by *Dp53* in germline cells during meiotic recombination in 8- and 16-cell cysts (Lu et al. 2010). Furthermore, this biosensor is selectively activated in stem cells after genotoxic or oncogenic stress (Wylie et al. 2014). Strikingly, overexpression of hp53 in the germline activated the p53 biosensor in 8- and 16-cell cysts and in early egg chambers of $dp53^{-/-}$ flies (Figure 3-2). Activation of the biosensor mimicked the expression pattern of nanos-Gal4 (Figure 3-2) rather than the *Dp53* activation pattern, suggesting that hp53 is constitutively active and does not respect negative regulation of *Dp53* activity. Unfortunately, because expression with nanos-Gal4 begins at the 8- and 16-cell cyst stage, I could not test whether hp53 activated the biosensor in stem cells after gamma-irradiation. Nevertheless, these results encouraged me to pursue the idea of using *Drosophila* as a system with which to study human p53 gain-of-function mutations.

Creating a platform to study human p53 cancer mutations in Drosophila

To study human p53 mutants, I decided to create humanized p53 flies (Figure 3-3). I considered replacing the native *Dp53* ORF with hp53 cDNA, however, the laborious nature of targeted recombination would undermine the versatility of this platform. Instead, I targeted

Dp53 on a BAC carrying the *Dp53* locus by *in vitro* recombineering and subsequent;y integrated this genomic fragment into the *Drosophila* genome using phiC31 site-directed recombination (See Materials and Methods and Figure 3-4). Additionally, to facilitate screening of transformants, I positively marked the humanized BACs with a RFP cassette that was later excised using Cre-recombinase (see Figure 3-5A). This approach allowed preservation of all native regulatory elements while providing versatile manipulation of the *Dp53* locus and efficient generation of transgenics.

Drosophila p53 encodes two isoforms – *Dp53* and *DΔNp53*. *Dp53* consists of exons A and B spliced into exons 2-8, while *DΔNp53* has an internal promoter that drives expression of only exons 1-8 (Figure 3-4A). *DΔNp53* is the originally described isoform described in the landmark paper by Abrams et al (Brodsky et al. 2000). Recently, both *Dp53* and *DΔNp53* were shown to induce apoptosis (Dichtel-Danjoy et al. 2013), but differences in spatiotemporal expression have not been examined. In order to preserve both the *Dp53* and *DΔNp53* promoters and 5'UTRs, I decided to only replace exons 1-8 with hp53 cDNA (Figure 3-4B). This humanized p53 line is referred to as $hp53^{1}$. Additionally, I mutated the start codon at exon A in one of the lines in order to preferentially drive expression of hp53 under control of the *DΔNp53* promoter. This line is referred to as $hp53^{2}$. The humanized mutant p53 lines do not contain a mutation in the exon A start codon and are referred to by their missense mutation.

By using the methods described above, I successfully generated 8 transgenic lines: one *Dp53* rescue line ($Dp53^{+}$), 2 wild-type humanized p53 lines ($hp53^{1}$ and $hp53^{2}$, referred to as wild-type hp53 lines) and 5 mutant humanized p53 lines (R175H, G245S, R248Q, R273C

and R273H, referred to as mutant hp53 lines) which represent five of the most common hot-spot mutations in human cancer (Brosh and Rotter 2009) (See Materials and Methods and Appendix B). In addition, humanized p53 BACs for the remaining 3 hot-spot mutations (R248W, G249S and R282W) were engineered and can be used to generate the respective mutant lines if so desired (see Appendix C).

When I initially received the hp53 lines, hp53 expression was significantly lower than native *Dp53* expression (Figure 3B) but after Cre-mediated excision of the 3' RFP cassette (Figure 3A), I found expression levels were comparable (Figure 3-5B). All of the humanized lines used in this study were first crossed to Cre to remove the RFP cassette, sequence confirmed, then placed into $Dp53^{-/-}$ genetic backgrounds and then verified by PCR (See Materials and Methods). After crossing into a $Dp53^{-/-}$ background, wild-type hp53 transcript levels were significantly reduced (compare Figure 3-5B and 3-5C), suggesting that perhaps *Dp53* positively regulates hp53 by binding to the native regulatory elements present in the humanized genomic fragment. Two alleles of *Dp53* were used for complementation: $Dp53^{5A-1-4}$ and $Dp53^{NS}$ (See Appendix B for collection). Interestingly, humanized lines were healthier in the $Dp53^{5A-1-4}$ background than in the $Dp53^{NS}$ background (data not shown), suggesting these alleles are functionally different or that one of them contains a background modifier.

Humanized p53 flies can induce apoptosis in the embryo and the developing wing

Dp53 robustly induces apoptosis in the embryo and the developing wing in response to genotoxic stressors such as gamma-irradiation (Figure 3-6). To test whether this apoptotic response is intact in humanized p53 flies, I stained irradiated embryos and wing discs with acridine orange (AO) to label dying cells. Humanized p53 embryos and wing discs do not

exhibit signs of apoptosis under normal conditions but, like *Dp53*$^{+}$ flies, can induce an apoptotic response upon irradiation (Figure 3-6). However, AO staining in the wing disc of humanized p53 flies is noticeably different than that of *Dp53*$^{+}$ flies. Dying cells in humanized p53 wing discs seem to clump together resulting in patches of AO^{+} cells, whereas they are more evenly distributed in *Dp53*$^{+}$ tissue (Figure 3-6B). These results demonstrate that humanized p53 flies can promote stress-induced apoptosis, showing that hp53 can complement *Dp53* function *in vivo*. Unexpectedly, hp53 failed to upregulate a set of radiation induced p53-dependent (RIPD) genes required for apoptosis in the embryo – rpr, skl and hid (Figure 3-7).

Wild-type but not mutant humanized p53 flies can activate the p53 biosensor

To determine whether humanized p53 flies can activate an *in vivo* p53 biosensor, I crossed the humanized p53 lines into a *Dp53*$^{-/-}$ background carrying the p53 biosensor (NS150, see Materials and Methods). NS150 flies were compromised for endogenous and stimulus-dependent biosensor activation, but this was rescued by the *Dp53*$^{+}$ rescue (Figure 3-8A), mapping reporter activation to in the germline to *Dp53*. Strikingly, the two wild-type humanized lines potently activated the biosensor throughout the germline (Figure 3-8A and 39A). Interestingly, biosensor activation by hp53 was upregulated after irradiation challenge without increase in protein levels (Figure 3-9A), suggesting that hp53 is being activated post-translationally by Dp53 upstream regulators Chk2 or ATM. This is significant as the current model for p53 activation centers around its stabilization, not activation. In contrast, the five hot-spot mutations were silent for biosensor activation *in vivo* as seen by immunofluorescence (Figure 3-8B) and western blot (Figure 3-9B). Failure to activate the

p53 biosensor was not due to decreased levels since humanized mutant lines express hp53 at levels comparable to humanized wild-type lines (Figure 3-10). Taken together, these results show that humanized p53 can activate a *Drosophila* p53 biosensor in the germline and that p53 mutants are compromised for transactivation of this reporter.

Human p53 mutants do not show increased stability

Accumulation of mutant p53 is a common hallmark of cancer (Lubin et al. 1995). To determine whether mutant p53 proteins show increased stability in humanized flies, I blotted lysates from wild-type and mutant ovaries with DO-1, a widely used monoclonal hp53 antibody that recognizes both wild-type and mutant protein (Figure 3-10). Both wild-type and mutant hp53 are expressed at comparable levels in the ovary, suggesting that p53 mutants are not inherently more stable than the wild-type protein in this heterologous system. Furthermore, *in vivo* staining with DO-1 shows that mutant hp53 does not accumulate in the germline of humanized p53 mutants (Figure 3-11A). These results are consistent with studies in mice and Li-Fraumeni patients (Lang et al. 2004; Olive et al. 2004) which show that mutant p53 proteins do not accumulate in untransformed tissue.

Hp53 forms nuclear foci in the germline of humanized p53 flies

To determine whether subcellular localization of hp53 mutant protein can account for the loss of transactivation potential in the germline, I stained ovaries from humanized mutant p53 flies with DO-1. Both wild-type and mutant protein was found in the nucleus of germline cells in the germarium as well as other tissues (not shown). Thus, inability to activate the p53 biosensor is not due to defective translocation into the nucleus.

Strikingly, humanized wild-type p53 flies exhibited prominent foci throughout the germarium (Figure 3-11A) and in early egg chambers. Staining the nuclear membrane with anti-lamin revealed that these foci were predominantly nuclear (Figure 3-11B) but also present in the cytoplasm (Figure 3-15F). In contrast, none of the mutant hp53 flies exhibited prominent foci in the germline (Figure 3-11A and 3-15A), showing that these proteins behave differently than their wild-type counterpart. This difference was not dependent on protein levels as both the wild-type and mutant proteins are expressed well in this tissue (Figure 3-11A).

These results show that although wild-type and mutant p53 proteins are all imported into the nucleus, mutant p53 is disrupted for its ability to form foci. Thus, mutant protein can be distinguished from wild-type protein, allowing stratification of oncogenic mutants. Furthermore, this shows that the ability of to transactivate the p53 biosensor correlates with the protein's ability to associate into prominent nuclear foci.

Hp53 foci localize to Drosophila p53 foci but not to known nuclear body markers

Like humanized p53 flies, wild-type flies form nuclear *Dp53* foci in the germline (Figure 3-12A). To determine whether hp53 foci behave like *Dp53* foci, I costained ovaries from humanized p53 flies in a $Dp53^{+/-}$ background using anti-hp53 and anti-*Dp53*. As expected, hp53 and *Dp53* foci colocalized frequently (Figure 3-12B), showing that hp53 interacts with the subnuclear architecture similarly to *Dp53*. This observation is consistent with our previous observations that hp53 can functionally complement *Dp53 in vivo* and suggests that hp53 is localizing to the same nuclear compartment as *Dp53*.

To determine the identity of these hp53/*Dp53* foci, I decided to costain with markers for nuclear architecture and nuclear bodies. In samples costained with anti-lamin, hp53 foci seemed to localize near the lamin signal (Figure 3-11B), suggesting that these foci are associated with the nuclear membrane. Later experiments revealed that this was indeed the case (Figure 3-15F). As seen in Figure 3-13, hp53 foci did not colocalize with markers for Cajal bodies, histone locus bodies, or insulator bodies. Additionally, hp53 foci did not localize to the nucleolus (as seen by DAPI staining, data not shown). Because humanized p53 flies typically have 2-4 prominent foci per nucleus, which resembles staining for centrosomal proteins, I costained with gamma-tubulin but did not observe colocalization (Figure 3-13D). Since p53 has been shown to bind to promyelocytic (PML) nuclear bodies in humans, I costained for the *Drosophila* ortholog of SUMO2 – a characteristic modification found in PML bodies (Fogal et al. 2000). Surprisingly, there were many instances of colocalization with hp53 (Figure 3-14), suggesting that perhaps hp53 foci are localizing to a PML body precursor in the fly.

Taken together, these results show that hp53 foci interact with subnuclear architecture like *Dp53* and that patterns of subnuclear localization can discriminate between wild-type and gain-of-function hp53 mutants. Furthermore, these foci might be localizing to a PML body precursor in *Drosophila*.

Hot spot mutants can be stratified by their foci

The overarching goal of this platform is to discover phenotypes that can allow us stratify human p53 mutations and test whether this stratification has prognostic value. Hp53 foci in humanized p53 flies might provide a read out that can be used to stratify these mutations.

To this end, I analyzed confocal micrographs of germaria from humanized p53 flies stained with anti-hp53 and quantified different properties of hp53 foci using Imaris software.

After processing the micrographs in Imaris (see Materials and Methods), the difference between wild-type and mutant hp53 foci became very apparent (Figure 3-15A and B). Notably, hp53 mutants show some instances of foci but they are greatly reduced both in size (Figure 3-15C) and in number (Figure 3-15D). Additionally, mutants display a higher incidence of foci in cytoplasm (Figure 3-15E), consistent with observations that p53 mutants preferentially accumulate in the cytoplasm (Morselli et al. 2008). Interestingly, localization to the nuclear membrane is not affected in hp53 mutants (Figure 3-15F), suggesting that although they are compromised for biosensor activation and foci formation, they can still localize to nuclear architecture. Furthermore, not all hp53 mutants behaved the same. R248Q, a conformational mutant, exhibited larger and more abundant foci than the rest of the mutants (Figure 3-15C,D). These results show that wild-type and missense mutant hp53 behave dramatically different at a cellular level *in vivo* and that stratification of hp53 mutants is possible by applying this parameter with our genetic platform.

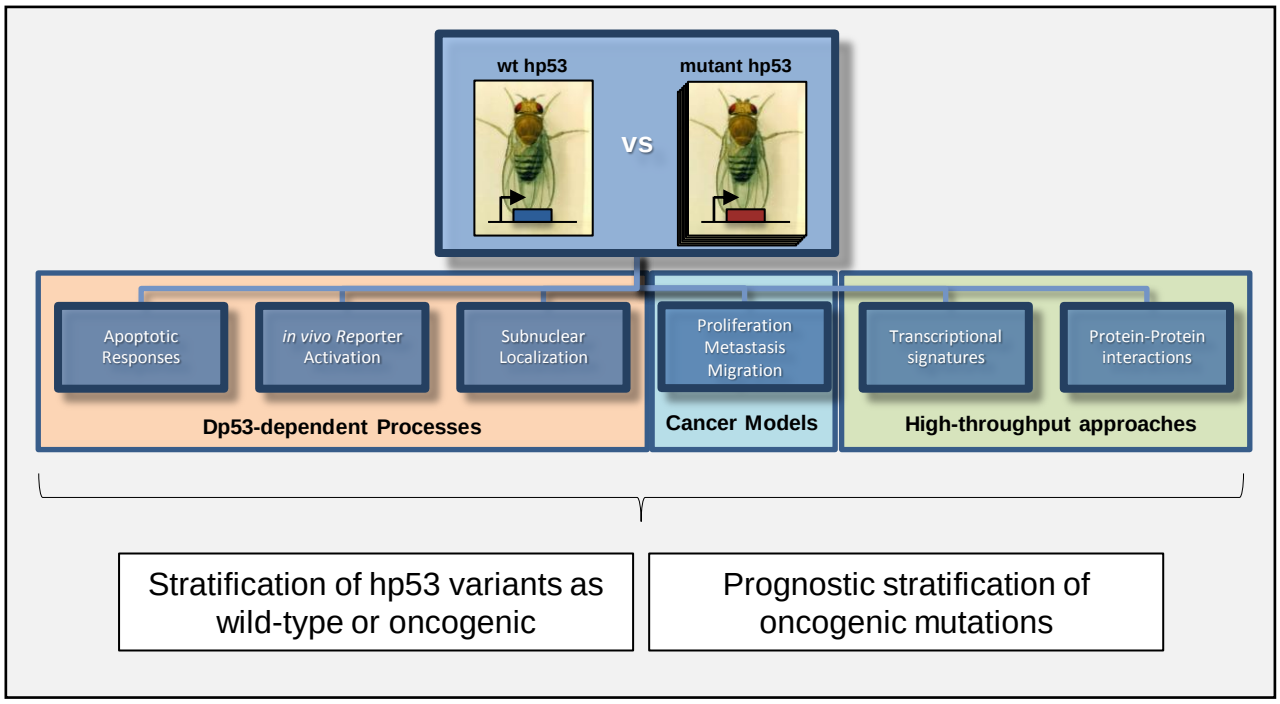

Figure 3-1. *Drosophila* as a platform to study oncogenic human p53 mutations. Schematic illustrating the power of a *Drosophila* platform. Various assays and approaches can be used to uncover novel gain-of-function activities in oncogenic hp53 mutants and discover common properties that allow us to differentiate oncogenic variants from wild-type variants. Furthermore, differences discovered between mutants might allow for prognostic stratification.

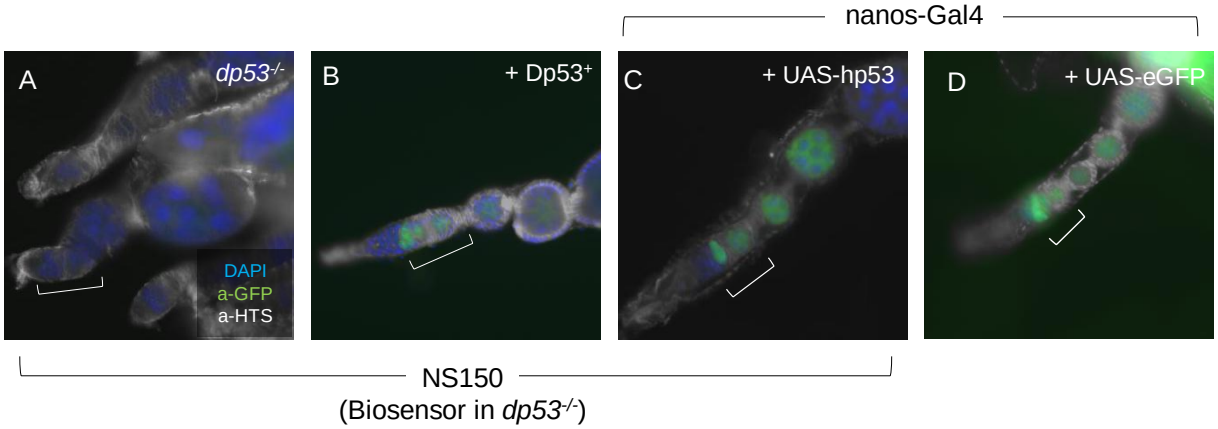

Figure 3-2. Overexpression of hp53 in the germline can activate a p53 biosensor. Light micrographs of whole mount immunofluorescence on ovaries from NS150 (A), $Dp53^{+}$;NS150 (B), nanos-Gal4>UAS-hp53;NS150 (C) or nanos-Gal4>UAS-eGFP (D). NS150 flies carry a p53 biosensor in a $dp53^{-/-}$ background. Biosensor activation in the region 2a/2b (white bracket) is absent in NS150 ovaries (A) but restored by presence of a *Dp53* genomic fragment (B). Overexpression of hp53 by nanos-Gal4, a germline driver, can activate the p53 biosensor in region 2a/2b as well as in early egg chambers (C). This pattern of reporter activation mimics the expression pattern of the nanos-Gal4 driver seen in in (D).

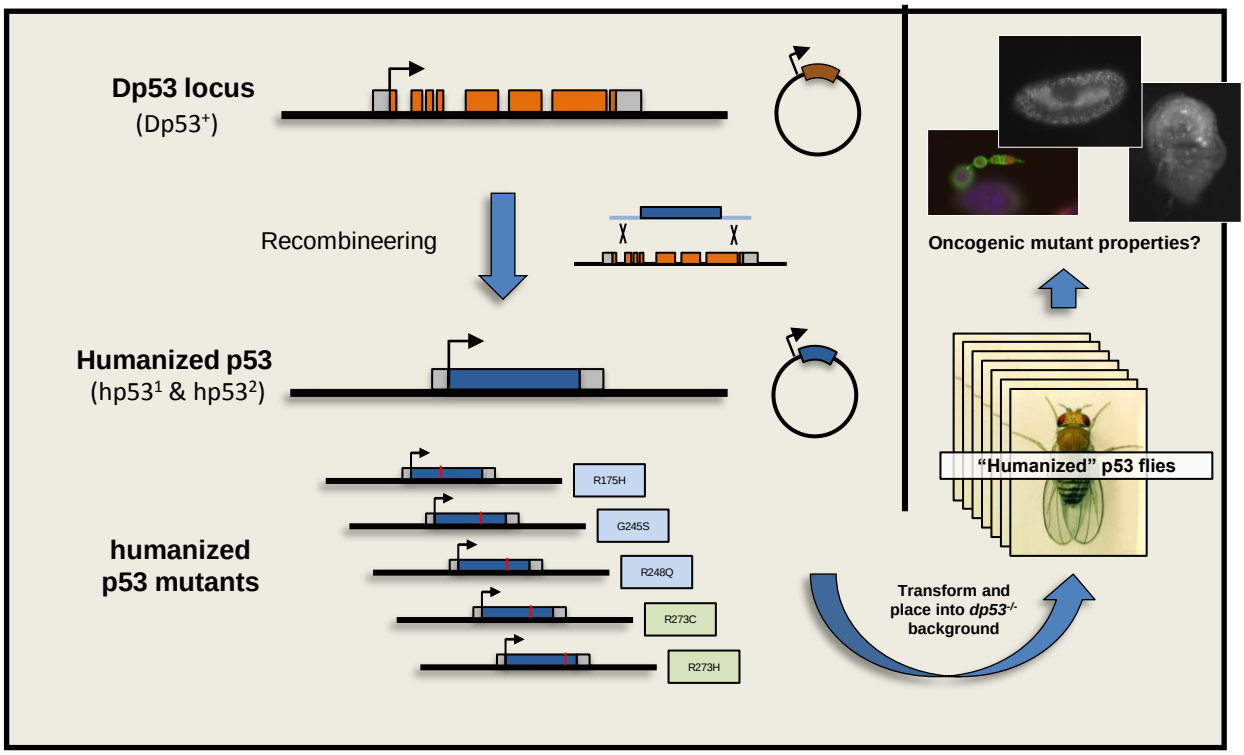

Figure 3-3. Generating humanized p53 flies. Schematic of how humanized p53 flies were generated. The *Dp53* ORF (orange) is replaced with hp53 cDNA (blue) in a BAC containing the *Dp53* locus, including all native regulatory elements. For humanized p53 mutants, hp53 cDNA with single missense mutations was recombineered into the *Dp53* BAC. Two of the mutations are classified as "conformational" mutants (light blue) and the other three as "contact site" mutants (light green). These humanized genomic fragments were injected into embryos carrying an attP-integration site for transformation and then transformants were placed in a $dp53^{-/-}$ background to assay for oncogenic mutant properties.

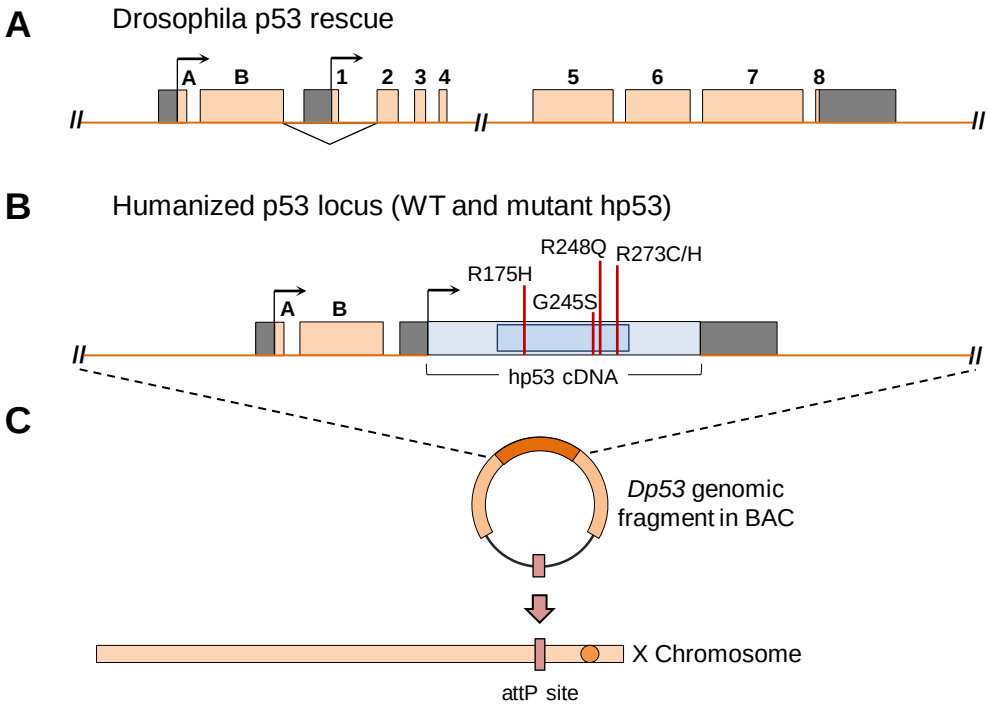

Figure 3-4. Humanizing the *Dp53* locus. Schematic showing how *Dp53* was "humanized." The *Dp53* rescue (A) and six humanized p53 lines (B) were generated by integrating a BAC containing an unmodified (A) or recombineered (B) 20kb genomic fragment of the *Dp53* locus into an attP landing site in the genome via phiC31-driven recombination (C). Exons 1-8 of the *Dp53* locus code for the predominant gene product (A). Exons A and B splice onto exon 2 to encode a longer and less prevalent isoform of *Dp53* (A). Translation start sites for both isoforms are shown as black arrows. To generate a wild-type humanized p53 line, exons 1-8 of *Dp53* were replaced with wild-type human p53 (hp53) cDNA via recombineering (B) and then integrated into the same attP landing site on the X chromosome used for the *Dp53* rescue (C). Directed point mutations were made in the wild-type hp53 cDNA to generate humanized p53 mutant lines comprising five of the most prevalent hot-spot mutations found in human tumors: R175H, G245S, R248Q, R273C and R273H. The respective prevalence of the five mutations are indicated by height of the red bars (B). Orange: *Drosophila* sequence and exons, gray: UTRs, blue: human sequence, dark blue: hp53 DNA binding domain.

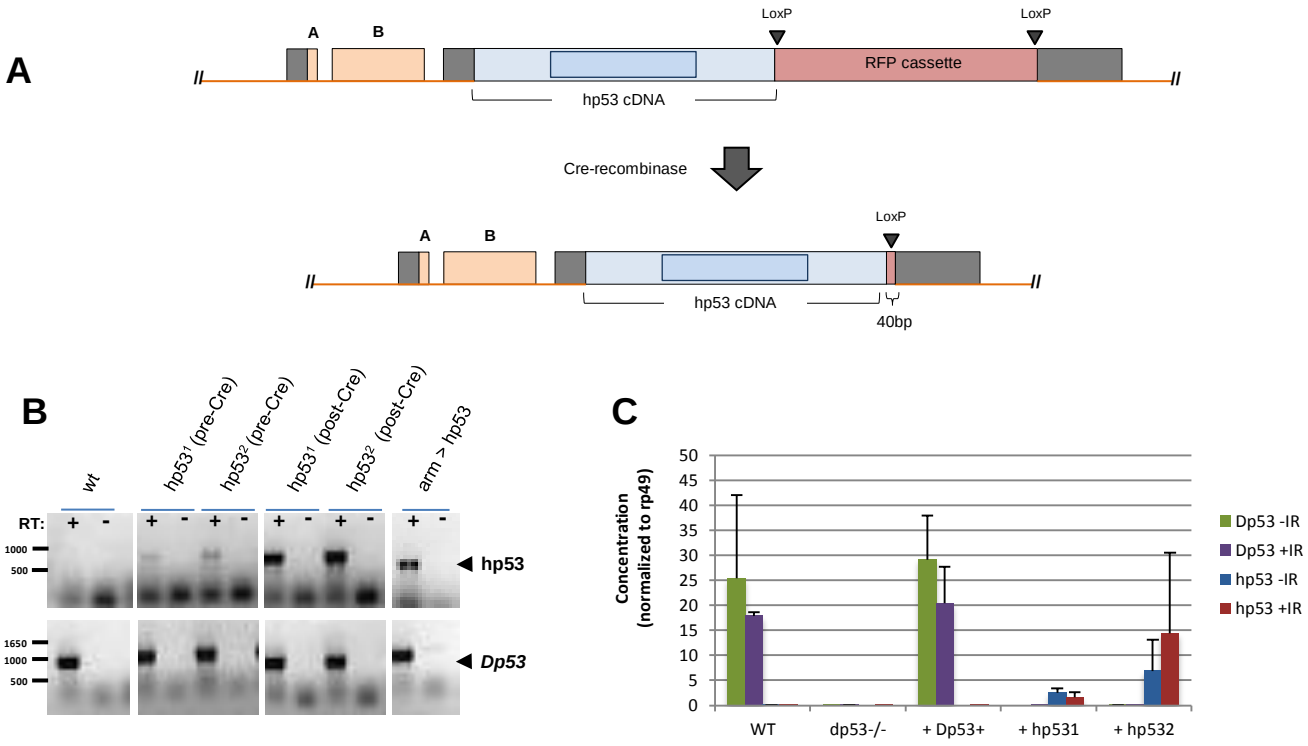

Figure 3-5. Excision of RFP cassette is required for hp53 expression. (A) To generate humanized p53 flies, a RFP/kanamycin cassette was used for selection during recombineering and as a marker for screening of transformants. This cassette was removed by crossing in a Cre-recombinase transgene, leaving only a 40 bp "scar." (B) Hp53 expression in humanized p53 flies with the RFP cassette (pre-Cre) was significantly lower than *Dp53* expression, but excision of the cassette (post-Cre) restored hp53 expression to levels comparable to those of *Dp53*. Armadillo-Gal4 driving UAS-hp53 was used as a hp53 positive control. (C) Quantitative RT-PCR normalized to *rp49* was used to compare transcript levels of *Dp53* and hp53 in a $dp53^{-/-}$ background (C). WT: *yw*, $dp53^{-/-}$: $dp53^{5A\text{-}1\text{-}4/5A\text{-}1\text{-}4}$, + $Dp53^{+}$: $Dp53^{+};dp53^{5A\text{-}1\text{-}4/5A\text{-}1\text{-}4}$, + $hp53^{1}$: $hp53^{1};dp53^{5A\text{-}1\text{-}4/5A\text{-}1\text{-}4}$.

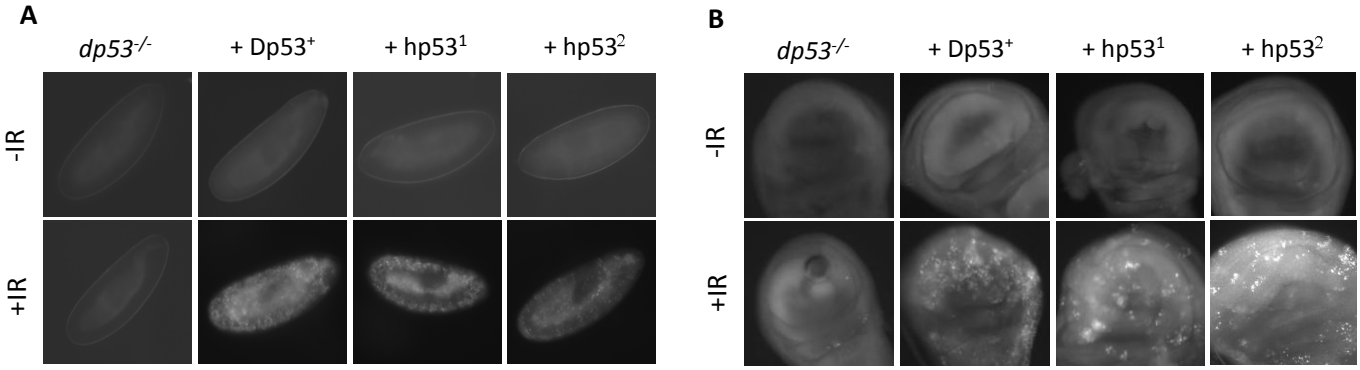

Figure 3-6. Hp53 restores IR-induced apoptosis in embryos and wing discs. Acridine Orange (AO) staining of embryos (A) and wing discs (B) before (-IR) and after (+IR) irradiation at 40 gray. Notice that *dp53*$^{-/-}$ embryos and wing discs do not elicit a radiation-induced apoptotic response. This response is restored in the presence the Dp53^{+} rescue fragment or wild-type hp53 (hp53^{1} or hp53^{2}). *dp53*$^{-/-}$: NS150/TM3,Sb, +Dp53^{+}: *Dp53*$^{+}$;NS150/TM3,Sb, +hp53^{1}: hp53^{1};NS150/TM3,Sb, +hp53^{2}: hp53^{2};NS150/ TM3,Sb.

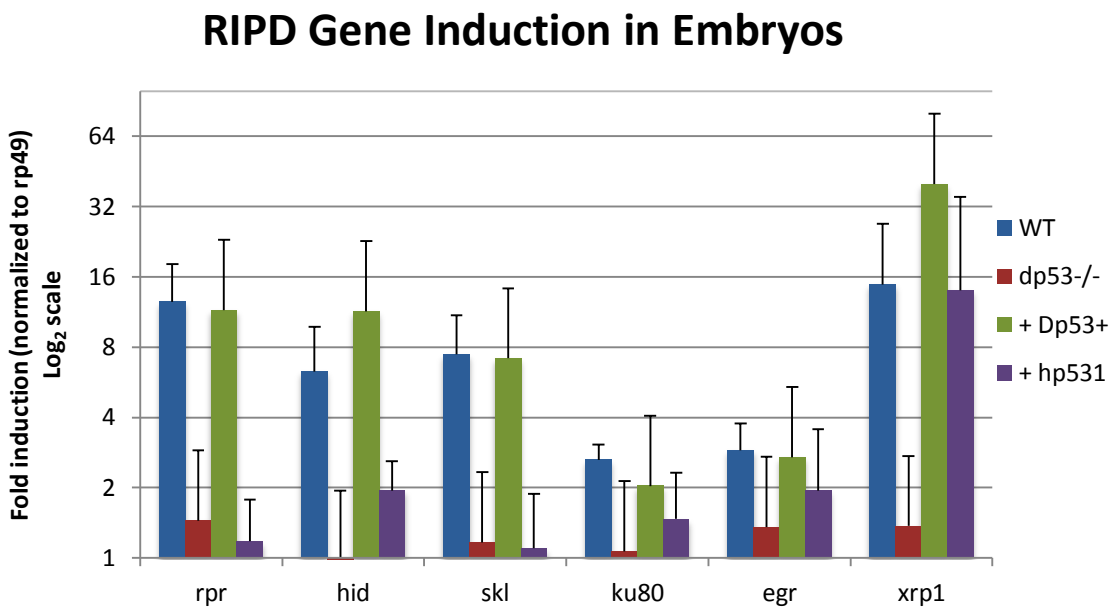

Figure 3-7. RIPD gene induction in embryos. Embryos of the indicated genotypes were collected, aged, mock treated or irradiated at 40 gray, allowed to recover and then processed for RNA (see Materials and Methods). WT embryos show induction of all RIPD genes after irradiation. This response is lost in *dp53*$^{-/-}$ embryos and rescued with the Dp53^{+} genomic fragment. hp53^{1} shows potent rescue of Xrp1 induction and modest rescue of hid, ku80 and egr induction but failed to induce rpr and skl. All signal was normalized to rp49 housekeeping gene levels. Note log scale to accommodate Dp53^{+} induction of Xrp1. WT: *yw*, dp53$^{-/-}$: *dp53*$^{5A\text{-}1\text{-}4/5A\text{-}1\text{-}4}$, + Dp53^{+}: *Dp53*$^{+}$;*dp53*$^{5A\text{-}1\text{-}4/5A\text{-}1\text{-}4}$, + hp53^{1}: hp53^{1};*dp53*$^{5A\text{-}1\text{-}4/5A\text{-}1\text{-}4}$.

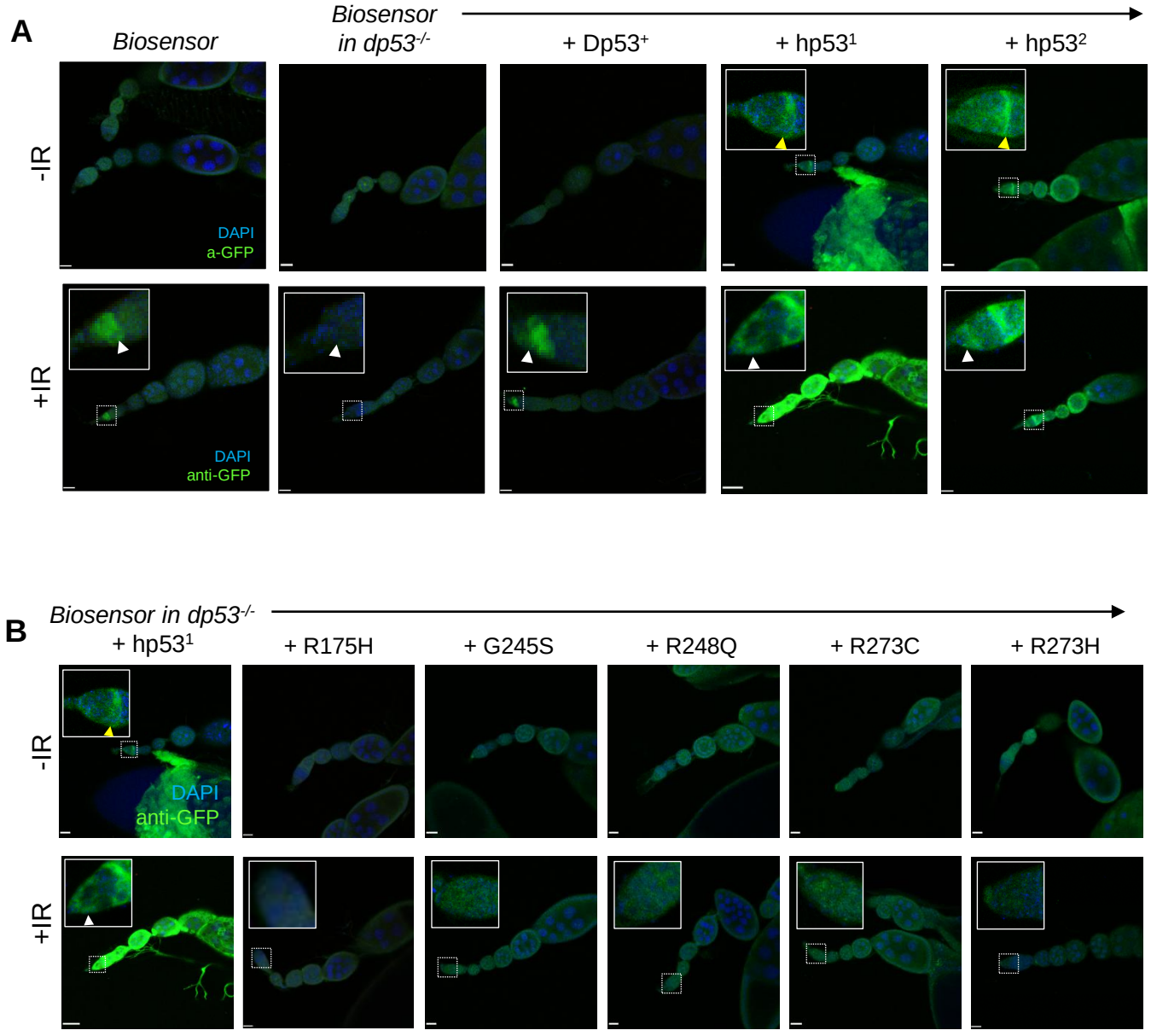

Figure 3-8. Wild-type but not mutant hp53 can activate a p53 biosensor. Confocal micrographs of immunofluorescence on ovaries before (-IR) or 24 hours after irradiation (+IR) at 40 gray. Ovaries from flies of the indicated genotypes were stained with anti-GFP to detect activation of a p53 biosensor. Insets focus on region 1 (white arrowheads) of the germarium, where stem cells reside. Wellow arrowheads indicate region 2a/2b where meiotic recombination normally activates *Dp53*. Black arrow indicates presence of a p53 biosensor in a *dp53*$^{-/-}$ background. Notice that the *Dp53* rescue (Dp53^{+}) can restore biosensor activation in the stem cells (A, inset) and that WT (hp53^{1} or hp53^{2}) but not mutant (R175H, G45S, R248Q, R273C, R273H) hp53 can activate the biosensor in the ovariole (B). Biosensor in *Dp53*$^{+/+}$: GHP150, biosensor in *dp53*$^{-/-}$: NS150/TM3,Sb. All other genotypes are the indicated BAC (*Dp53*$^{+}$, hp53^{1}, etc) in a NS150/TM3,Sb background.

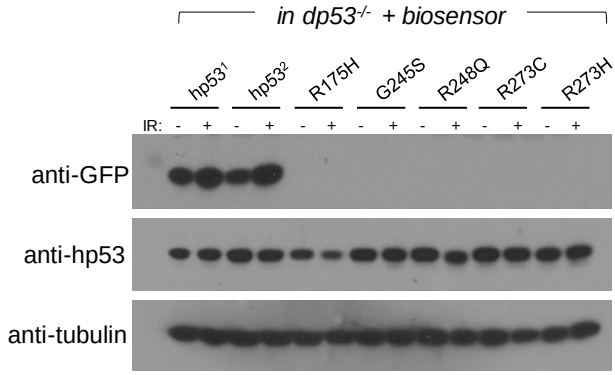

Figure 3-9. Stimulus activates wild-type hp53 without increase in stabilization. Western blots of ovary lysates from humanized p53 flies carrying a p53 biosensor in a $dp53^{-/-}$ background before (-) or 24 hours after (+) irradiation at 40 gray. Wild-type hp3 flies ($hp53^{1}$ and $hp53^{2}$) show radiation-induced upregulation of the biosensor (anti-GFP) without increased stabilization of hp53 (anti-hp53). Notice that the five oncogenic mutants fail to activate the biosensor. All flies were $dp53^{-/-}$ + biosensor: NS150/TM3,Sb. Anti-tubulin serves as a loading control. Anti-hp53: DO-1 monoclonal antibody.

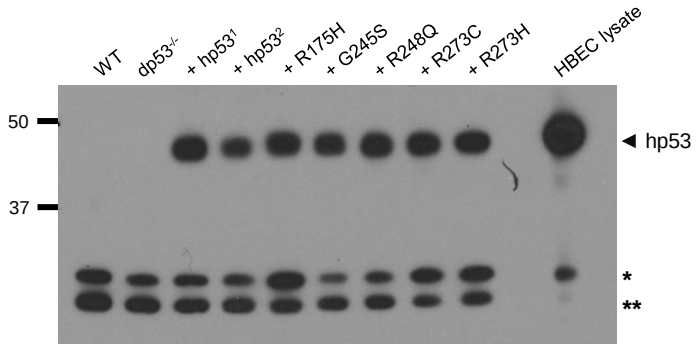

Figure 3-10. Wild-type and mutant p53 humanized lines express hp53 at similar levels. Western blot for hp53 levels in ovary lysates from flies before (-) or 24 hours after irradiation (+) at 40 gray. Wild-type and all five mutant hp53 lines express hp53 (black arrow) at similar levels. HBEC lysate was included as a positive control for full-length hp53. Notice that wild-type or $dp53^{-/-}$ ovary lysates do not have any DO-1 signal around 50kD. * and ** denote non-specific cross-reacting bands. ** serves as a loading control. WT: *yw*, $dp53^{-/-}$: $dp53^{5A\text{-}1\text{-}4/5A\text{-}1\text{-}4}$. All other genotypes are the indicated BAC ($hp53^1$, $hp53^2$, etc) in a $dp53^{5A\text{-}1\text{-}4/5A\text{-}1\text{-}4}$ background. Anti-hp53: DO-1 monoclonal antibody. HBEC: human bronchial epithelial cells.

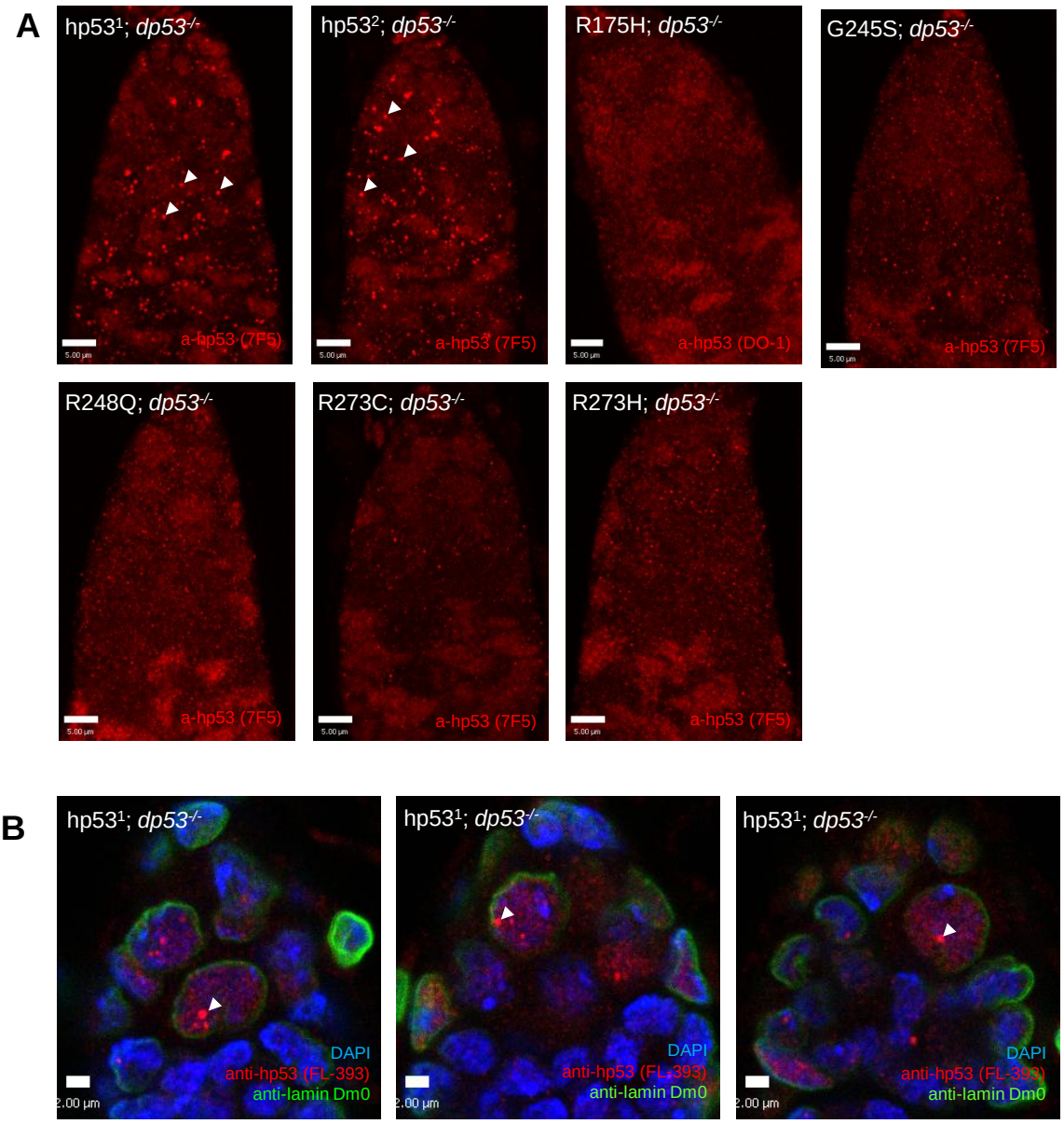

Figure 3-11. Wild-type but not mutant hp53 can form nuclear foci in the germline. Confocal micrographs of immunofluorescence on whole mount ovaries. (A) Collapsed Z-stacks (~50um) of germaria from wild-type hp53 ($hp53^1$ or $hp53^2$) or mutant p53 in a $dp53^{-/-}$ background stained with anti-hp53 7F5 or DO-1. Arrowheads indicate representative foci. Notice lack of foci in mutants. (B) Single Z-slices of wild-type hp53 costained with anti-lamin and anti-hp53 FL-393. Arrowheads indicate representative foci. Notice that foci colocalize with DAPI lie within the nuclear membrane (lamin signal) and sometimes appear associated with lamin. *dp53-/-*: $dp53^{5A\text{-}1\text{-}4/5A\text{-}1\text{-}4}$.

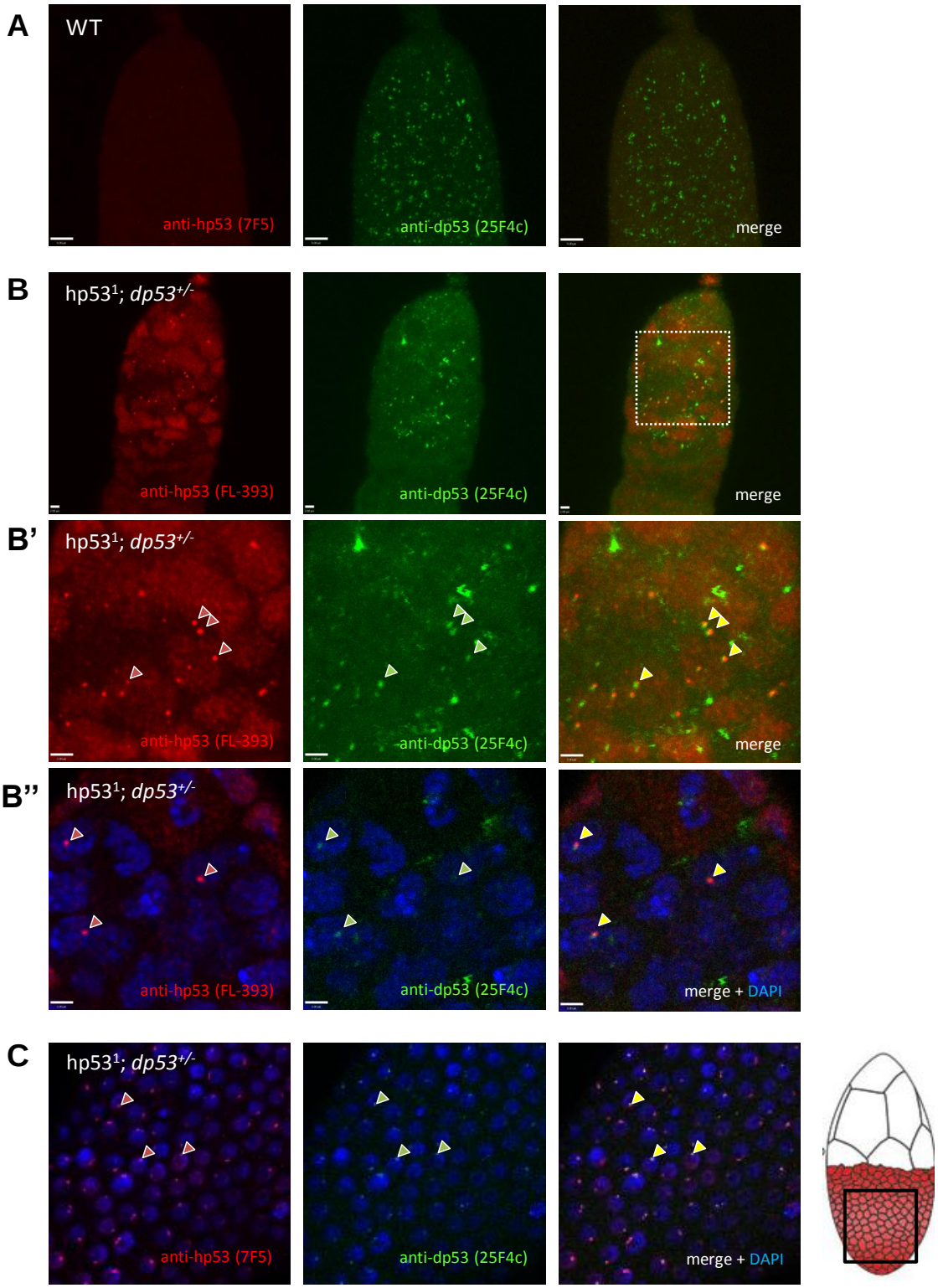

Figure 3-12. hp53 foci colocalize with Dp53 foci. Confocal micrographs of immunofluorescence on whole mount ovaries. (A) Collapsed Z-stacks (~50um) of wild-type germaria showing Dp53 foci. Notice that there is very little background with anti-hp53. (B and B'') Collapsed Z-stacks (~50um) of germaria showing hp53 and Dp53 colocalization. (B') is a higher magnification image of the dotted area in (B). (B'') A single z-slice from the dotted region in (B)showing hp53 and Dp53 colocalization. (C) A collapsed Z-stack of egg chamber follicle cells (see cartoon on right) showing hp53 and Dp53 colocalization. Arrowheads indicate representative foci colocalization. All genotypes are: $hp53^{1}$; +/TM3,Sb.

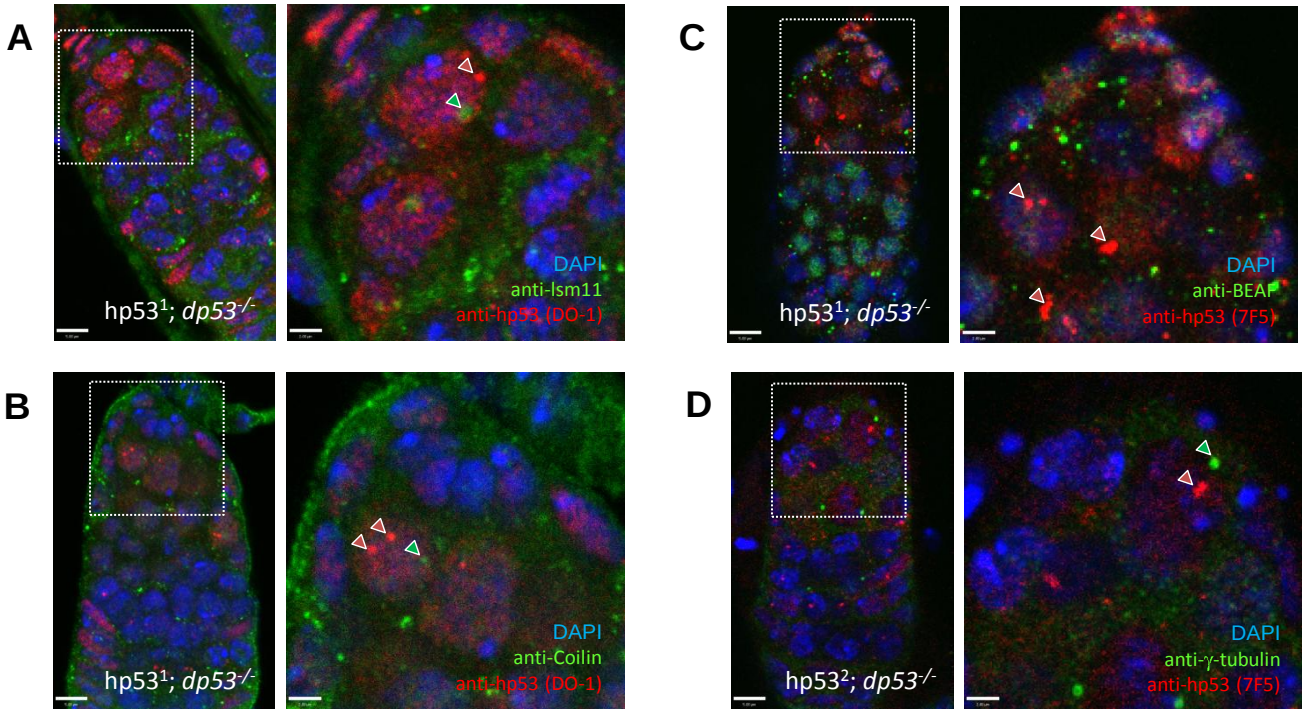

Figure 3-13. hp53 foci do not colocalize with known nuclear body markers. Confocal micrographs of immunofluorescence on whole mount ovaries. (A-D) are single Z-slices from a Z-stack. Costaining with anti-hp53 and markers for histone locus bodies (A), Cajal bodies (B), insulator bodies (C) or the cetrosome (D) did not show colocalization. Boxed regions are shown in higher magnification. Arrowheads indicate representative foci. *dp53*$^{-/-}$: *dp53*$^{5A\text{-}1\text{-}4/5A\text{-}1\text{-}4}$.

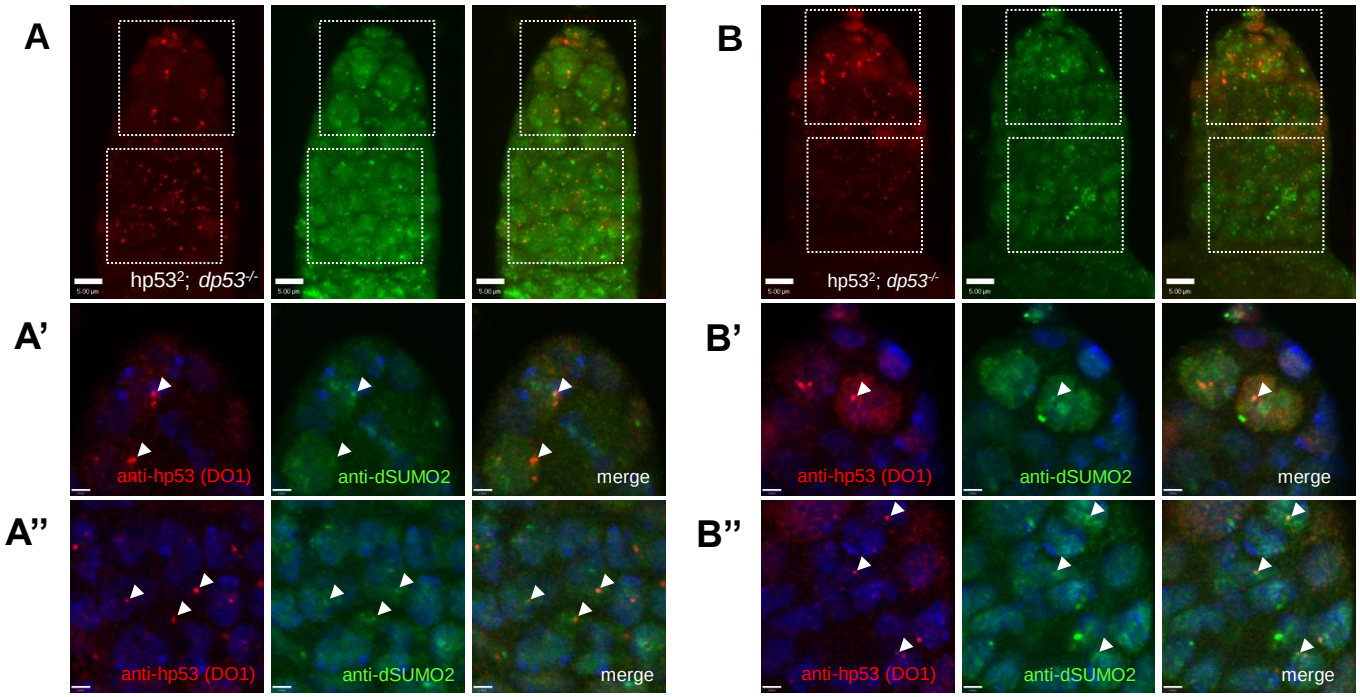

Figure 3-14. hp53 foci colocalize with dSUMO2 staining. Confocal micrographs of immunofluorescence on whole mount ovaries. (A and B) Collapsed Z-stacks (~50um) of germaria showing colocalizatoin of hp53 foci with dSUMO2 staining. (A' and B') Single Z-slices of boxed region 1 in (A) and (B) showing examples of hp53 and dSUMO2 colocalization. (A" and B") Single Z-slices of boxed region 2a/2b in (A) and (B) showing examples of hp53 and dSUMO2 colocalization. Arrowheads indicate representative foci. *dp53*$^{-/-}$: *dp53*$^{5A\text{-}1\text{-}4/5A\text{-}1\text{-}4}$.

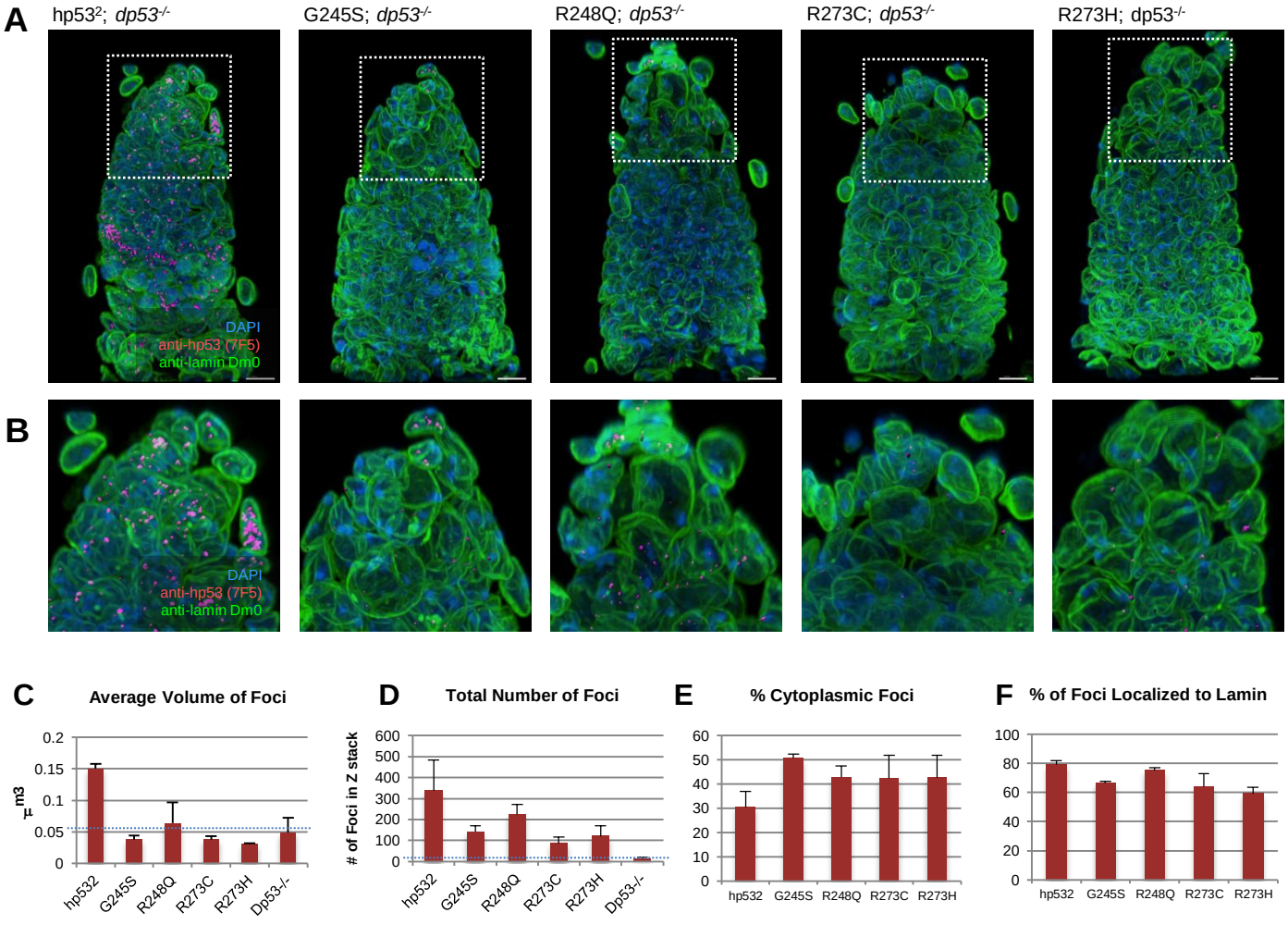

Figure 3-15. Hp53 mutants can be stratified by their foci. Confocal micrographs of immunofluorescence on whole mount ovaries processed with Imaris software. (A-B) Germaria of indicated genotypes showing hp53 nuclear foci in magenta, lamin in green and DAPI in blue. Notice hp53 mutants are compromised for foci seen in hp53[2]. For image processing see Materials and Methods. (C-F) Quantification of confocal micrographs in (A-B). Data represents two Z-stacks. (C) Average volume of foci in samples (in um3). (D) Total number of foci present within a ~50um Z-stack. (E) Percentage of foci that are cytoplasmic. (F) Percentage of foci that localize to lamin. Dotted blue line in (C) and (D) represent level of background. Genotype of *dp53*$^{-/-}$: *dp53*$^{5A\text{-}1\text{-}4/5A\text{-}1\text{-}4}$.

Discussion

Here I've shown the creation of a powerful *in vivo* genetic platform aimed at uncovering novel behaviors and activities that distinguish oncogenic p53 mutants from wild-type p53. Humanized p53 complements *Drosophila* p53 *in vivo* while mutants fail do so. Additionally, I discovered that hot-spot mutants fail to form subnuclear foci properly – a shared property that allows stratification of oncogenic mutants.

Human p53 studies in the fly have been limited to ectopic expression systems which are hampered because overexpression of hp53, like *Dp53*, potently induces cell death (Yamaguchi et al. 1999). I bypassed this limitation by humanizing *Drosophila* p53, where hp53 is under control of the same native regulatory elements that control *Dp53* expression. These flies express hp53 in the same tissues as *Dp53* and with the same dynamics, thus allowing the study of hp53 in biologically and developmentally relevant contexts.

To our surprise, humanized p53 flies were viable and competent for radiation-induced apoptosis (Figure 3-6) and for activation of a p53 biosensor (Figures 3-8A and 3-9A), thus validating *Drosophila* as a viable system in which to study human p53 and its mutant variants. Strikingly, although wild-type hp53 embryos are competent for radiation induced-apoptosis in the embryo, they do not induce strong expression of rpr, skl or hid like $Dp53^{+}$. This could be explained by the modest upregulation of hid (Figure 3-7) or upregulation of grim (which was not tested because it is not a RIPD gene). Interestingly, hp53 expression was reduced in a $Dp53^{-/-}$ background compared to a wild-type background (Figure 3-5C), suggesting that perhaps *Dp53* positively regulates the genomic hp53 fragment. However,

the lower transcript levels were not a concern since humanized p53 flies exhibit abundant hp53 protein and can rescue apoptosis (Figures 3-10 and 3-6).

Several observations in our humanized p53 system are consistent with what is known about p53 gain-of-function mutants from other studies. In knock-in mice for R172H and R270H (the mouse equivalent to R175H and R273H), p53 mutants were unable to transactivate the p53 target genes p21 and Mdm2 (Olive et al. 2004). Likewise, *in vivo* transcriptional activation of the p53 biosensor was abolished in humanized p53 mutant flies (Figures 3-8B and 3-9B). Interestingly, this observation correlates with the inability of p53 mutants to induce apoptosis or activate the p53 biosensor, suggesting that formation of foci might be a prerequisite for proper p53 function in the germline. Furthermore, p53 mutant knock-in mice revealed that hp53 mutants do not accumulate in normal tissue (Lang et al. 2004; Olive et al. 2004), debunking the long-held theory that mutant p53 imparts its oncogenic activity in part by its increased stability. Similarly, humanized mutant p53 flies do not show increased levels of hp53 when compared to humanized wild-type flies (Figure 3-10) nor do they show cellular accumulation of the mutant protein in the germline (Figure 3-11). This observation suggests that p53 mutant protein is not inherently more stable or prone to accumulation, but rather, supports the hypothesis that additional lesions are required for full oncogenic transformation. This might explain why humanized mutant p53 flies do not exhibit tumors or over-proliferative phenotypes of any kind.

To our surprise, hp53 upregulation of the biosensor in response to stress (Figure 3-9A) was not due to increased protein levels, as the current model of p53 activation suggests. Instead, I propose that hp53 is being postranslationally modified by the upstream kinases Chk2 and

ATM. This not only indicates that human p53 can replace Dp53 in its endogenous regulatory network, but challenges the conventional model of p53 activation.

A novel observation that has come out of this humanized p53 system is that subnuclear localization of hp53 can discriminate between wild-type and gain-of-function mutants (Figure 3-15). These hp53 foci are not artifactual since they colocalize with *Dp53* foci in the germline (Figure 3-12), suggesting that formation of hp53 foci in these cells is biologically relevant. Hp53 subnuclear localization has been described previously in the context of cellular stress (Fogal et al. 2000; Carbone et al. 2002) but what role localization plays in hp53 function and how mislocalization might contribute to mutant p53 gain-of-function has not been studied. Because these foci are disrupted in flies carrying p53 mutations found in human cancer (Figure 3-15C,D), understanding the nature of hp53 foci in humanized p53 flies might help get at these questions.

The observation that hp53 foci colocalize with dSmt3 (*Drosophila* SUMO2) in humanized p53 flies (Figure 3-14), might provide the key to identifying the nature of hp53 foci in humanized flies. SUMO2 is a modification characteristic of promyelocytic leukemia (PML) which has been associated with various disorders and pathologies including cancer (Gurrieri et al. 2004). PML forms higher-order nuclear domains PML nuclear bodies which recruit and modify p53 in response to stress (Ferbeyre et al. 2000; Fogal et al. 2000; Pearson et al. 2000). Interestingly, knockdown of PML in cell lines harboring p53 mutations is shown to impair their growth and cell cycle progression (Haupt et al. 2009), suggesting that PML might be involved in mutant p53 gain of function activity. Although *Drosophila* does not have a PML ortholog, nuclear foci containing SUMO2 and *Drosophila* Daxx-like protein, a protein

also found in mammalian PML nuclear bodies (Mauri et al. 2008) suggest that these might be the precursors to PML nuclear bodies in mammals. Interestingly, ectopically expressed *Dp53* localizes to these proto-PML bodies *in vivo* (Mauri et al. 2008). It will be interesting to see whether hp53 is in fact associating with proto-PML bodies and whether this interaction is modified in p53 mutants.

Lastly, one of the major aims of project is uncover differences in behavior among p53 mutants that might allow prognostic stratification of p53 mutations. Analyzing nuclear foci in the humanized p53 lines revealed that one mutant in particular, R248Q, a conformational mutant, exhibited larger and more numerous foci than the other mutants. Interestingly, conformational mutants are prone to aggregation when transiently expressed in human cell lines whereas contact site mutants like R273H are not (Xu et al. 2011). Thus, the larger foci in R248Q mutants might reflect aggregation of this mutant protein compared to the other mutants. Furthermore, knock-in mice for this mutation happen to exhibit accelerated tumor onset and greater lethality when compared to R172H, R248W and R270H knock-in mice (Hanel et al. 2013). Compellingly, in our *Drosophila* system, males carrying this mutation are sterile in a $p53^{NS}$ background, showing that differences in behavior at the cellular level correlate with phenotypes at the organismal level.

In conclusion, the results shown in this chapter of my dissertation work show that humanized p53 flies are a viable platform with which to study oncogenic p53 mutants. The powerful genetic tools available in *Drosophila* and the absence of p63- and p73- dependent gain-of-function effects poise this as a valuable system for discovering novel gain-of-function properties of human p53 mutants and new insight how they exert oncogenic activity.

Future Directions

Although this project is still in its infancy, it has already yielded a few interesting observations and I suspect it will produce many more. Recommendations for future study include further characterization of humanized p53 flies, follow up on the nuclear foci phenotype and testing hp53 mutants in *Drosophila* cancer models.

In order to correctly interpret data and make conclusions using this platform, more detailed characterization of the humanized p53 lines is required. Because the $hp53^{+}$ and the hp53 mutant have upstream coding exons for the larger Dp53 isoform, its possible that chimeric transcripts are being transcribed. Additionally, the identity of the transcript being expressed in these humanized lines should be determined. Additionally, determining the sequence identity of the human protein is strongly suggested as it runs below the expected molecular weight for hp53 on SDS-PAGE (Figure 3-10). Furthermore, discrepancies between $Dp53^{-/-}$ backgrounds must be sorted out. For instance, all of the humanized p53 lines are more viable and fertile in combination with $Dp53^{5A\text{-}1\text{-}4}$ than with $Dp53^{NS}$. Consistent with this idea, wild-type hp53 lines can rescue radiation-induced apoptosis in $Dp53^{NS}$ homozygotes but not $Dp53^{5A\text{-}1\text{-}4}$ homozygotes.

Hp53 can induce reporter activation in response to radiation (Figure 3-9A). This pivotal observation suggests that hp53 post-translational modification is sufficient for activation. It will be important to address whether this is the case. Does hp53 get phosphorylated? Is it activated in the absence of Chk2 or ATM? Additionally, it is interesting that although hp53 does not completely rescue RIPD gene induction (Figure 3-7), it can induce apoptosis in the embryo in response to radiation. These deaths are most likely caused by the modest

induction seen in *hid* expression (Figure 3-7), but it is also possible that hp53 is engaging a non-canonical death pathway.

Loss- of-function phenotypes of the hp53 mutants should also be examined. It will be important to test whether radiation-induced apoptosis remains intact or whether it is abolished in humanized mutant p53 embryos and wing discs. Preliminary evidence shows that mutant R175H is compromised for radiation-induced apoptosis in the embryo (data not shown). Furthermore, other p53-dependent phenotypes such as genomic instability should be tested in the mutant lines and examined for suppression or enhancement. Although *in vivo* data clearly demonstrates that hp53 mutants exert gain-of-function activities (Lang et al. 2004; Olive et al. 2004; Hanel et al. 2013), the contribution of dominant-negative effects to the oncogenicity of these mutants is still debated. To examine this, one could examine effects of p53 mutants on p53 biosensor activation by wild-type hp53 as well as effects on wild-type hp53 nuclear foci.

The observation that warrants the most follow up is the disruption of nuclear foci in the humanized p53 mutants (Figure 3-15). This common property of p53 mutants might provide insight into pivotal gain-of-function activities and could serve as a useful tool to stratify p53 mutants for prognostic use. Determining whether p53 mutants simply fail to form foci or whether they are actively disrupting the subnuclear architecture could shed light on gain-of-function mechanisms. Furthermore, because of the accessibility of the *Drosophila* germline, this system could be used to ask whether small molecules can restore nuclear foci in humanized p53 mutants. In order to establish pathological relevance, it will be important to

test whether human cells harboring p53 gain-of-function mutations are also compromised for hp53 subnuclear localization.

Identifying the composition of these foci will undoubtedly provide insight into what protein interactions might be disrupted in p53 mutants. The observation that hp53 colocalizes to *Drosophila* SUMO2 in germline cells (Figure 3-14) is exciting and warrants further investigation. Because SUMO2 is a characteristic component of PML nuclear bodies, it would be interesting to test for whether other known PML nuclear body components such as NF-YA and Daxx-like protein (DLP) also colocalize with hp53 foci. Co-immunoprecipitation studies could be used to support these observations.

Lastly, as a future effort, I think it would be enlightening to place the humanized p53 lines in cancer models in order to determine whether p53 mutants exert oncogenic gain-of-function in the *Drosophila* system. RasV12 and EGFR overexpression models in the fly promote proliferative tumors and have been used to identify novel oncogenes involved in cellular transformation (Brumby and Richardson 2003; Pagliarini and Xu 2003; Dow et al. 2008; Herranz et al. 2012). Additionally, by using the MARCM technique, one can localize expression of RasV12 to specific tissues and positively label RasV12 cells in order to screen for genes that cooperate to promote metastasis and invasion of these cells (Pagliarini and Xu 2003). Testing hp53 mutants for enhancement of proliferative or metastatic phenotypes in these models would determine whether they exhibit oncogenic gain-of-function in the fly and allow for prognostic stratification.

Chapter 3 Acknowledgements

I wish to acknowledge Erin Regan for the innumerable qPCRs she ran that contributed to figures 3-5 and 3-7. Many thanks to Melissa O'neal for being a cloning boss and helping me create the constructs for humanized lines. Thanks also to Paula Kurtz for being interested in this project and helping with experiments that did not make it on here but one day will make it somewhere else.

CHAPTER FOUR:

IN VIVO FUNCTION OF P53 IN THE *DROSOPHILA* GERMLINE

Introduction

When one first joins a research lab in graduate school, one is either thrust into a specific project with a defined roadmap or into a forest of possibilities where one can explore and pave their own road. One of the appeals of John's lab was that I was free to do the latter. So before I decided to develop the two projects that make up chapters 2 and 3 of this dissertation, I wandered the woods and carried out several experiments with the aim of understanding the role of p53 in the germline. Although these experiments do not directly feed into my dissertation work, they are nonetheless a memorable part of my graduate career. Many of them gave negative or inconclusive results but are included in hopes that they provide valuable insight for future students in the lab examining roles of p53 in germline stem cells (GSCs). Thus, this chapter exists primarily to document – a fact reflected by its brevity and lack of story.

p53 is a highly conserved gene in evolution spanning from protists to man (Lu et al. 2009). Although p53 is most famously known as a tumor suppressor, invertebrates do not deal with cancer in the wild, suggesting that tumor suppression is a recent feature that was co-opted from more ancestral roles. What might these ancestral functions be? *Drosophila* is a great system in which to study this question as it does not get cancer in the wild yet contains a highly conserved p53 regulatory network (discussed in Chapter 3: Introduction). Recently, Wan Jin Lu, a former grad student from our lab, discovered that *Drosophila p53* is active in

germline cells undergoing meiotic recombination (Lu et al. 2010) and, together with Annika Wylie, showed that it is selectively licensed in GSCs after stress (Wylie et al. 2014). These studies establish roles for p53 in the germline distinct from those classically associated with tumor suppression such as apoptosis or cell cycle arrest. At the outset of this work, we already knew that p53 was selectively activated in GSCs but did not understand what its roles were in this context. The following experiments were aimed at uncovering these ancestral roles.

Materials and Methods

Fly Strains and Husbandry

CantonS flies were used as wild-type controls unless noted otherwise. All lines were obtained from the Bloomington Stock Center except for flies for Rr3 assay which were kindly provided by William R. Engels (Preston et al. 2006). $Dp53^{NS}$, $Dp53^{5A\text{-}1\text{-}4}$ and GHP150 were inherited lab stocks. All flies were reared at 25ºC or room temperature.

Immunofluorescence

Whole ovaries were dissected in PBS, tips teased apart, fixed in PT (1X PBS, 0.1%Triton) with 4% Formaldehyde and heptane at a 1:3 volume/volume ratio for 15 minutes. Fixed samples were then washed with PT 4x7 minutes, blocked with PTA (1X PBS, 0.1% Triton, 1.5%BSA) for 1 hr, and incubated overnight at 4ºC with primary antibody diluted in PTA. On the second day, the samples were rinsed 3 times with PT, washed with PTA 4x7 minutes, incubated with appropriate secondary antibody for 2 hrs at room temperature, rinsed again with PT 3 times and washed with PT overnight at 4ºC. On the third day, the samples were rinsed with PBS once and mounted with VECTASHIELD + DAPI (Vector Labs).

The following antibodies and dilutions were used: anti-Dp53 25F4 concentrated (Developmental Studies Hybridoma Bank) at 1:1000, anti-Dp53 ID3 at 1:2000 (pre-absorbed against $p53^{5A\text{-}1\text{-}4}$ ovaries), anti-dmp53 IF6 at 1:2000 (pre-absorbed against $p53^{5A\text{-}1\text{-}4}$ ovaries), Alexa-488 and Alexa-568 secondary antibodies (Invitrogen Molecular Probes) were used at 1:250. Custom monoclonal antibodies against Dp53 (ID3 and IF6) were raised at Abmart Antibody Company (Shanghai, China) against epitope QDERQLNSKK.

Microscopes and Image Processing

Light micrographs were taken with a Zeis Axioplan 2E microscope. Confocal micrographs were taken with a Zeiss LSM780 laser confocal microscopes using Zen software.

Stem cell division assay

Ovaries from WT or dp53-/- flies before or 24 hours , 48 hours and 5 days after irradiation at 40 gray were dissected and stained with anti-HTS, which stains the fusome. GSCs were identified by fusome morphology and dividing cells (indicated by an elongated fusome) were scored and plotted.

Radiosensitivity assay

Ovaries from WT or $dp53^{-/-}$ flies 5 days or 2 weeks after irradiation at 40 gray were dissected and stained with DAPI, anti-vasa, a germline marker, and anti-HTS, a cytoskeletal marker.

Stem cell differentiation assay

A hs-Bam transgene was crossed into bam^{hv} and bam^{hv}; $dp53^{NS}$ mutants. 10 mutant females were then mated with 10 wild-type males in vials and heatshocked every day except for weekends for 30 minutes. Vials were flipped every two days and examined for progeny. Vials that had at least one progeny were considered a fertile vial. This was continued for 15 days.

Rr3 assay

Rr3 assay was conducted using strains and methods detailed in (Preston et al. 2006). Single strand annealing (SSA) rates were determined by taking the ratio of red progeny without endonuclease ($endo^-$) over total (red and non-red) $endo^-$ progeny from each male assayed and then plotting the average rate for 10 males. Non-homologous end joining (NHEJ) and homologous recombination (HR) rates were determined from non-red endonuclease positive progeny ($endo^+$). The two were distinguished by using PCR primers that can detect HR specific repair (see Appendix C for primer sequences). NHEJ and HR rates are determined by the ratio of $NHEJ^+$ or HR^+ progeny over the total number of non-red $endo^+$ progeny. For WT, 1,435 progeny from 10 males were scored; for $dp53^{5A\text{-}1\text{-}4}$, 1,463 progeny from 9 males were scored; for $dp53^{NS}$, 946 progeny from 5 males were scored.

Dihydroethidium staining

DHE staining was conducted as in (Owusu-Ansah and Banerjee 2009).

Metabolic flux assay

Assays were modified from (Bricker et al. 2012). 20 female flies of the respective genotype were fattened for 2 days on yeast paste and then transferred to chambers with glucose-only plates for 24 hours. After acclimatization, flies were fed 5% ^{13}C-labelled glucose for 12 hours (Figure 4A-C) or 1, 2, or 3 hours (Figure 4-7D-G). For this, flies were transferred to a chamber with 250ul of 5% ^{13}C-Glucose (Cambridge Isotope Laboratories) in 1X PBS pipetted onto two 1.5cm^2 whatman filter papers stacked together. All genotypes and time points assayed were done in triplicate.

Results

p53 status affects germline stem cell division after stress

In mammals, p53 plays a critical role in the controlling the cell cycle checkpoint during stress (Kastan et al. 1992), and although hotly contested, this activity is now thought to be dispensable for preventing tumorigenesis (Brady et al. 2011; Li et al. 2012; Valente et al. 2013). To determine whether p53 is involved in cell cycle control in germline stem cells (GSCs) after stress, I decided to quantify dividing stem cells in wild-type and *dp53*$^{-/-}$ flies after irradiation by staining the stem cell fusome, a cytoskeletal structure which is elongated during cell division. Interestingly, unirradiated *dp53*$^{-/-}$ flies exhibited slightly lower steady-state stem cell division rates (Figure 4-1). Contrary to what I expected, stem cell division rate dipped in *dp53*$^{-/-}$ flies by ~15% 24 hours after IR (Figure 4-1). However, by 5 days, *dp53*$^{-/-}$ division rates returned to levels similar to those of wild-type (Figure 4-1). These results show that *Dp53* deficient stem cells undergo greater proliferative arrest but eventually recover. This observation was pursued more in depth by others in the lab using BrdU incorporation studies (Wylie et al. 2014) and is discussed later.

p53 preserves integrity of the germline during stress

The previous stem cell division rate experiments revealed that *dp53*$^{-/-}$ ovaries may be more sensitive to challenge with irradiation than their wild-type counterparts in that they exhibit more frequent morphological abnormalities. To determine whether this phenotype might give clues to p53 function in the germline, I conducted a time course radio-sensitivity assay in ovaries from wild-type or *dp53*$^{-/-}$ flies by staining them with markers for germline cells (anti-

vasa), the cytoskeleton (anti-HTS), and DAPI at 24 hours, 5 days, and 2 weeks after irradiation. Both wild-type and transheterozygous *dp53*$^{-/-}$ ovaries did not show any morphological phenotypes after 24 hours of irradiation (data not shown). After 5 days, however, 30% of *dp53*$^{-/-}$ ovaries exhibited morphological abnormalities (Figure 4-2A) compared to 2% of wild-type ovaries. Interestingly, *dp53*$^{-/-}$ ovaries presented a reproducible stem cell depletion phenotype which was often accompanied by presence of an enlarged germ cell (Figure 4-2A). Furthermore, *dp53*$^{-/-}$ ovaries exhibited highly deranged morphology two weeks after irradiation at higher penetrance than wild-type ovaries (Figure 4-2B). Although the pleiotropic nature of these phenotypes do not help determine what specific roles p53 might have in stem cells, they do support the hypothesis that p53 plays an important role in stem cell behavior during stress.

p53 is not required for germline stem cell differentiation after developmental arrest

Work in our lab now published in Wylie et al showed that p53 is activated in mutants for bag of marbles (*Bam*), which display massive stem cell tumors due to deregulated differentiation signals (Wylie et al. 2014). To determine whether p53 impacts GSC differentiation, I transiently expressed *Bam* in the germline of *bam*$^{-/-}$ or *bam*$^{-/-}$, *dp53*$^{-/-}$ mutants and assayed fertility recovery as a read out for successful differentiation of arrested GSCs. Both *bam*$^{-/-}$ and *bam*$^{-/-}$, *dp53*$^{-/-}$ mutants displayed similar rates of fertility recovery (Figure 4-3), demonstrating that p53 status does not majorly impact differentiation of GSCs. However, double mutants exhibited a slight dip in fertility after 6 days (Figure 4-3), suggesting that *dp53*$^{-/-}$ GSCs might become exhausted more quickly than their wild-type counterparts.

Does p53 regulate DNA repair during meiotic recombination?

Another central p53 role that might be important in germline cells is controlling DNA repair. To examine whether p53 might be transactivating DNA repair genes during meiotic recombination, I performed *in situ* hybridization in wild-type and *dp53*$^{-/-}$ ovaries. I decided to probe for DNA repair genes included in a collection of radiation-induced p53-dependent (RIPD) genes in the embryo (Akdemir et al. 2007). These genes are involved in a variety of DNA repair pathways including the DNA damage checkpoint (rad50, mre11, mus304), non-homologous end joining (ku80), homologous recombination (mus205) or nucleotide-excision repair (mus210), as well as a gene involved in meiotic cell cycle progression (sra). All but two of these genes were found to be strictly p53-dependent (ku80 and rad50 are only partly p53-dependent). Interestingly, *in situ* with DIG-labelled RNA probes suggested that many of these genes are expressed in region 2a/2b of the germarium (Figure 4-4A) where the p53 biosensor is activated during meiotic recombination (see Figure 3-1). However, as seen in Figure 4-4B, all of the probes exhibited highly variable signal in this region, ranging from weak to strong. Additionally, no appreciable difference was seen when comparing wild-type and *dp53*$^{-/-}$ ovaries (data not shown). I hypothesized that perturbing DNA repair during meiosis might sensitize region 2a/2b to p53 activity. To this end, I used *okra*$^{-/-}$ mutants (the *Drosophila* rad54 ortholog), which are defective for homologous recombination (Kooistra et al. 1997). Although probe signal was not increased in this background, the *okra*$^{-/-}$, p53$^{-/-}$ double mutants exhibited a modest decrease of signal compared to *okra*$^{-/-}$ mutants (Figure 4-4B). Unfortunately, antisense probes for *okra* exhibited signal in *okra*$^{-/-}$ mutants, suggesting that this probe might not be specific for its target genes. This called other probes into question which had not been validated against mutant tissue. The variability of this

assay and the uncertainty of probe specificity do not make this a reliable method to address whether p53 plays a role in regulating DNA repair in the germline.

Rr3 is an *in vivo* reporter assay that can be used to determine usage of DNA repair pathways in the *Drosophila* germline (Johnson-Schlitz et al. 2007). It relies on the fact that each DNA repair pathway has a unique repair product that can be inherited by progeny if the repair is carried out in germ cells. The assay consists of a DsRed transgene that is interrupted by an I-SceI site which results in a single double-stranded break upon induction of the I-SceI endonuclease in the male germline (where there is no endogenous meiotic recombination). If the germ cell used non-homologous end-joining (NHEJ) to repair the break, then the future progeny will not express DsRed. In contrast, homologous recombination (HR - using a sister chromosome with the intact DsRed sequence as template) or single strand annealing (SSA - if the progeny do not carry the intact DsRed sister chromosome) will remove the non-DsRed sequence interrupting the gene, thus restoring the reading frame and causing the progeny to glow red. Interestingly, the $Dp53^{5A\text{-}1\text{-}4}$ allele exhibited a modest increase in NHEJ compared to wild-type flies (Figure 4-5A and B). The $Dp53^{NS}$ allele, however, had wild-type frequencies of NHEJ (Figure 4-5A and B), suggesting that the difference seen in the $Dp53^{5A\text{-}1\text{-}4}$ allele do not map to *Dp53*. This methodology was not pursued further.

Does p53 regulate metabolism in germline cells?

Recently, p53 has emerged as a metabolic regulator (Spike and Wahl 2011) and has been implicated in stem cell metabolism (Meletis et al. 2006; Qin et al. 2007; Zheng et al. 2008)(Meletis et al. 2006; Qin et al. 2007; Zheng et al. 2008)(Meletis et al. 2006; Qin et al.

2007; Zheng et al. 2008)(Meletis et al. 2006; Qin et al. 2007; Zheng et al. 2008)(Meletis et al. 2006; Qin et al. 2007; Zheng et al. 2008)(Meletis et al. 2006; Qin et al. 2007; Zheng et al. 2008)(Meletis et al. 2006; Qin et al. 2007; Zheng et al. 2008)(Meletis et al. 2006; Qin et al. 2007; Zheng et al. 2008)(Meletis et al. 2006; Qin et al. 2007; Zheng et al. 2008)(Meletis et al. 2006; Qin et al. 2007; Zheng et al. 2008). To determine whether p53 is controlling metabolism in female germ cells, I used dihydroethidium (DHE), an *in vivo* dye which enters the nucleus and intercalates with DNA upon activation by reactive oxygen species (ROS) (Owusu-Ansah and Banerjee 2009), as a readout for oxidative phosphoryation (OXPHOS). Strikingly, unirradiated wild-type germaria exhibited a bight band of DHE staining in region 2a/2b (Figure 4-6A) where p53 is activated during meiotic recombination (see Figure 3-1), indicating increased OXPHOS. Although not quantified, this signal was not majorly affected in *dp53*$^{-/-}$ germaria (Figure 4-6B), suggesting that although ROS is produced in this region, it is not regulated by p53.

Next, I sought collaboration with Andrew Mullen and Ralph Deberardinis to determine whether p53 null flies exhibited phenotypes in metabolic flux. For this, flies were fed ^{13}C-labelled glucose and metabolic flux of glucose was determined by the amount of ^{13}C labeling present in each the metabolic intermediates. We ran a preliminary trial with 12 hours of labeling which yielded uninterpretable results due to extensive saturation of ^{13}C labeling as revealed by the high abundance of M+6 labeled citrate and M+4 labeled fumarate intermediates (Figures 4-7A and B). However, these results showed that both *Dp53* mutants exhibited difference in glycolitic flux as indicated by labeled (M+3) lacatate (Figure 4-7C). To decrease saturation, we opted to repeat the experiment with shorter labeling periods of 1, 2

and 3 hours. Strikingly, *dp53*$^{-/-}$ mutants exhibited increased glycolitic flux as indicated by the increase of M+3 labeled lactate at 3 hours (Figure 4-7D). Unfortunately, the *Dp53*$^{+}$ rescue failed to restore glycolysis to wild-type rates (Figure 4-7D), indicating that this phenotype does not map to p53. Failure to rescue might be due to a background mutation in the Dp53^{NS} or differences in genetic background (which was not controlled for in this experiment). Although I did not pursue these studies further, the methodology is promising and could be used to directly test for metabolic phenotypes in *dp53*$^{-/-}$ germaria.

SIRT1 does not regulate p53 activity in the germline

Finally, SIRT1 has been shown to be intimately involved in regulating p53 action via deacetylation (Vaziri et al. 2001). To test whether Sir2, the *Drosophila* SIRT1 ortholog, has an effect on Dp53 activation in the germline, I ectopically expressed Sir2 in germline cells of flies carrying a p53 biosensor and examined them before and after irradiation (for biosensor, see Figure 3-1). Sir2 overexpression did not abolish endogenous p53 activation of the biosensor in region 2a/2b (Figure 4-8A) or stimulus-dependent activation of the biosensor in GSCs 24 hours or 5 days after irradiation (Figure 4-8B). Expression of Sir2 in the germline did produce ectopic stem-like cells 24 hours and 5 days after irradiation (white arrows, Figure 4-4B). This observation was not pursued further as it did not seem to be connected to p53 activity in the germline, as indicated by biosensor activation in the GSCs.

Generation of Dp53 monoclonal antibodies

Currently, the *Drosophila* p53 field is hampered by the lack of good antibodies against Dp53 - especially for Western blotting - which has left many important experiments about p53 biology in stem cells on paper. To confront this issue, we hired Abmart to raise monoclonal

antibodies against Dp53 using a QDERQLNSKK peptide (See Materials and Methods). I received 10 ascites samples, of which two yielded signal in wild-type ovaries but not in a *dp53*$^{-/-}$ ovaries by immunofluorescence (Figure 4-9A and B). Both antibodies stained foci in the germarium (white arrows in Figures 4-9A and B) and in nurse cell nuclei (yellow arrows in Figures 4-9A and B). One of the clones in particular, 1D3, stained differently in the germarium than an existing monoclonal antibody, 25F4, which we have recently gotten to work for immunofluorescence (compare Figure 4-9A to 4-9C). Unfortunately, neither of these antibodies picked up a Dp53-specific signal when tested for Western blotting on cell lysates overexpressing Dp53 and on lysates from wild-type and *dp53*$^{-/-}$ embryos but (data not shown). These antibodies (1D3 in particular) may prove to be useful tools to complement 25F4 in immunofluorescent studies.

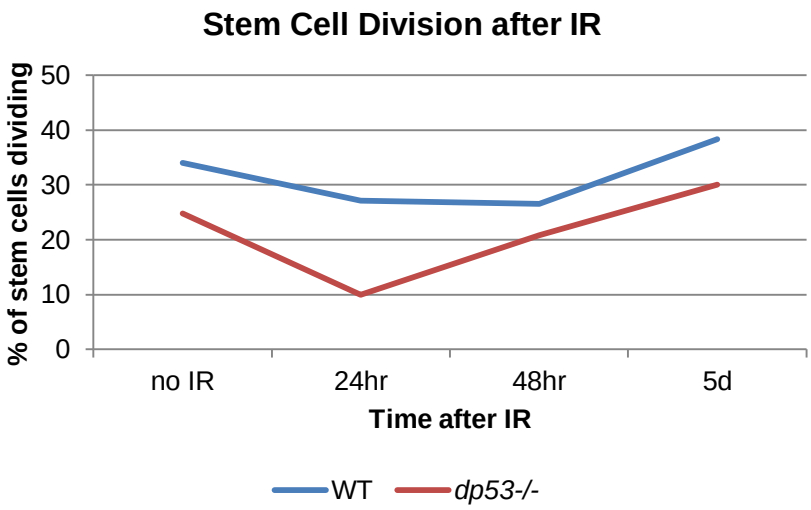

Figure 4-1. p53 is not required for division of germline stem cells after genotoxic stress. Ovaries from WT or *dp53*$^{-/-}$ flies before or 24 hours , 48 hours and 5 days after irradiation at 40 gray were dissected and stained with anti-HTS, which stains the fusome. GSCs were identified by presence of round fusome and dividing cells (indicated by an elongated fusome) were scored and plotted. WT: *Canton S, dp53*$^{-/-}$: *dp53*$^{NS/5A\text{-}1\text{-}4}$.

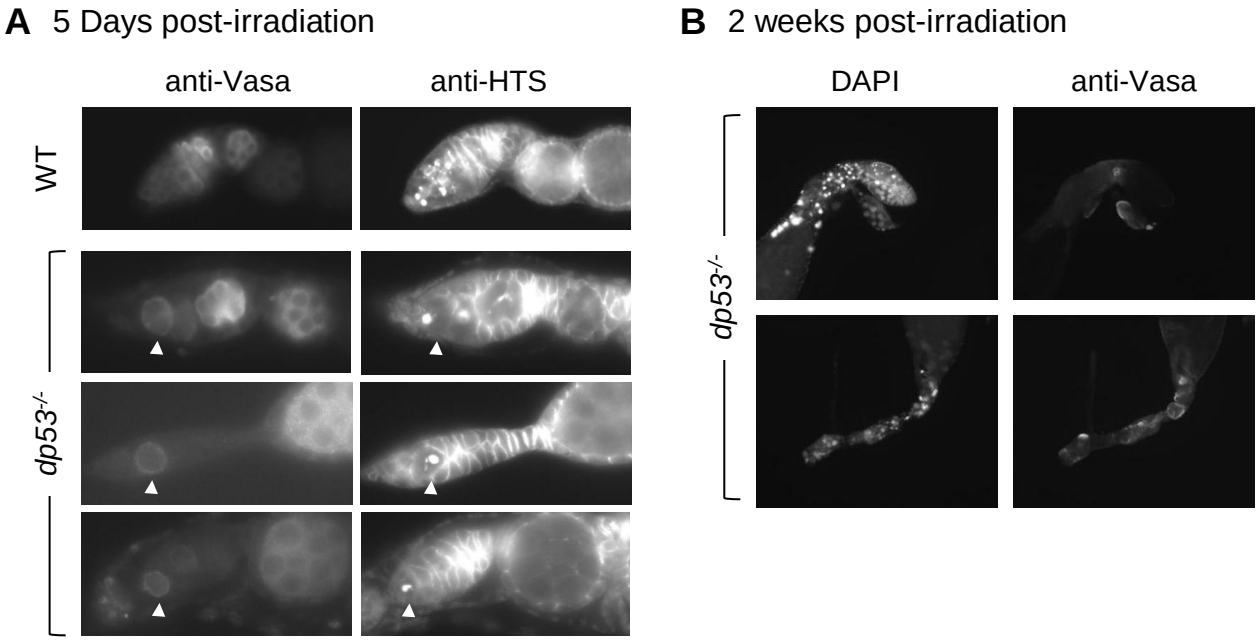

Figure 4-2. p53 preserves germline integrity after genotoxic stress. Radiosensitivity assay. Ovaries from WT or *dp53*$^{-/-}$ flies 5 days or 2 weeks after irradiation at 40 gray were dissected and stained with DAPI, anti-vasa, a germline marker, and anti-HTS, a cytoskeletal marker. WT: *Canton S*, *dp53*$^{-/-}$: *dp53*$^{NS/K1}$.

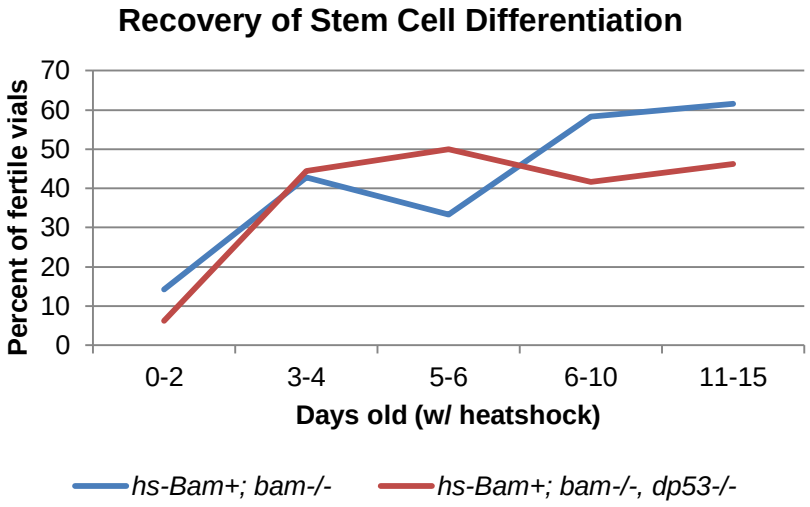

Figure 4-3. p53 is not required for differentiation of germline stem cells after developmental arrest. A heat-shock inducible *Bam* rescue transgene (*hs-Bam*$^{+}$) was crossed into *bam*$^{-/-}$ and *bam*$^{-/-}$, *dp53*$^{-/-}$ double mutants. These flies were then mated with wild-type males and heat-shocked every day except for weekends for 30 minutes. Vials were flipped every two days and examined for progeny. Vials that had at least one progeny were considered a fertile vial. This was continued for 15 days. Notice that *bam*$^{-/-}$ and *bam*$^{-/-}$; *dp53*$^{-/-}$ double mutants displayed similar rates of fertility recovery but dipped ~20% after day 6 . *bam*$^{-/-}$: *bam*$^{hv/hv}$, *dp53*$^{-/-}$: *dp53*$^{NS/NS}$.

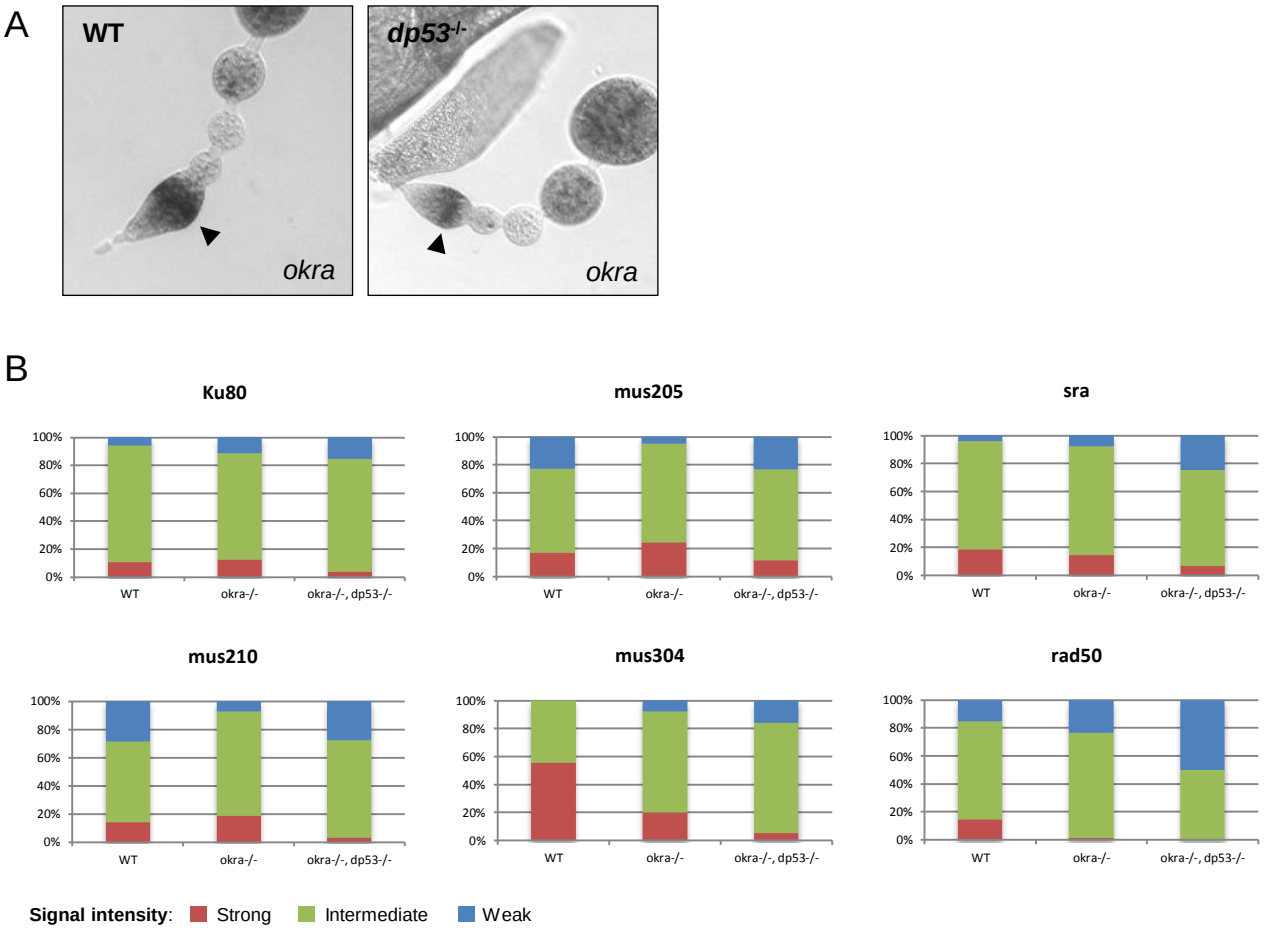

Figure 4-4. *in situ* hybridization of RIPD DNA repair genes. *in situ* hybridizations on whole mount dissected ovaries. (A) Representative images of probe signal in region 2a/2b (black arrows) in both WT and *dp53*$^{-/-}$ ovaries. (B) Ovaries from WT, *okra*$^{-/-}$ and *okra*$^{-/-}$, *dp53*$^{-/-}$ flies were dissected and probed with DIG-labeled antisense or sense RNA probes (see Materials and Methods). Signal intensity was binned into strong (red), intermediate (green) or weak (blue) signal intensity and percentages plotted. Genotypes: WT: *yw*, *okra*$^{-/-}$: *okra*$^{RU/AA}$, *dp53*$^{-/-}$: *dp53*$^{NS/5A-1-4}$.

A

SSA/HR/NHEJ Rates in WT vs *dp53*$^{-/-}$ (% ± StdDev)

	SSA	HR	NHEJ
WT	94.26% ± 7.20	0.74% ± 15.96	5.00% ± 15.96
dp53^{5A-1-4}	86.09% ± 24.57	0.72% ± 6.53	13.19% ± 8.16
dp53^{NS}	94.27% ± 8.16	0.00% ± 0.00	5.73% ± 0.00

B

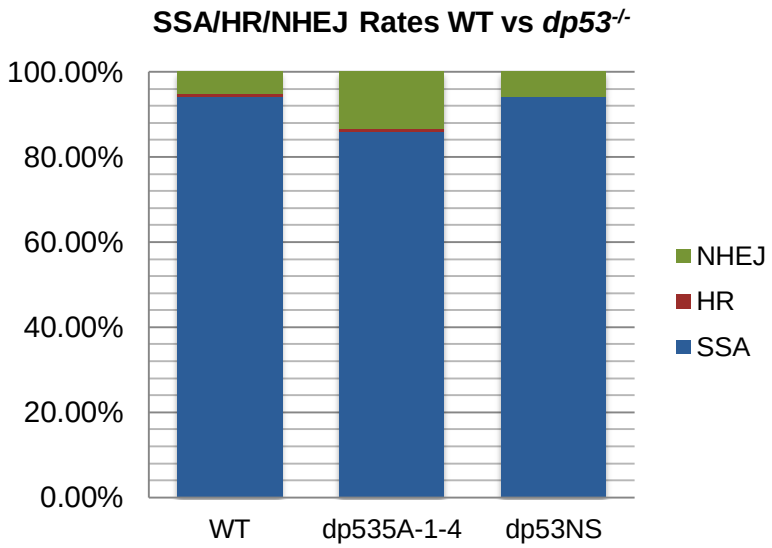

Figure 4-5. p53 status in the germline does not affect DNA repair pathway usage. Rr3 assay measuring DNA repair rates in the germline of WT or *dp53*$^{-/-}$ (dp53^{5A-1-4} or dp53^{NS}) male flies (See Materials and Methods). Single strand annealing (SSA) rates were determined by taking the ratio of red progeny not carrying endonuclease (endo^{-}) over total endo^{-} progeny for each parental male assayed. Non-homologous end joining (NHEJ) and homologous recombination (HR) rates were determined from non-red progeny carrying endonuclease (endo^{+}). The two were distinguished by using PCR primers that can detect HR-specific repair (see Appendix C for primer sequences). NHEJ rates are determined by the ratio of NHEJ^{+} progeny over total number of endo^{+} progeny and HR rates are determined by the ratio of HR^{+} progeny over the total number of endo^{+} progeny. Notice that although dp53^{5A-1-4} showed increased NHEJ rates, dp53^{NS} did not. For WT, 1,435 progeny from 10 males were scored; for dp53^{5A-1-4}, 1,463 progeny from 9 males were scored; for dp53^{NS}, 946 progeny from 5 males were scored. dp53^{NS}: *dp53*$^{NS/NS}$, dp53^{5A-1-4}: *dp53*$^{5A-1-4/5A-1-4}$.

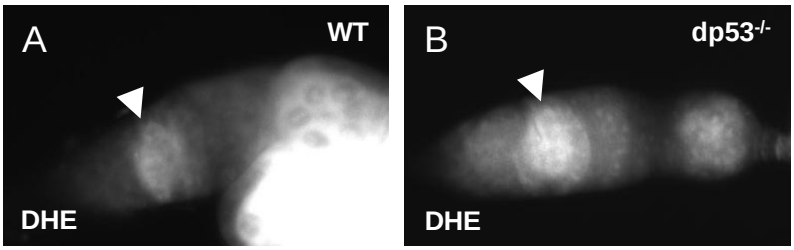

Figure 4-6. *dp53*$^{-/-}$ flies are not affected for oxidative phosphorylation in the germline. Light micrographs of ovaries stained with dihydroethidium (DHE), a dye that detects reactive oxygen species. (A) Wild-type flies exhibit DHE staining at region 2a/2b where p53 is activated by meiotic recombination (white arrow). (B) This signal was not affected in *dp53*$^{-/-}$ germaria (white arrow). WT: *yw/Canton S*, *dp53*$^{-/-}$: *dp53*$^{NS/NS}$.

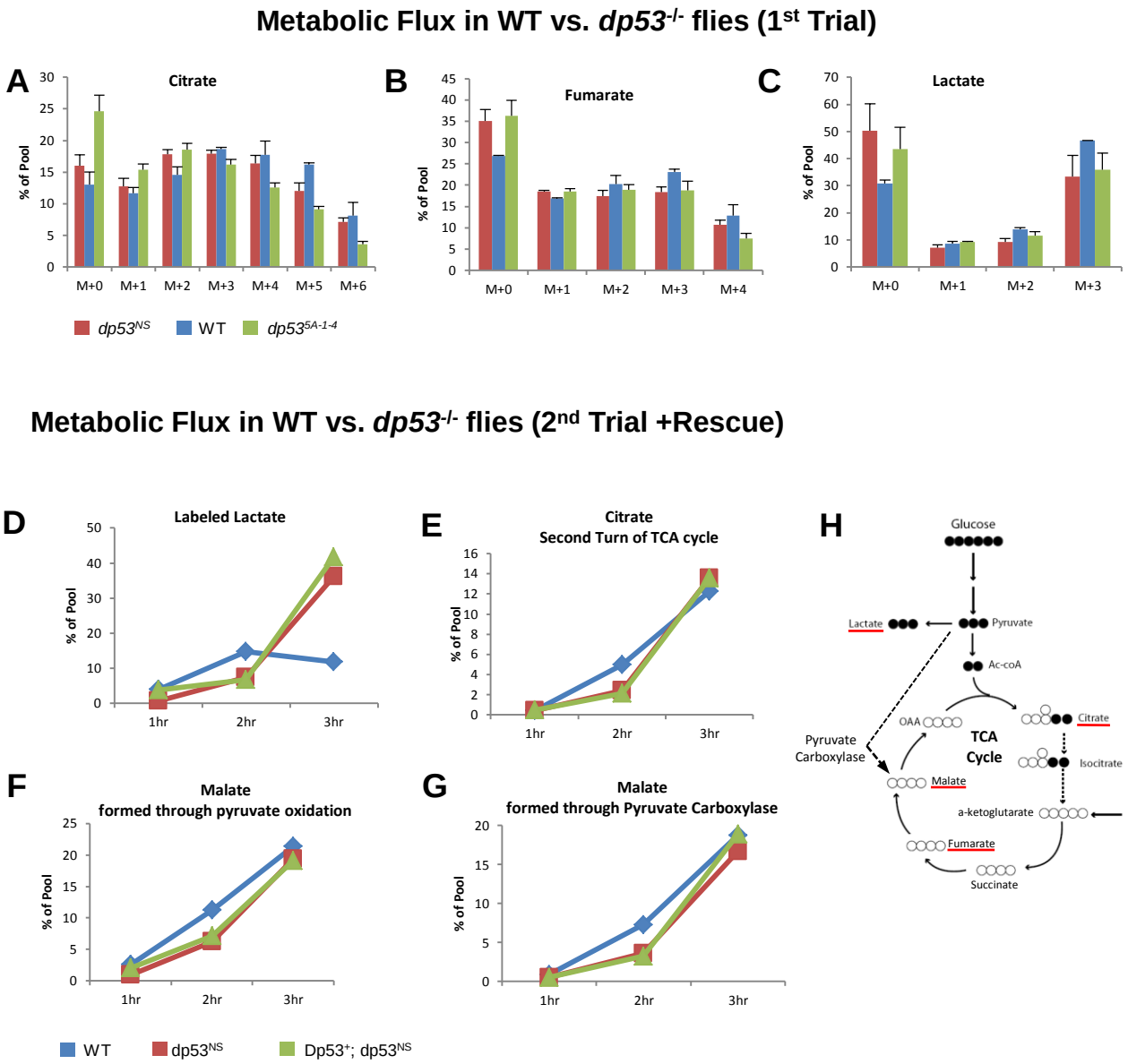

Figure 4-7. dp53^{NS} flies exhibit an increase in glycolysis that does not map to p53. Metabolic flux analysis done in collaboration with Andrew Mullen in Ralph Deberardinis' lab. Whole female flies of the indicated genotype were labeled with C^{13}-glucose for the time-points indicated and assayed for metabolite levels (See Materials and Methods). (A-C) A preliminary trial in which flies were labeled for 12 hours. This experiment exhibited high levels of saturation as indicated by presence of M+2-M+6 citrate intermediates above 10% of the total citrate pool (A). M+number designates how many labeled carbon atoms are present in that intermediate. Typically, one pass through the TCA cycle will result in an M+2 labeled intermediate and two passes will result in an M+4 intermediate (see diagram in H). (D-G) Flies of the indicated genotypes were labeled with C^{13}-glucose for 1, 2 or 3 hours. Notice the increase in labeled lactate in *dp53$^{NS/NS}$* flies at 3 hours (D). This increase did not map to *Dp53* as the Dp53^{+} genomic rescue fragment did not lower levels of glycolysis back to normal levels (D, green line). Citrate (E) and malate (F,G) remained relatively unaltered. (H) Diagram of glucose metabolism through the TCA cycle and glycolytic pathway. Circles represent carbon atoms. Black circles represent C^{13}-labeled carbon atoms. Intermediates shown in A-G are underlined in red. WT: *yw*, dp53^{NS}: *dp53$^{NS/NS}$*, dp53^{5A-1-4}: *dp53$^{5A-1-4/5A-1-4}$*.

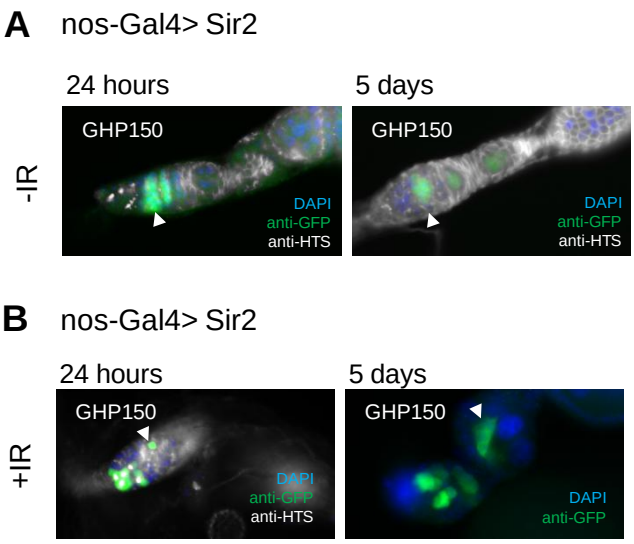

Figure 4-8 .SIRT1 does not inhibit p53 activity in the germline. Light micrographs of immunofluorescence on whole mount ovaries from flies carrying a p53 biosensor (GHP150) and ectopically expressing Sir2 in the germline with the nanos-Gal4 driver. nos-Gal4>Sir2 = nanos-gal4 driving Sir2. These flies were irradiated at 40 gray, dissected 24hours or 5days later, fixed and stained with DAPI, anti-GFP, which reports biosensor activation, and anti-HTS, which stains the cytoskeleton. (A) Ovaries from unirradiated nos-Gal4>Sir2, GHP150 flies. Notice biosensor activation in region 2a/2b, suggesting that Sir2 expression does not inhibit p53 activity in region 2a/2b. (B) Ovaries from nos-Gal4>Sir2, GHP150 flies 24 hours or 5 days after irradiation. Notice that after 24 hours, nos>Sir2 germaria have ectopic stem cells outside of the niche (white arrows), and after 5 days, nos>Sir2 germaria still have robust reporter activation in ectopic stem-like cells (white arrows).

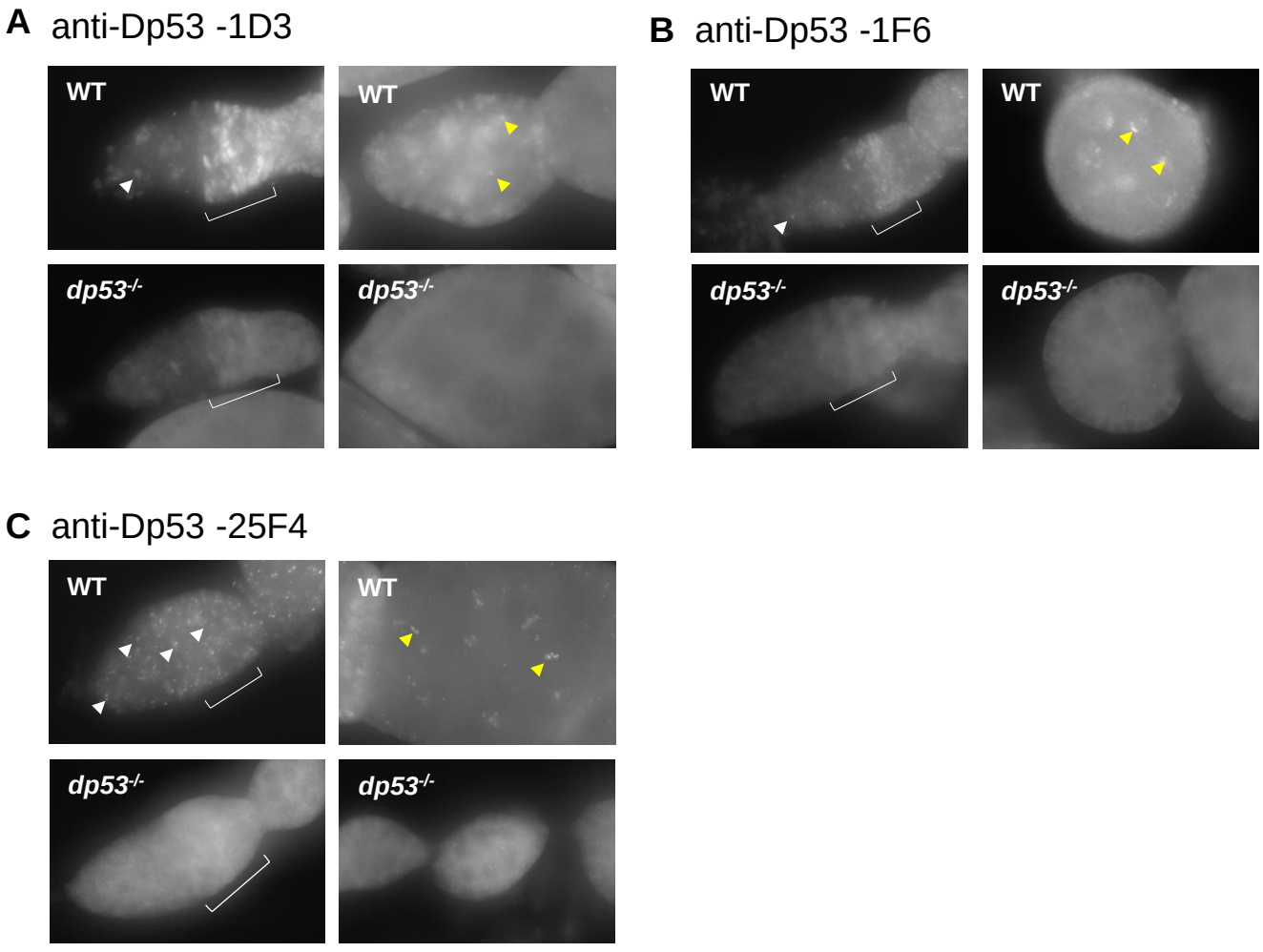

Figure 4-9. Generating Dp53 monoclonal antibodies. Two monoclonal antibodies (A and B) were raised at Abmart Inc. against epitope QDERQLNSKK . These antibodies detect p53 specific signal in germaria (A and B). ID3 (A) and IF6 (B) were diluted at 1:2000, pre-absorbed against mutant tissue overnight and then used to incubate WT or *dp53*$^{-/-}$ sample overnight for two nights. Notice Dp53-specific signal in both germaria (white arrows) and nurse cells (yellow arrows) in both clones. (C) A monoclonal Dp53 antibody, 25F4, that has recently yielded consistent and distinguishable staining in germaria (white arrows) as well as nurse cell nuclei (yellow arrows). White brackets indicate region 2a/2b of the germarium. Genotypes are WT: *yw*, *dp53*$^{-/-}$: *dp53*$^{5A\text{-}1\text{-}4/5A\text{-}1\text{-}4}$.

Discussion and Future Directions

p53 is activated in the germline undergoing meiotic recombination {Lu et al. 2010} and in germline stem cells (GSCs) following genotoxic and oncogenic stress {Wylie et al. 2014}. Importantly, flies do not get cancer, which establishes function of p53 in the germline as an ancestral role predating that of tumor suppression. However, it is not clear what p53 activation is doing in this context.

The experiments described in this chapter were aimed at examining different aspects of p53 function in germline and stem cell biology but failed to yield any positive results. Currently, one of the only functional consequences of p53 depletion in the germline is a loss of fertility recovery after irradiation {Wylie et al. 2014}. This is supported by the observation that *Dp53* is required for integrity of the germline after irradiation challenge (Figure 4-2). But how might *Dp53* be acting to protect stem cells after genotoxic stress? As seen in Figure 4-1, *Dp53* depleted stem cells undergo greater proliferative arrest, suggesting that p53 might regulate stem cell programs that are required for re-entry into the cell cycle. This observation was pursued more in depth by Wan Jin Lu who used BrdU incorporation studies to examine cell cycle kinetics of $dp53^{-/-}$ GSCs (Wylie et al. 2014). She showed that both $dp53^{-/-}$ and wild-type GSCs enter proliferative arrest 4 hours after irradiation, but $dp53^{-/-}$ GSCs are delayed for cell cycle re-entry suggesting that p53 might play a role in GSC cell cycle checkpoint regulation. Perhaps p53 is regulating DNA repair in GSCs? Unfortunately, data from in situ hybridization and the Rr3 assay were inconclusive and do not prove or disprove this hypothesis. Recently, Wylie et al showed that clearance of γ-H2Ax foci in irradiated GSCs

does not depend on *Dp53* status, showing that *Dp53* does not affect DNA repair in the stem cells (Wylie et al. 2014).

More compelling, however, are emerging roles for p53 as a regulator of metabolism (Vousden and Ryan 2009) and stem cell plasticity and differentiation (Qin et al. 2007; Zheng et al. 2008; Marion et al. 2009). Studies using *bam*$^{-/-}$ flies show that *Dp53* status did not affect differentiation of arrested stem cells into mature eggs (Figure 4-3). However, the observation that *bam*$^{-/-}$; *dp53*$^{-/-}$ flies dip in fertility at days 6-15 during Bam^{+} rescue, suggest that p53 is might be involved in stem cell renewal. The experiments attempted to address p53's role in germline metabolism but were inconclusive. While DHE staining did show OXPHOS was happening in the germline, I did not see a significant difference compared to wild-type. This experiment would be worth repeating with irradiated ovaries and with quantification of signal. Additionally, increase in glycolytic flux in *dp53*$^{-/-}$ mutants was confounded by failure of *Dp53*$^{+}$ to rescue increased lactate levels (Figure 4-7D). Nevertheless, metabolic flux analysis yields reproducible results and is relatively straightforward, begging examination of *dp53*$^{-/-}$ stem cells for metabolic phenotypes. Because samples can be snap frozen before processing, it would be feasible to collect enough *bam*$^{-/-}$ and *bam*$^{-/-}$, *dp53*$^{-/-}$ ovaries or ovary tips to enrich for stem cells for this assay.

Chapter 4 Acknowledgements

I would like to thank Shulin Ye, who is a brilliant TAMS student and helped me screen the *Dp53* antibodies; Cara Spanel-Weber for being fascinated with life and helping with *the in situ* hybridization studies; Andrew Mullen and Ralph Deberardinis for being innovators in science and for collaborating on the metabolic flux studies; lastly, Wan Jin Lu for passing on a wealth of knowledge to me and so many others and for being the mastermind behind the conceptual design of many of the experiments in this chapter.

APPENDIX A: Tango7 Fly Stocks

Tango7^{L} stocks	
Tango7^{L} parental strain	yw; W358*/SM6a;Pol/+
Tango7^{L} 1st round clean up	al^{1}, bl^{1}, pr^{1}, Tango7^{L}
al^{1}, FRT42D, Tango7^{L}, sp^{1}	al^{1}, P{ry$^{+t7.2}$,neo,FRT}42D, Tango7^{L}, sp^{1}/CyO, w^{+}, twist-GFP
Tango7^{VK006}; al^{1}, FRT42D, Tango7^{L}, sp^{1}	PBac{CH321-18D10}VK00006; al^{1}, P{ry$^{+t7.2}$, neoFRT}42D, Tango7^{L}, sp^{1}
Tango7^{E} stocks	
Tango7^{E} parental strain	yw; Q135*/SM6a;Pol/+
Tango7^{E} 1st round clean up	al1, dp1, cn1, Tango7E
FRT42D, Tango7^{E}	P{ry$^{+t7.2}$,neoFRT}42D, Tango7^{E}/CyO, w^{+}, twist-GFP
Tango7^{VK006}; FRT42D, Tango7^{E}	PBac{CH321-18D10}VK00006; P{ry$^{+t7.2}$, neoFRT}42D, Tango7^{E}
TILLING mutations	
E33K	yw; E33K/SM6a;Pol/+
C53S	yw; C53S/SM6a;Pol/+
G268S	yw; G268S/SM6a;Pol/+
E292K	yw; E292K/SM6a;Pol/+
V230H, DFLEG232-235, I244H	yw; V230H, DFLEG232-235, I244H/SM6a;Pol/+
Deficiencies	
Df(2R)Exel7130	w^{1118}; Df(2R)Exel7130/CyO
Df(2R)50C-38	Df(2R)50C-38, al^{1} b^{1} cn^{1} P{CaSpeR}Cp1^{50C-38}/CyO, amos^{Roi-1} bw^{1}
Df(2R)BSC401	w^{1118}; Df(2R)BSC401/CyO
FLP stocks	
hs-FLP;FRT42D, GFP	yw, hs-FLP; P{ry$^{+t7.2}$, neoFRT}42D P{ w^{+},Ubi-GFP(S65T)nls}2R/CyO
hs-FLP;FRT42D, RFP	yw, hs-FLP; P{ry$^{+t7.2}$, neoFRT}42D P{ w^{+},Ubi-mRFP.nls}2R
ey-FLP;FRT42D, GFP	yw, ey-FLP; P{ry$^{+t7.2}$, neoFRT}42D P{ w^{+},Ubi-GFP(S65T)nls}2R/CyO
ey-FLP;FRT42D, RFP	yw, ey-FLP;; P{ry$^{+t7.2}$, neoFRT}42D P{ w^{+},Ubi-mRFP.nls}2R
MS1096-FLP;FRT42D, GFP	MS1096-Gal4, UAS-FLP; P{ry$^{+t7.2}$, neoFRT}42D P{ w^{+}, Ubi-GFP(S65T)nls}2R/CyO
MS1096-FLP;FRT42D, RFP	MS1096-Gal4, UAS-FLP; P{ry$^{+t7.2}$, neoFRT}42D P{w^{+},Ubi-mRFP.nls}2R
Ey-Flp; FRT42D-w+, l(2)cl-R11[1]	yw, P{ry$^{+t7.2}$,ey-FLP.N}2 P{GMR-lacZ.C(38.1)}TPN1; P{ry$^{+t7.2}$, neoFRT}42D P{w^{t*} ry^{+t*},white-un1}47A l(2)cl-R11[1]/CyO, y^{+}
Tango7 UASp lines	
UASp-FLAG-3xHA-Tango7^{FL}	w;CyO/Sp; P{UASp-FLAG-3xHA-Tango7^{FL}}
UASp-FLAG-3xHA-Tango7^{L}	w;CyO/Sp; P{UASp-FLAG-3xHA-Tango7^{L}}
UASp-FLAG-3xHA-Tango7$^{PCI+30aa}$	w;CyO/Sp; P{UASp-FLAG-3xHA-Tango7$^{PCI+30aa}$}
Other	
Tango7^{L}; GMR-rpr	al^{1}, P{ry$^{+t7.2}$, neoFRT}42D, Tango7^{L}, sp^{1}/CyO; GMR-rpr
FRT42D, Tango7^{L}; GMR-grim	al^{1}, P{ry$^{+t7.2}$, neoFRT}42D, Tango7^{L}, sp^{1}/CyO; GMR-grim
GMR-hid; FRT42D, Tango7^{L}	P{GMR-hid}SS1, yw, P{neoFRT}19A; al^{1}, P{ry$^{+t7.2}$, neoFRT}42D, Tango7^{L}, sp^{1}/CyO

FRT42D, Tango7^{L}; He-Gal4, UAS-GFP	w*; P{w^{+mC}, He-GAL4.Z}85, P{w^{+mC}, UAS-GFP.nls}8
Tango7^{L}; ppk-GFP	al^{1}, P{ry$^{+t7.2}$, neoFRT}42D, Tango7^{L}, sp^{1}/CyO, twist-GFP; ppk-GFP/TM6,Tb
FRT42D, Tango7^{L}; SREBP^{reporter}	w*; P{ry$^{+t7.2}$, neoFRT}42D, Tango7^{L}, sp^{1}/CyO, P{w^{+mC}, ActGFP}JMR1; P{w^{+mC}, GAL4-dSREBPg.K}B31, P{w^{+m*}, UAS-GFP.U}3
Tango7^{HSM00667}	y^{1} sc* v^{1}; P{TRiP.HMS00667}attP2
hsp83-Gal4	yw; sna^{Sco}/CyO; al^{1}, hsp83-gal4/TM3, Sb

APPENDIX B: Humanized p53 Collection

X Chromosome	3rd Chromosome					
	wild-type	$Dp53^{5A-1-4}$	$Dp53^{NS}$/TM3,Sb	$Dp53^{NS}$/TM3,Sb,Tb-RFP	NS150/TM3,Sb	NS150/TM3,Sb,Tb-RFP
wild-type		x	x	x	x	x
$Dp53^{+}$ (A1)	x	x	x	x	x	x
hp531 (B2)	x	x	x	x	x	x
hp532 (C4)	x	x	x	x	x	x
R175H		x	x	x	x	x
G245S		x	x	x	x	x
R248Q		x	x	x	x	x
R273C		x	x	x	x	x
R273H		x	x	x	x	x
$Dp53^{+}$ $(A1)^{RFP}$	x					
hp531 $(B2)^{RFP}$	x					
hp532 $(C4)^{RFP}$	x					
$R175H^{RFP}$	x					
$G245S^{RFP}$	x					
$R248Q^{RFP}$	x					
$R273C^{RFP}$	x					
$R273H^{RFP}$	x					

APPENDIX C: PRIMERS USED

Primers used in Chapter 2		
Primers for cell culture plasmids:		
1	Tango7-V5-6xHis Fwd	CGCGGTACCTCAGTGATGATGGTGATGGTGATGATGACCGGTACGCGT
2	Tango7-V5-6xHis Rev	GCGCGAGCTCATGACTTCGCATCCGGTTTTCATAGACC
3	Flag-Dronc Fwd	ATCGACGGATCCTAATGCAGCCGCCGGAGCTAGAGATTGG
4	Flag-Dronc Rev	TACGTAGAATTCCTATTCGTTGAAAAACCCG
Primers for UASp lines:		
5	UASp-FLAG-3xHA-Tango7^{FL}	ATCGACGTCGACATGACTTCGCATCCGGTTTTCATAG
6	UASp-FLAG-3xHA-Tango7^{FL}	TACGTAGCGGCCGCCTAGTGTATCAGCTTCTGGG
7	UASp-FLAG-3xHA-Tango7^{L}	ATCGACGTCGACATGACTTCGCATCCGGTTTTCATAG
8	UASp-FLAG-3xHA-Tango7^{L}	TACGTAGCGGCCGCCTATGCCTGCAGCAAATCGCG
9	UASp-FLAG-3xHA-Tango7$^{PCI+30aa}$	ATCGACGTCGACGACCTCATCCACGACCTGCTG
10	UASp-FLAG-3xHA-Tango7$^{PCI+30aa}$	TACGTAGCGGCCGCCTAGTGTATCAGCTTCTGGG
11	UASp-FLAG-3xHA-Tango7$^{\Delta PCI}$	CTGTGCGCTTTTTGGAAGGCAAGGAGAACCTCAGCACAGT
12	UASp-FLAG-3xHA-Tango7$^{\Delta PCI}$	ACTGTGCTGAGGTTCTCCTTGCCTTCCAAAAAGCGCACAG

Primers used in Chapter 3		
Primers for amplifying left half of hp53 part of targeting fragment (including arm of homology)		
13	hp53/dmp53-XhoI-Fwd	TAGTTTCTCGAGTCAGTCTGAGTCAGGCCCTTC
14	hp53-Rev (GC-hp53-dmp53-Fwd)	CAGATATAGCCGACTAAGATGGAGGAGCCGCAGTCAG
Primers for amplifying right half of hp53 part of targeting fragment (including overlap with RFP cassette)		
15	RA-hp53-dmp53-Fwd	CTGACTGCGGCTCCTCCATCTTAGTCGGCTATATCTG
16	hp53/dmp53-NotI-Rev	CGTCTAGTTTGCGGCCGCGTGCACAGCCGTGAGTCTTCAC
Primers for creating left half of RFP/kan part of targeting fragment:		
17	RFP 3' half Fwd	TGTGGCAAGTGTAGCAGCAGG
18	RFP/Kan-XhoI-Rev	TTTACTAGTTGCTGCTGCGCATAA
Primers for creating right half of RFP/kan part of targeting fragment:		
19	RA-RFP/Kan-KpnI-Fwd#2	GACTAAGGTACCCACATTTCAAAGGTATCTGATACCTGGGAGATTGTCGAC CAGATCAGAAGATAACTTCGTATAGCATACATTATACG
20	RFP 5' half Rev	CCAAGTGCATGCCACACTGC
Primers for stitching together both halves of RFP/kan cassette		
21	5' RA-RFP/Kan-KpnI-Fwd#2	GACTAAGGTACCCACATTTC
22	5' RFP/Kan-XhoI-Rev	ACTCAGACTGACTCGAG
Primers for checking left arm of targeted product		
23	RA-hp53-dmp53-Fwd	CTGACTGCGGCTCCTCCATCTTAGTCGGCTATATCTG

24	Hp53-RAChk-Rev	TTGCTGTGCTGTTTTCC
Primers for checking right arm of targeted product		
25	Hp53-LAChk-Fwd	GCATCCTCGCACATGTGC
26	RFP/Kan_seq_Rev	ATAGTCTGGTATGTCGGCAGG
Primers for site-directed mutagenesis of hp53 mutants		
27	hp53_mutagenesis_R175H-G524A	GAGGTTGTGAGGCACTGCCCCCACCATG
28	GC - hp53_mutagenesis_R175H-G5	CATGGTGGGGGCAGTGCCTCACAACCTC
29	hp53_mutagenesis_G245S-G733A	GTTCCTGCATGGGCAGCATGAACCGGAG
30	GC - hp53_mutagenesis_G245S-G7	CTCCGGTTCATGCTGCCCATGCAGGAAC
31	hp53_mutagenesis_R248Q-C742T	CATGGGCGGCATGAACTGGAGGCCCATCCTCAC
32	GC - hp53_mutagenesis_R248Q-C7	GTGAGGATGGGCCTCCAGTTCATGCCGCCCATG
33	hp53_mutagenesis_R248W-G743A	GCGGCATGAACCAGAGGCCCATCCTC
34	GC - hp53_mutagenesis_R248W-G7	GAGGATGGGCCTCTGGTTCATGCCGC
35	hp53_mutagenesis_R249S-G747T	CATGAACCGGAGTCCCATCCTCACC
36	GC - hp53_mutagenesis_R249S-G7	GGTGAGGATGGGACTCCGGTTCATG
37	hp53_mutagenesis_R273H-C817T	GAACAGCTTTGAGGTGTGTGTTTGTGCCTGTC
38	GC - hp53_mutagenesis_R273H-C8	GACAGGCACAAACACACACCTCAAAGCTGTTC
39	hp53_mutagenesis_R273C-G818A	CAGCTTTGAGGTGCATGTTTGTGCCTGTC
40	GC - hp53_mutagenesis_R273C-G8	GACAGGCACAAACATGCACCTCAAAGCTG
41	hp53_mutagenesis_R282W-C844T	GTCCTGGGAGAGACTGGCGCACAGAGGAAG
42	GC - hp53_mutagenesis_R282W-C8	CTTCCTCTGTGCGCCAGTCTCTCCCAGGAC
Primers for qRT-PCR		
43	GFP_qPCR_3_Fwd	CAACCACTACCTGAGCACCC
44	GFP_qPCR_3_Rev	AGCTCGTCCATGCCGAGAGTG
45	hp53_qPCR_Fwd	GTACCACCATCCACTACAACTAC
46	hp53_qPCR_Rev	CACAAACACGCACCTCAAAG
47	dp53_qPCR_Fwd	CTATTGAGCTGGCGTTCGTCTTGGAT
48	dp53_qPCR_Rev	TCTGCCAAAACTCGTGTATCGGGCG

Primers used in Chapter 4		
Primers for DIG-labeled RNA probes		
49	mre11_Fwd-T7	ACAACCACCTGGGCTATGG
50	mre11_Rev-T7	ATTCTAATACGACTCACTATAGGGTGGCTGCTTAGGATGACC
51	rad50_Fwd-T7	CCATATTCGGCATCACCGAG
52	Rad50_Rev-T7	ATTCTAATACGACTCACTATAGGGAACACTCGGCAACTAGC
53	mus210_Fwd-T7	TGGAAGCCGAGCAAGGACG
54	mus210_Rev-T7	ATTCTAATACGACTCACTATAGGGTGCTCCTTCGTAGGACG
55	mus304_Fwd-T7	ACGACGATGACGATGTCATCC
56	mus304_Rev-T7	ATTCTAATACGACTCACTATAGGGCTCCGTGAATACCTTGC
57	mus309_Fwd-T7	ACGCCACACCATGGCGTCC
58	mus309_Rev-T7	ATTCTAATACGACTCACTATAGGGTTTGATCCTGGCAGTG

59	sra_Fwd-T7	AATGCGTCCGCCGATGC
60	sra_Rev-T7	ATTCTAATACGACTCACTATAGGGCAAACATACGAACGTAGC
61	mus205_Fwd-T7	AAGCCGCGTCGCAGTGC
62	mus205_Rev-T7	ATTCTAATACGACTCACTATAGGGCTGCAACATTGCCAGGC
63	okr_Fwd-T7	ATCCGATGGCCTGCAACG
64	okr_Rev-T7	ATTCTAATACGACTCACTATAGGGTTGTAATGTCTGCCAGC
65	lig4_Fwd-T7	AGGCCTCGCCTGAGGAAC
66	lig4_Rev-T7	ATTCTAATACGACTCACTATAGGGATTGTTGGCAACCACTCC
67	rpr_Fwd-T7	GTGTGTGCGCCAGCAAC
68	rpr_Rev-T7	ATTCTAATACGACTCACTATAGGGAACTTCGACTCATCTTCG
69	Ku80_Fwd-T7	CCTGCGAGGATGGAGAATG
70	Ku80_Rev-T7	ATTCTAATACGACTCACTATAGGGAGTGTGCACTCCAGATC
71	Ku70-Fwd-T7	GCGGCAAGAAGCTAAACAAC
72	Ku70-Rev-T7	ATTCTAATACGACTCACTATAGGGCGTCAGCAGTGTTTTCCGTA
Rr3 assay primers for distinguishing NHEJ vs HR		
73	EJ3	CCGGCTAGGGATACGGCCGGG
74	Red06	GCCGTCCTCGAAGTTCATCA

BIBLIOGRAPHY

Abbott MK, Lengyel JA. 1991. Embryonic head involution and rotation of male terminalia require the Drosophila locus head involution defective. *Genetics* **129**: 783-789.

Abrams JM, White K, Fessler LI, Steller H. 1993. Programmed cell death during Drosophila embryogenesis. *Development* **117**: 29-43.

Adorno M, Cordenonsi M, Montagner M, Dupont S, Wong C, Hann B, Solari A, Bobisse S, Rondina MB, Guzzardo V et al. 2009. A Mutant-p53/Smad complex opposes p63 to empower TGFbeta-induced metastasis. *Cell* **137**: 87-98.

Akdemir F, Christich A, Sogame N, Chapo J, Abrams JM. 2007. p53 directs focused genomic responses in Drosophila. *Oncogene* **26**: 5184-5193.

Akdemir F, Farkas R, Chen P, Juhasz G, Medved'ova L, Sass M, Wang L, Wang X, Chittaranjan S, Gorski SM et al. 2006. Autophagy occurs upstream or parallel to the apoptosome during histolytic cell death. *Development* **133**: 1457-1465.

Amarneh B, Matthews KA, Rawson RB. 2009. Activation of sterol regulatory element-binding protein by the caspase Drice in Drosophila larvae. *J Biol Chem* **284**: 9674-9682.

Arama E, Agapite J, Steller H. 2003. Caspase activity and a specific cytochrome C are required for sperm differentiation in Drosophila. *Dev Cell* **4**: 687-697.

Arama E, Bader M, Rieckhof GE, Steller H. 2007. A ubiquitin ligase complex regulates caspase activation during sperm differentiation in Drosophila. *PLoS Biol* **5**: e251.

Arama E, Bader M, Srivastava M, Bergmann A, Steller H. 2006. The two Drosophila cytochrome C proteins can function in both respiration and caspase activation. *EMBO J* **25**: 232-243.

Baker SJ, Fearon ER, Nigro JM, Hamilton SR, Preisinger AC, Jessup JM, vanTuinen P, Ledbetter DH, Barker DF, Nakamura Y et al. 1989. Chromosome 17 deletions and p53 gene mutations in colorectal carcinomas. *Science* **244**: 217-221.

Bard F, Casano L, Mallabiabarrena A, Wallace E, Saito K, Kitayama H, Guizzunti G, Hu Y, Wendler F, Dasgupta R et al. 2006. Functional genomics reveals genes involved in protein secretion and Golgi organization. *Nature* **439**: 604-607.

Bjorklund M, Taipale M, Varjosalo M, Saharinen J, Lahdenpera J, Taipale J. 2006. Identification of pathways regulating cell size and cell-cycle progression by RNAi. *Nature* **439**: 1009-1013.

Bonke M, Turunen M, Sokolova M, Vaharautio A, Kivioja T, Taipale M, Bjorklund M, Taipale J. 2013. Transcriptional networks controlling the cell cycle. *G3 (Bethesda)* **3**: 75-90.

Boutros M, Kiger AA, Armknecht S, Kerr K, Hild M, Koch B, Haas SA, Paro R, Perrimon N, Heidelberg Fly Array C. 2004. Genome-wide RNAi analysis of growth and viability in Drosophila cells. *Science* **303**: 832-835.

Brady CA, Jiang D, Mello SS, Johnson TM, Jarvis LA, Kozak MM, Kenzelmann Broz D, Basak S, Park EJ, McLaughlin ME et al. 2011. Distinct p53 transcriptional programs dictate acute DNA-damage responses and tumor suppression. *Cell* **145**: 571-583.

Bressac C, Bre MH, Darmanaden-Delorme J, Laurent M, Levilliers N, Fleury A. 1995. A massive new posttranslational modification occurs on axonemal tubulin at the final step of spermatogenesis in Drosophila. *Eur J Cell Biol* **67**: 346-355.

Bricker DK, Taylor EB, Schell JC, Orsak T, Boutron A, Chen YC, Cox JE, Cardon CM, Van Vranken JG, Dephoure N et al. 2012. A mitochondrial pyruvate carrier required for pyruvate uptake in yeast, Drosophila, and humans. *Science* **337**: 96-100.

Brodsky MH, Nordstrom W, Tsang G, Kwan E, Rubin GM, Abrams JM. 2000. Drosophila p53 binds a damage response element at the reaper locus. *Cell* **101**: 103-113.

Brodsky MH, Weinert BT, Tsang G, Rong YS, McGinnis NM, Golic KG, Rio DC, Rubin GM. 2004. Drosophila melanogaster MNK/Chk2 and p53 regulate multiple DNA repair and apoptotic pathways following DNA damage. *Molecular and cellular biology* **24**: 1219-1231.

Broihier HT, Skeath JB. 2002. Drosophila homeodomain protein dHb9 directs neuronal fate via crossrepressive and cell-nonautonomous mechanisms. *Neuron* **35**: 39-50.

Brosh R, Rotter V. 2009. When mutants gain new powers: news from the mutant p53 field. *Nat Rev Cancer* **9**: 701-713.

Brumby AM, Richardson HE. 2003. scribble mutants cooperate with oncogenic Ras or Notch to cause neoplastic overgrowth in Drosophila. *EMBO J* **22**: 5769-5779.

Carbone R, Pearson M, Minucci S, Pelicci PG. 2002. PML NBs associate with the hMre11 complex and p53 at sites of irradiation induced DNA damage. *Oncogene* **21**: 1633-1640.

Carlile GW, Smith DH, Wiedmann M. 2004. Caspase-3 has a nonapoptotic function in erythroid maturation. *Blood* **103**: 4310-4316.

Chen P, Rodriguez A, Erskine R, Thach T, Abrams JM. 1998. Dredd, a novel effector of the apoptosis activators reaper, grim, and hid in Drosophila. *Dev Biol* **201**: 202-216.

Chen SX, Cherry A, Tari PK, Podgorski K, Kwong YK, Haas K. 2012. The transcription factor MEF2 directs developmental visually driven functional and structural metaplasticity. *Cell* **151**: 41-55.

Chew SK, Akdemir F, Chen P, Lu WJ, Mills K, Daish T, Kumar S, Rodriguez A, Abrams JM. 2004. The apical caspase dronc governs programmed and unprogrammed cell death in Drosophila. *Dev Cell* **7**: 897-907.

Chew SK, Chen P, Link N, Galindo KA, Pogue K, Abrams JM. 2009. Genome-wide silencing in Drosophila captures conserved apoptotic effectors. *Nature* **460**: 123-127.

Cooper JL, Greene EA, Till BJ, Codomo CA, Wakimoto BT, Henikoff S. 2008a. Retention of induced mutations in a Drosophila reverse-genetic resource. *Genetics* **180**: 661-667.

Cooper JL, Till BJ, Henikoff S. 2008b. Fly-TILL: reverse genetics using a living point mutation resource. *Fly (Austin)* **2**: 300-302.

Croft DR, Coleman ML, Li S, Robertson D, Sullivan T, Stewart CL, Olson MF. 2005. Actin-myosin-based contraction is responsible for apoptotic nuclear disintegration. *J Cell Biol* **168**: 245-255.

Daish TJ, Mills K, Kumar S. 2004. Drosophila caspase DRONC is required for specific developmental cell death pathways and stress-induced apoptosis. *Dev Cell* **7**: 909-915.

De Botton S, Sabri S, Daugas E, Zermati Y, Guidotti JE, Hermine O, Kroemer G, Vainchenker W, Debili N. 2002. Platelet formation is the consequence of caspase activation within megakaryocytes. *Blood* **100**: 1310-1317.

Dekanty A, Romero NM, Bertolin AP, Thomas MG, Leishman CC, Perez-Perri JI, Boccaccio GL, Wappner P. 2010. Drosophila genome-wide RNAi screen identifies multiple regulators of HIF-dependent transcription in hypoxia. *PLoS Genet* **6**: e1000994.

DeLeo AB, Jay G, Appella E, Dubois GC, Law LW, Old LJ. 1979. Detection of a transformation-related antigen in chemically induced sarcomas and other transformed cells of the mouse. *Proc Natl Acad Sci U S A* **76**: 2420-2424.

Dichtel-Danjoy ML, Ma D, Dourlen P, Chatelain G, Napoletano F, Robin M, Corbet M, Levet C, Hafsi H, Hainaut P et al. 2013. Drosophila p53 isoforms differentially regulate apoptosis and apoptosis-induced proliferation. *Cell Death Differ* **20**: 108-116.

Doumanis J, Wada K, Kino Y, Moore AW, Nukina N. 2009. RNAi screening in Drosophila cells identifies new modifiers of mutant huntingtin aggregation. *PLoS One* **4**: e7275.

Dow LE, Elsum IA, King CL, Kinross KM, Richardson HE, Humbert PO. 2008. Loss of human Scribble cooperates with H-Ras to promote cell invasion through deregulation of MAPK signalling. *Oncogene* **27**: 5988-6001.

Eliyahu D, Michalovitz D, Eliyahu S, Pinhasi-Kimhi O, Oren M. 1989. Wild-type p53 can inhibit oncogene-mediated focus formation. *Proc Natl Acad Sci U S A* **86**: 8763-8767.

Eliyahu D, Michalovitz D, Oren M. 1985. Overproduction of p53 antigen makes established cells highly tumorigenic. *Nature* **316**: 158-160.

Eliyahu D, Raz A, Gruss P, Givol D, Oren M. 1984. Participation of p53 cellular tumour antigen in transformation of normal embryonic cells. *Nature* **312**: 646-649.

Enari M, Sakahira H, Yokoyama H, Okawa K, Iwamatsu A, Nagata S. 1998. A caspase-activated DNase that degrades DNA during apoptosis, and its inhibitor ICAD. *Nature* **391**: 43-50.

Fabrizio JJ, Hime G, Lemmon SK, Bazinet C. 1998. Genetic dissection of sperm individualization in Drosophila melanogaster. *Development* **125**: 1833-1843.

Fan Y, Bergmann A. 2010. The cleaved-Caspase-3 antibody is a marker of Caspase-9-like DRONC activity in Drosophila. *Cell Death Differ* **17**: 534-539.

Feinstein-Rotkopf Y, Arama E. 2009. Can't live without them, can live with them: roles of caspases during vital cellular processes. *Apoptosis* **14**: 980-995.

Ferbeyre G, de Stanchina E, Querido E, Baptiste N, Prives C, Lowe SW. 2000. PML is induced by oncogenic ras and promotes premature senescence. *Genes Dev* **14**: 2015-2027.

Finlay CA, Hinds PW, Tan TH, Eliyahu D, Oren M, Levine AJ. 1988. Activating mutations for transformation by p53 produce a gene product that forms an hsc70-p53 complex with an altered half-life. *Molecular and cellular biology* **8**: 531-539.

Fogal V, Gostissa M, Sandy P, Zacchi P, Sternsdorf T, Jensen K, Pandolfi PP, Will H, Schneider C, Del Sal G. 2000. Regulation of p53 activity in nuclear bodies by a specific PML isoform. *EMBO J* **19**: 6185-6195.

Fuchs Y, Steller H. 2011. Programmed cell death in animal development and disease. *Cell* **147**: 742-758.

Geisbrecht ER, Montell DJ. 2004. A role for Drosophila IAP1-mediated caspase inhibition in Rac-dependent cell migration. *Cell* **118**: 111-125.

Gong WJ, Golic KG. 2003. Ends-out, or replacement, gene targeting in Drosophila. *Proc Natl Acad Sci U S A* **100**: 2556-2561.

Grether ME, Abrams JM, Agapite J, White K, Steller H. 1995. The head involution defective gene of Drosophila melanogaster functions in programmed cell death. *Genes Dev* **9**: 1694-1708.

Guo Y, Walther TC, Rao M, Stuurman N, Goshima G, Terayama K, Wong JS, Vale RD, Walter P, Farese RV. 2008. Functional genomic screen reveals genes involved in lipid-droplet formation and utilization. *Nature* **453**: 657-661.

Gurrieri C, Capodieci P, Bernardi R, Scaglioni PP, Nafa K, Rush LJ, Verbel DA, Cordon-Cardo C, Pandolfi PP. 2004. Loss of the tumor suppressor PML in human cancers of multiple histologic origins. *J Natl Cancer Inst* **96**: 269-279.

Hanel W, Marchenko N, Xu S, Yu SX, Weng W, Moll U. 2013. Two hot spot mutant p53 mouse models display differential gain of function in tumorigenesis. *Cell Death Differ* **20**: 898-909.

Hao Z, Duncan GS, Chang CC, Elia A, Fang M, Wakeham A, Okada H, Calzascia T, Jang Y, You-Ten A et al. 2005. Specific ablation of the apoptotic functions of cytochrome C reveals a differential requirement for cytochrome C and Apaf-1 in apoptosis. *Cell* **121**: 579-591.

Harvey M, McArthur MJ, Montgomery CA, Jr., Bradley A, Donehower LA. 1993. Genetic background alters the spectrum of tumors that develop in p53-deficient mice. *FASEB J* **7**: 938-943.

Harvey M, Vogel H, Morris D, Bradley A, Bernstein A, Donehower LA. 1995. A mutant p53 transgene accelerates tumour development in heterozygous but not nullizygous p53-deficient mice. *Nat Genet* **9**: 305-311.

Haupt S, di Agostino S, Mizrahi I, Alsheich-Bartok O, Voorhoeve M, Damalas A, Blandino G, Haupt Y. 2009. Promyelocytic leukemia protein is required for gain of function by mutant p53. *Cancer Res* **69**: 4818-4826.

Hay BA, Guo M. 2006. Caspase-dependent cell death in Drosophila. *Annu Rev Cell Dev Biol* **22**: 623-650.

Herranz H, Hong X, Hung NT, Voorhoeve PM, Cohen SM. 2012. Oncogenic cooperation between SOCS family proteins and EGFR identified using a Drosophila epithelial transformation model. *Genes Dev* **26**: 1602-1611.

Hinds P, Finlay C, Levine AJ. 1989. Mutation is required to activate the p53 gene for cooperation with the ras oncogene and transformation. *J Virol* **63**: 739-746.

Honarpour N, Du C, Richardson JA, Hammer RE, Wang X, Herz J. 2000. Adult Apaf-1-deficient mice exhibit male infertility. *Dev Biol* **218**: 248-258.

Huesmann GR, Clayton DF. 2006. Dynamic role of postsynaptic caspase-3 and BIRC4 in zebra finch song-response habituation. *Neuron* **52**: 1061-1072.

Hughes JR, Meireles AM, Fisher KH, Garcia A, Antrobus PR, Wainman A, Zitzmann N, Deane C, Ohkura H, Wakefield JG. 2008. A microtubule interactome: complexes with roles in cell cycle and mitosis. *PLoS Biol* **6**: e98.

Huh JR, Vernooy SY, Yu H, Yan N, Shi Y, Guo M, Hay BA. 2004. Multiple apoptotic caspase cascades are required in nonapoptotic roles for Drosophila spermatid individualization. *PLoS Biol* **2**: E15.

Isaji M, Lenartowska M, Noguchi T, Frank DJ, Miller KG. 2011. Myosin VI regulates actin structure specialization through conserved cargo-binding domain sites. *PLoS One* **6**: e22755.

Ishizaki Y, Jacobson MD, Raff MC. 1998. A role for caspases in lens fiber differentiation. *J Cell Biol* **140**: 153-158.

Jekely G, Sung HH, Luque CM, Rorth P. 2005. Regulators of endocytosis maintain localized receptor tyrosine kinase signaling in guided migration. *Dev Cell* **9**: 197-207.

Jenkins JR, Rudge K, Currie GA. 1984. Cellular immortalization by a cDNA clone encoding the transformation-associated phosphoprotein p53. *Nature* **312**: 651-654.

Jiao R, Daube M, Duan H, Zou Y, Frei E, Noll M. 2001. Headless flies generated by developmental pathway interference. *Development* **128**: 3307-3319.

Joerger AC, Fersht AR. 2007. Structure-function-rescue: the diverse nature of common p53 cancer mutants. *Oncogene* **26**: 2226-2242.

-. 2010. The tumor suppressor p53: from structures to drug discovery. *Cold Spring Harb Perspect Biol* **2**: a000919.

Johnson-Schlitz DM, Flores C, Engels WR. 2007. Multiple-pathway analysis of double-strand break repair mutations in Drosophila. *PLoS Genet* **3**: e50.

Kaplan Y, Gibbs-Bar L, Kalifa Y, Feinstein-Rotkopf Y, Arama E. 2010. Gradients of a ubiquitin E3 ligase inhibitor and a caspase inhibitor determine differentiation or death in spermatids. *Dev Cell* **19**: 160-173.

Kastan MB, Zhan Q, el-Deiry WS, Carrier F, Jacks T, Walsh WV, Plunkett BS, Vogelstein B, Fornace AJ, Jr. 1992. A mammalian cell cycle checkpoint pathway utilizing p53 and GADD45 is defective in ataxia-telangiectasia. *Cell* **71**: 587-597.

Kato S, Han SY, Liu W, Otsuka K, Shibata H, Kanamaru R, Ishioka C. 2003. Understanding the function-structure and function-mutation relationships of p53 tumor suppressor protein by high-resolution missense mutation analysis. *Proc Natl Acad Sci U S A* **100**: 8424-8429.

Knudson AG, Jr. 1971. Mutation and cancer: statistical study of retinoblastoma. *Proc Natl Acad Sci U S A* **68**: 820-823.

Kondo S, Senoo-Matsuda N, Hiromi Y, Miura M. 2006. DRONC coordinates cell death and compensatory proliferation. *Molecular and cellular biology* **26**: 7258-7268.

Kooistra R, Vreeken K, Zonneveld JB, de Jong A, Eeken JC, Osgood CJ, Buerstedde JM, Lohman PH, Pastink A. 1997. The Drosophila melanogaster RAD54 homolog, DmRAD54, is involved in the repair of radiation damage and recombination. *Molecular and cellular biology* **17**: 6097-6104.

Kosman D, Small S, Reinitz J. 1998. Rapid preparation of a panel of polyclonal antibodies to Drosophila segmentation proteins. *Dev Genes Evol* **208**: 290-294.

Kress M, May E, Cassingena R, May P. 1979. Simian virus 40-transformed cells express new species of proteins precipitable by anti-simian virus 40 tumor serum. *J Virol* **31**: 472-483.

Kroemer G, Galluzzi L, Brenner C. 2007. Mitochondrial membrane permeabilization in cell death. *Physiol Rev* **87**: 99-163.

Kunte AS, Matthews KA, Rawson RB. 2006. Fatty acid auxotrophy in Drosophila larvae lacking SREBP. *Cell Metab* **3**: 439-448.

Kuo CT, Zhu S, Younger S, Jan LY, Jan YN. 2006. Identification of E2/E3 ubiquitinating enzymes and caspase activity regulating Drosophila sensory neuron dendrite pruning. *Neuron* **51**: 283-290.

Lane DP, Crawford LV. 1979. T antigen is bound to a host protein in SV40-transformed cells. *Nature* **278**: 261-263.

Lang GA, Iwakuma T, Suh YA, Liu G, Rao VA, Parant JM, Valentin-Vega YA, Terzian T, Caldwell LC, Strong LC et al. 2004. Gain of function of a p53 hot spot mutation in a mouse model of Li-Fraumeni syndrome. *Cell* **119**: 861-872.

Lavigueur A, Maltby V, Mock D, Rossant J, Pawson T, Bernstein A. 1989. High incidence of lung, bone, and lymphoid tumors in transgenic mice overexpressing mutant alleles of the p53 oncogene. *Molecular and cellular biology* **9**: 3982-3991.

Lehembre F, Badenhorst P, Muller S, Travers A, Schweisguth F, Dejean A. 2000. Covalent modification of the transcriptional repressor tramtrack by the ubiquitin-related protein Smt3 in Drosophila flies. *Molecular and cellular biology* **20**: 1072-1082.

Li T, Kon N, Jiang L, Tan M, Ludwig T, Zhao Y, Baer R, Gu W. 2012. Tumor suppression in the absence of p53-mediated cell-cycle arrest, apoptosis, and senescence. *Cell* **149**: 1269-1283.

Lindquist RA, Ottina KA, Wheeler DB, Hsu PP, Thoreen CC, Guertin DA, Ali SM, Sengupta S, Shaul YD, Lamprecht MR et al. 2011. Genome-scale RNAi on living-cell

microarrays identifies novel regulators of Drosophila melanogaster TORC1-S6K pathway signaling. *Genome Res* **21**: 433-446.

Linzer DI, Levine AJ. 1979. Characterization of a 54K dalton cellular SV40 tumor antigen present in SV40-transformed cells and uninfected embryonal carcinoma cells. *Cell* **17**: 43-52.

Lippens S, Kockx M, Knaapen M, Mortier L, Polakowska R, Verheyen A, Garmyn M, Zwijsen A, Formstecher P, Huylebroeck D et al. 2000. Epidermal differentiation does not involve the pro-apoptotic executioner caspases, but is associated with caspase-14 induction and processing. *Cell Death Differ* **7**: 1218-1224.

Lu WJ, Amatruda JF, Abrams JM. 2009. p53 ancestry: gazing through an evolutionary lens. *Nat Rev Cancer* **9**: 758-762.

Lu WJ, Chapo J, Roig I, Abrams JM. 2010. Meiotic recombination provokes functional activation of the p53 regulatory network. *Science* **328**: 1278-1281.

Lubin R, Schlichtholz B, Teillaud JL, Garay E, Bussel A, Wild CP. 1995. p53 antibodies in patients with various types of cancer: assay, identification, and characterization. *Clin Cancer Res* **1**: 1463-1469.

Lucas EP, Khanal I, Gaspar P, Fletcher GC, Polesello C, Tapon N, Thompson BJ. 2013. The Hippo pathway polarizes the actin cytoskeleton during collective migration of Drosophila border cells. *J Cell Biol* **201**: 875-885.

Luke-Glaser S, Roy M, Larsen B, Le Bihan T, Metalnikov P, Tyers M, Peter M, Pintard L. 2007. CIF-1, a shared subunit of the COP9/signalosome and eukaryotic initiation factor 3 complexes, regulates MEL-26 levels in the Caenorhabditis elegans embryo. *Molecular and cellular biology* **27**: 4526-4540.

Marion RM, Strati K, Li H, Murga M, Blanco R, Ortega S, Fernandez-Capetillo O, Serrano M, Blasco MA. 2009. A p53-mediated DNA damage response limits reprogramming to ensure iPS cell genomic integrity. *Nature* **460**: 1149-1153.

Mashima T, Naito M, Tsuruo T. 1999. Caspase-mediated cleavage of cytoskeletal actin plays a positive role in the process of morphological apoptosis. *Oncogene* **18**: 2423-2430.

Mauri F, McNamee LM, Lunardi A, Chiacchiera F, Del Sal G, Brodsky MH, Collavin L. 2008. Modification of Drosophila p53 by SUMO modulates its transactivation and pro-apoptotic functions. *J Biol Chem* **283**: 20848-20856.

Meier P, Silke J, Leevers SJ, Evan GI. 2000. The Drosophila caspase DRONC is regulated by DIAP1. *EMBO J* **19**: 598-611.

Meletis K, Wirta V, Hede SM, Nister M, Lundeberg J, Frisen J. 2006. p53 suppresses the self-renewal of adult neural stem cells. *Development* **133**: 363-369.

Mendes CS, Arama E, Brown S, Scherr H, Srivastava M, Bergmann A, Steller H, Mollereau B. 2006. Cytochrome c-d regulates developmental apoptosis in the Drosophila retina. *EMBO Rep* **7**: 933-939.

Mills AA, Zheng B, Wang XJ, Vogel H, Roop DR, Bradley A. 1999. p63 is a p53 homologue required for limb and epidermal morphogenesis. *Nature* **398**: 708-713.

Mills K, Daish T, Harvey KF, Pfleger CM, Hariharan IK, Kumar S. 2006. The Drosophila melanogaster Apaf-1 homologue ARK is required for most, but not all, programmed cell death. *J Cell Biol* **172**: 809-815.

Montell DJ. 2003. Border-cell migration: the race is on. *Nat Rev Mol Cell Biol* **4**: 13-24.

Morselli E, Tasdemir E, Maiuri MC, Galluzzi L, Kepp O, Criollo A, Vicencio JM, Soussi T, Kroemer G. 2008. Mutant p53 protein localized in the cytoplasm inhibits autophagy. *Cell Cycle* **7**: 3056-3061.

Mowat M, Cheng A, Kimura N, Bernstein A, Benchimol S. 1985. Rearrangements of the cellular p53 gene in erythroleukaemic cells transformed by Friend virus. *Nature* **314**: 633-636.

Muller H, Schmidt D, Steinbrink S, Mirgorodskaya E, Lehmann V, Habermann K, Dreher F, Gustavsson N, Kessler T, Lehrach H et al. 2010. Proteomic and functional analysis of the mitotic Drosophila centrosome. *EMBO J* **29**: 3344-3357.

Muller PA, Caswell PT, Doyle B, Iwanicki MP, Tan EH, Karim S, Lukashchuk N, Gillespie DA, Ludwig RL, Gosselin P et al. 2009. Mutant p53 drives invasion by promoting integrin recycling. *Cell* **139**: 1327-1341.

Ni JQ, Markstein M, Binari R, Pfeiffer B, Liu LP, Villalta C, Booker M, Perkins L, Perrimon N. 2008. Vector and parameters for targeted transgenic RNA interference in Drosophila melanogaster. *Nat Methods* **5**: 49-51.

Noguchi T, Lenartowska M, Miller KG. 2006. Myosin VI stabilizes an actin network during Drosophila spermatid individualization. *Mol Biol Cell* **17**: 2559-2571.

Noguchi T, Miller KG. 2003. A role for actin dynamics in individualization during spermatogenesis in Drosophila melanogaster. *Development* **130**: 1805-1816.

Nordling CO. 1953. A new theory on cancer-inducing mechanism. *Br J Cancer* **7**: 68-72.

Olive KP, Tuveson DA, Ruhe ZC, Yin B, Willis NA, Bronson RT, Crowley D, Jacks T. 2004. Mutant p53 gain of function in two mouse models of Li-Fraumeni syndrome. *Cell* **119**: 847-860.

Owusu-Ansah E, Banerjee U. 2009. Reactive oxygen species prime Drosophila haematopoietic progenitors for differentiation. *Nature* **461**: 537-541.

Pagliarini RA, Xu T. 2003. A genetic screen in Drosophila for metastatic behavior. *Science* **302**: 1227-1231.

Parada LF, Land H, Weinberg RA, Wolf D, Rotter V. 1984. Cooperation between gene encoding p53 tumour antigen and ras in cellular transformation. *Nature* **312**: 649-651.

Pearson M, Carbone R, Sebastiani C, Cioce M, Fagioli M, Saito S, Higashimoto Y, Appella E, Minucci S, Pandolfi PP et al. 2000. PML regulates p53 acetylation and premature senescence induced by oncogenic Ras. *Nature* **406**: 207-210.

Petitjean A, Mathe E, Kato S, Ishioka C, Tavtigian SV, Hainaut P, Olivier M. 2007. Impact of mutant p53 functional properties on TP53 mutation patterns and tumor phenotype: lessons from recent developments in the IARC TP53 database. *Hum Mutat* **28**: 622-629.

Pozniak CD, Radinovic S, Yang A, McKeon F, Kaplan DR, Miller FD. 2000. An anti-apoptotic role for the p53 family member, p73, during developmental neuron death. *Science* **289**: 304-306.

Preston CR, Flores CC, Engels WR. 2006. Differential usage of alternative pathways of double-strand break repair in Drosophila. *Genetics* **172**: 1055-1068.

Qin H, Yu T, Qing T, Liu Y, Zhao Y, Cai J, Li J, Song Z, Qu X, Zhou P et al. 2007. Regulation of apoptosis and differentiation by p53 in human embryonic stem cells. *J Biol Chem* **282**: 5842-5852.

Quon KC, Berns A. 2001. Haplo-insufficiency? Let me count the ways. *Genes Dev* **15**: 2917-2921.

Rodriguez A, Oliver H, Zou H, Chen P, Wang X, Abrams JM. 1999. Dark is a Drosophila homologue of Apaf-1/CED-4 and functions in an evolutionarily conserved death pathway. *Nat Cell Biol* **1**: 272-279.

Rogulja-Ortmann A, Luer K, Seibert J, Rickert C, Technau GM. 2007. Programmed cell death in the embryonic central nervous system of Drosophila melanogaster. *Development* **134**: 105-116.

Ryoo HD, Baehrecke EH. 2010. Distinct death mechanisms in Drosophila development. *Curr Opin Cell Biol* **22**: 889-895.

Seegmiller AC, Dobrosotskaya I, Goldstein JL, Ho YK, Brown MS, Rawson RB. 2002. The SREBP pathway in Drosophila: regulation by palmitate, not sterols. *Dev Cell* **2**: 229-238.

Sepp KJ, Hong P, Lizarraga SB, Liu JS, Mejia LA, Walsh CA, Perrimon N. 2008. Identification of neural outgrowth genes using genome-wide RNAi. *PLoS Genet* **4**: e1000111.

Sordet O, Rebe C, Plenchette S, Zermati Y, Hermine O, Vainchenker W, Garrido C, Solary E, Dubrez-Daloz L. 2002. Specific involvement of caspases in the differentiation of monocytes into macrophages. *Blood* **100**: 4446-4453.

Soussi T. 2007. p53 alterations in human cancer: more questions than answers. *Oncogene* **26**: 2145-2156.

Spike BT, Wahl GM. 2011. p53, Stem Cells, and Reprogramming: Tumor Suppression beyond Guarding the Genome. *Genes Cancer* **2**: 404-419.

Thompson CB. 1995. Apoptosis in the pathogenesis and treatment of disease. *Science* **267**: 1456-1462.

Till BJ, Colbert T, Tompa R, Enns LC, Codomo CA, Johnson JE, Reynolds SH, Henikoff JG, Greene EA, Steine MN et al. 2003. High-throughput TILLING for functional genomics. *Methods Mol Biol* **236**: 205-220.

Valente LJ, Gray DH, Michalak EM, Pinon-Hofbauer J, Egle A, Scott CL, Janic A, Strasser A. 2013. p53 efficiently suppresses tumor development in the complete absence of its cell-cycle inhibitory and proapoptotic effectors p21, Puma, and Noxa. *Cell Rep* **3**: 1339-1345.

Vaziri H, Dessain SK, Ng Eaton E, Imai SI, Frye RA, Pandita TK, Guarente L, Weinberg RA. 2001. hSIR2(SIRT1) functions as an NAD-dependent p53 deacetylase. *Cell* **107**: 149-159.

Venken KJ, Carlson JW, Schulze KL, Pan H, He Y, Spokony R, Wan KH, Koriabine M, de Jong PJ, White KP et al. 2009. Versatile P[acman] BAC libraries for transgenesis studies in Drosophila melanogaster. *Nat Methods* **6**: 431-434.

Vousden KH, Lane DP. 2007. p53 in health and disease. *Nat Rev Mol Cell Biol* **8**: 275-283.

Vousden KH, Ryan KM. 2009. p53 and metabolism. *Nat Rev Cancer* **9**: 691-700.

Wang X, Zelenski NG, Yang J, Sakai J, Brown MS, Goldstein JL. 1996. Cleavage of sterol regulatory element binding proteins (SREBPs) by CPP32 during apoptosis. *EMBO J* **15**: 1012-1020.

Williams DW, Kondo S, Krzyzanowska A, Hiromi Y, Truman JW. 2006. Local caspase activity directs engulfment of dendrites during pruning. *Nat Neurosci* **9**: 1234-1236.

Wolf D, Harris N, Rotter V. 1984. Reconstitution of p53 expression in a nonproducer Ab-MuLV-transformed cell line by transfection of a functional p53 gene. *Cell* **38**: 119-126.

Wolf D, Rotter V. 1984. Inactivation of p53 gene expression by an insertion of Moloney murine leukemia virus-like DNA sequences. *Molecular and cellular biology* **4**: 1402-1410.

-. 1985. Major deletions in the gene encoding the p53 tumor antigen cause lack of p53 expression in HL-60 cells. *Proc Natl Acad Sci U S A* **82**: 790-794.

Wylie A, Lu WJ, D'Brot A, Buszczak M, Abrams JM. 2014. p53 activity is selectively licensed in the Drosophila stem cell compartment. *Elife* **3**: e01530.

Xu D, Li Y, Arcaro M, Lackey M, Bergmann A. 2005. The CARD-carrying caspase Dronc is essential for most, but not all, developmental cell death in Drosophila. *Development* **132**: 2125-2134.

Xu J, Reumers J, Couceiro JR, De Smet F, Gallardo R, Rudyak S, Cornelis A, Rozenski J, Zwolinska A, Marine JC et al. 2011. Gain of function of mutant p53 by coaggregation with multiple tumor suppressors. *Nat Chem Biol* **7**: 285-295.

Yamaguchi M, Hirose F, Inoue YH, Shiraki M, Hayashi Y, Nishi Y, Matsukage A. 1999. Ectopic expression of human p53 inhibits entry into S phase and induces apoptosis in the Drosophila eye imaginal disc. *Oncogene* **18**: 6767-6775.

Yang A, Schweitzer R, Sun D, Kaghad M, Walker N, Bronson RT, Tabin C, Sharpe A, Caput D, Crum C et al. 1999. p63 is essential for regenerative proliferation in limb, craniofacial and epithelial development. *Nature* **398**: 714-718.

Yang A, Walker N, Bronson R, Kaghad M, Oosterwegel M, Bonnin J, Vagner C, Bonnet H, Dikkes P, Sharpe A et al. 2000. p73-deficient mice have neurological, pheromonal and inflammatory defects but lack spontaneous tumours. *Nature* **404**: 99-103.

Yuan S, Akey CW. 2013. Apoptosome structure, assembly, and procaspase activation. *Structure* **21**: 501-515.

Yuan S, Yu X, Topf M, Dorstyn L, Kumar S, Ludtke SJ, Akey CW. 2011. Structure of the Drosophila apoptosome at 6.9 a resolution. *Structure* **19**: 128-140.

Zeng L, Wan Y, Li D, Wu J, Shao M, Chen J, Hui L, Ji H, Zhu X. 2013. The m-subunit of murine translation initiation factor eIF3 maintains the integrity of the eIF3 complex and is required for embryonic development, homeostasis, and organ size control. *J Biol Chem*.

Zheng H, Ying H, Yan H, Kimmelman AC, Hiller DJ, Chen AJ, Perry SR, Tonon G, Chu GC, Ding Z et al. 2008. p53 and Pten control neural and glioma stem/progenitor cell renewal and differentiation. *Nature* **455**: 1129-1133.

Zhou C, Arslan F, Wee S, Krishnan S, Ivanov AR, Oliva A, Leatherwood J, Wolf DA. 2005. PCI proteins eIF3e and eIF3m define distinct translation initiation factor 3 complexes. *BMC Biol* **3**: 14.